

NORTHWESTERN UNIVERSITY

Body Heat-Activated Polymer-Mineral Composites for Vertebral Body Fractures

A DISSERTATION

SUBMITTED TO THE GRADUATE SCHOOL  
IN PARTIAL FULFILLMENT OF THE REQUIREMENTS

for the degree

DOCTOR OF PHILOSOPHY

Field of Biomedical Engineering

By

Samantha E Huddleston

EVANSTON, ILLINOIS

September 2022

© Copyright by Samantha E Huddleston 2022

All Rights Reserved

## ABSTRACT

### Body Heat-Activated Polymer-Mineral Composites for Vertebral Body Fractures

Polymer and polymer/ceramic composites known as bone cements are commonly used in musculoskeletal reconstructive surgeries where bone tissue fixation, reinforcement, or void filling may be needed<sup>1</sup>. Polymethylmethacrylate, PMMA, was the initial (and currently only) FDA-approved bone cement for bone-void filling applications yet faces many inherent material-based challenges that impacts its use and success as a viable material in biomedical applications<sup>2,3</sup>. This work presents an alternate bone cement design for bone-void filling applications composed of citrate-based biomaterials (CBBs), ceramic, and a thermoresponsive initiator to address the shortcomings of clinically used bone cements.

Vertebral compression fractures due to osteoporosis require materials that are easy to handle, quickly fill and set within a bone cavity, provide similar mechanics to the surrounding bone, and effectively integrate within the bone structure, though these materials are currently based on the non-degradable, mechanically stiff PMMA which relies on peroxide-initiated polymerization to quickly set the cement at the cost of high exothermic temperatures. Recently, there has been interest in developing degradable, bone mechanic-matching alternatives that pursue physiologically induced polymerization to both augment the handling of the material before application and to reduce high localized temperatures that may lead to tissue damage. Thermoresponsive polymers such as CBBs have shown potential use in orthopedic applications as pre-molded biomaterials<sup>4</sup>. However, their ability to mimic the quick-setting ability of bone cements has not been explored. The objective of this research was to investigate whether CBBs could be functionalized to mimic bone cement polymerization mechanics via methacrylation of poly(1,8-octanediol co-citrate) (mPOC) and introduction of an azo-based radical initiator. We show that the addition of a ceramic com-

ponent (hydroxyapatite, HA) and a thermoresponsive component (2,2'-Azobis(4-methoxy-2,4-dimethylvaleronitrile, V70) produces a quick-setting, tunable polymer composite suitable for bone void filling applications. mPOC-60HA was the most viable composite *in vitro* and *in vivo*, producing results on par with clinically used PMMA. The HA provided a modular platform that tailors to specific bone mechanics. The results support the use of the thermoresponsive mPOC for bone cement applications over clinically used PMMA.



## ACKNOWLEDGEMENTS

This dissertation and my graduate work as a whole would not have been possible without the many individuals I relied on for support, mentorship, and understanding. Quite honestly I would have dropped out by now and started a bakery. Maybe check back on that in 20 years. This work has been supported by the IMSD CLIMB Program and the NSF GRFP.

I would not have even pursued graduate school without the training and support from the IMSD EXPRESS Program at Mizzou, especially in regard to Brian Booton. I will always appreciate your involvement and care in my academic career and I look forward to coming back to Mizzou.

I would like to thank my advisor, Professor Guillermo Ameer. I hold a lot of respect for his ability to make a pitch and I appreciate his earnest interest and help when I pursued an industrial internship and post graduate careers. I would also like to thank my committee members Dr. Jason Koh, Dr. Evan Scott, and Dr. Shu Liu. Each of their perspectives were incredibly enlightening and have helped me become a more well-rounded researcher. Additionally, Dr. Bret Ulery has provided extensive mentorship over the past few months while I have prepared my manuscript, thesis, and transition towards my next position. It was not necessary to provide this support, especially when I am not his student, lab member, or collaborator as of yet, but it has made me excited to continue to pursue academia and learn from him and his laboratory members as I pursue a postdoc at Mizzou.

There are so many lab members, past and present, that have enriched my time and effort over all these years. Thank you to Dr. Bin Jiang for being an excellent, if not initially intimidating, mentor. Thank you to Chongwen Duan, Banu Akar, Sherry Zhu, Simona Morochnik, Anthony Petty, Cole Fuerste, Paul Puglisi, Anamika Chatterjee, Shwetha Ramachandra, Jacqueline Burke, Nancy Rivera Bolaños, Juan Sanabria, Jimmy Su, María Mendez-Santos, Maddy Goedegebuure, Nicole Flores, Rebecca Keate, Huifeng Wang, and Xinlong Wang.

I would like to thank all of the wonderful friends I have made at Northwestern through my BME co-hort, organizations, and sports. Clayton Rische, Cole, Max Greenberg, Yuni Teh, Joseph Sombeck, Chandler Clark, and Shwetha, I care for you all very much and you made the first year in Chicago well worth the experience. Nilou Sarvian, Christian Contreras, Patrick Krantz, Jaime McFarlin, Carissa Heath, and Justin Finkle, I got to know you all while playing sports and they have each turned into wonderful friendships where we complain about grad school and various things. Patrick, you have made this past year significantly more bearable and I look forward to many more. Thank you to everyone I met through the graduate gardens, graduate board game group, GradSWE, and the BME DEI group, you have given me an outlet to meet and interact with many graduate students outside of my department.

Thank you to Big Fun and especially Sean O'Brien, Ryan Hoffman, Carly Ilg, and Clay Houser. You were the first thing that I found that made Chicago a home and thank goodness I talk to random strangers with frisbee discs. Thank you Eva Lopez for letting me spend my first Thanksgiving in Chicago with you and for being a rock solid friend no matter how much time passes. I send all my love to my CoMo crew, Nick Pemberton, Ginny Pemberton, Joey Kopp, Michael Castleman, Dalton Juern, Josh Garton, Kevin Coleman, Paige Martz, Andrew Notch, and Jeremy Davis. We shall have many more fancy dinners, board games, TTRPGs, anime/coffee sessions, and Discord chats now that I will also have a real job.

Thank you to Shwetha, again for the third time, but you're kind of important. You have been the best roommate, basically a sister, and I could not have done most of this without you. Thank you Tristen for being almost nearly the sole reason I am an engineer, without all those video games I probably wouldn't like problem solving all that much. Thank you mom and dad for being the best support during all these years and forcing me to pursue biomedical engineering. It has been relatively fun. Except for that cancer bit, try not to jinx me again. Dad, you are responsible for

my interest in science fiction and nerdism. Mom, you showed me how all that nonsense can be applicable by opening me up to the medical world at such a young age.

Finally, thank you to Nano. You were brought into my life on the second day I moved to Chicago to start this journey and you have brought aggravation and mostly joy since. Thank you for being my companion since nearly day one and I promise we will eventually have a bigger space for you to constantly meow at me in.

## ABBREVIATIONS

$\alpha$ -MEM – Alpha Minimum Essential Medium

AIBN – Azobisisobutyronitrile

ALP – Alkaline Phosphatase

ANOVA – Analysis of Variance

ASTM – American Society for Testing and Materials

BHT – Butylated Hydroxytoluene

BMD – Bone Mineral Density

BP – Benzoyl Peroxide

BSA – Bovine Serum Albumin

CBB – Citrate-Based Biomaterial

CCK8 – Cell Counting Kit 8

CPC – Calcium Phosphate Cement

D<sub>2</sub>O – Deuterium Oxide

DCPD – Dicalcium Phosphate Dihydrate

DI – Deionized

DMAP - 4-Dimethylaminopyridine

DMPT – N,N-Dimethyl-p-Toluidine

DMSO-d<sub>6</sub> – Deuterated Dimethyl Sulfoxide

EDAB - Ethyl 4-(Dimethylamino) Benzoate

EDTA - Ethylenediaminetetraacetic Acid

eNOS – Endothelial Nitric Oxide Synthase

ESI – Electrospray Ionization

FBR – Foreign Body Response

FBS – Fetal Bovine Serum

FDA – Food and Drug Administration

FT-IR – Fourier Transform Infrared Spectroscopy

GMA – Glycidyl Methacrylate

H&E – Hematoxylin and Eosin

HA – Hydroxyapatite

HMDS – Hexamethyldisiloxane

HMG – 3-Hydroxy-3-Methylglutaryl

hMSC – Human Mesenchymal Stem Cell

HUVECs – Human Umbilical Vein Endothelial Cells

ISO – International Organization for Standardization

KP – Kyphoplasty

MC3T3-E1 – Mouse Calvarial Pre-Osteoblast Cells

mPOC – Methacrylated Poly (1,8-Octanediol-co-Citrate)

MSC – Mesenchymal Stem Cell

MSI – Museum of Science and Industry

MT – Masson's Trichrome

NIH – National Institutes of Health

NMR – Nuclear Magnetic Resonance

NSF – National Science Foundation

OD – Optical Density

OPN – Osteopontin

OSX - Osterix

OVX – Ovariectomy

PBS – Phosphate Buffered Saline

PMMA – Poly (Methyl Methacrylate)

pNP – Para-Nitrophenol

pNPP – Para-Nitrophenylphosphate

POC - Poly (1,8-Octanediol-co-Citrate)

PPF – Poly Propylene Fumarate

RIPA – Radioimmunoprecipitation Assay

RUNX2 - Runt-related Transcription Factor 2

SEM – Scanning Electron Microscopy

TCP – Tri-Calcium Phosphate

THF – Tetrahydrofuran

V70 - 2,2'-Azobis(4-Methoxy-2,4-Dimethylvaleronitrile)

VCF – Vertebral Compression Fracture

VEGF - Vascular Endothelial Growth Factor

VP – Vertebroplasty

## TABLE OF CONTENTS

<b>Abstract</b> . . . . .	2
<b>Acknowledgments</b> . . . . .	4
<b>List of Figures</b> . . . . .	16
<b>List of Tables</b> . . . . .	25
<b>Chapter 1: Overview</b> . . . . .	27
1.1 Motivation . . . . .	27
1.2 Thesis Outline . . . . .	28
1.3 Specific Aims . . . . .	29
<b>Chapter 2: Background</b> . . . . .	30
2.1 Bone . . . . .	30
2.1.1 Bone Remodeling . . . . .	30
2.1.2 Fractures and Medical Interventions . . . . .	32
2.1.3 Bone Cement . . . . .	33

	12
2.2 PMMA . . . . .	35
2.3 Citrate-Based Biomaterials . . . . .	38
2.4 V70 . . . . .	40
2.5 HA . . . . .	41
<b>Chapter 3: POC Synthesis and Characterization . . . . .</b>	<b>43</b>
3.1 Objective . . . . .	43
3.2 Experimental Section . . . . .	43
3.2.1 Materials . . . . .	43
3.2.2 Synthesis Scheme of mPOC . . . . .	43
3.2.3 Nuclear Magnetic Resonance (NMR) . . . . .	45
3.2.4 Electrospray Ionization (ESI) . . . . .	45
3.2.5 Fourier-Transform Infrared Spectroscopy (FT-IR) . . . . .	46
3.2.6 Doughing and Setting Times . . . . .	46
3.2.7 Thermal Reaction . . . . .	47
3.2.8 Rheology . . . . .	47
3.2.9 Swelling and Mass Loss . . . . .	48
3.2.10 Mechanical Compression . . . . .	48
3.2.11 Startistical Analysis . . . . .	49
3.3 Results . . . . .	49
3.3.1 Characterization of POC . . . . .	49



	13
3.3.2 Rheology . . . . .	54
3.3.3 Mechanical Compression . . . . .	57
3.4 Discussion . . . . .	57
3.5 Conclusion . . . . .	61
<b>Chapter 4: <i>In Vitro</i> Studies of Cellular Response . . . . .</b>	<b>62</b>
4.1 Objective . . . . .	62
4.2 Experimental Section . . . . .	62
4.2.1 Culture of Undifferentiated Cells . . . . .	62
4.2.2 Cytotoxicity (MTT) Assay . . . . .	62
4.2.3 Proliferation (CCK8) Assay . . . . .	63
4.2.4 LIVE/DEAD Assay . . . . .	64
4.2.5 Scanning Electron Microscopy (SEM) Imaging . . . . .	64
4.2.6 Statistical Analysis . . . . .	65
4.3 Results . . . . .	65
4.3.1 HA increases cell viability . . . . .	65
4.3.2 HA increases cell proliferation . . . . .	65
4.4 Discussion . . . . .	67
4.5 Conclusion . . . . .	72
<b>Chapter 5: <i>In Vivo</i> Model for Inflammatory Effect . . . . .</b>	<b>73</b>

	14
5.1 Objective . . . . .	73
5.2 Experimental Section . . . . .	73
5.2.1 Rat Model and Preparation of Materials . . . . .	73
5.2.2 Tissue Processing . . . . .	74
5.2.3 Histological Assessment . . . . .	75
5.2.4 Immunohistochemistry Assessment . . . . .	75
5.2.5 Statistical Analysis . . . . .	77
5.3 Results . . . . .	77
5.3.1 HA reduces inflammatory response . . . . .	77
5.3.1.1 Histology Imaging . . . . .	77
5.3.1.2 Immunohistochemistry Imaging . . . . .	78
5.4 Discussion . . . . .	78
5.5 Conclusion . . . . .	83
<b>Chapter 6: Thesis Summary and Outlook . . . . .</b>	<b>84</b>
6.1 Summary of Thesis Work . . . . .	84
6.2 Future Work . . . . .	86
6.2.1 Alkaline Phosphatase/Alizarin Red <i>In Vitro</i> Study . . . . .	86
6.2.2 <i>In Vivo</i> Femoral Defect . . . . .	90
6.2.3 <i>In Vivo</i> Osteoporotic VP/KP Model . . . . .	92
6.2.4 <i>Ex Vivo</i> Vertebral Mechanics . . . . .	94

	15
6.2.5 Research Necessary for FDA Approval . . . . .	97
6.3 Significance and Outlook . . . . .	99
<b>References . . . . .</b>	<b>109</b>
<b>Appendix A: Appendix . . . . .</b>	<b>111</b>
A.1 Adjusted POC Synthesis . . . . .	111
A.2 Efficacy of Statins . . . . .	121
A.3 Component Cell Cytotoxicity . . . . .	124
A.4 OPN <i>In Vivo</i> Results . . . . .	129
<b>Vita . . . . .</b>	<b>132</b>

## LIST OF FIGURES

1.1	Schematic of the thesis outline. . . . .	29
2.1	The three stages of bone remodeling: resorption, reversal, and formation. During resorption, osteoclasts dissolve the bone matrix by secreting hydrochloric acid. Reversal oversees mononuclear cells preparing the exposed surface for new osteoblasts. Lastly, osteoblast precursors are recruited and differentiated into osteoblasts to form new bone during formation. . . . .	31
2.2	Schematic for vertebroplasty (VP) and kyphoplasty (KP). VP involves directly injecting bone cement into a fractured vertebral segment to stabilize the fracture. KP begins by introducing a balloon catheter into the fractured vertebrae, expanding the balloon to the vertebrae's original height, and then filling the created cavity with bone cement. . . . .	34
2.3	Chemical structure of a monomer unit of POC. Citrate moieties (black) confer antioxidant activity and are linked by 1,8-octanediol (blue). . . . .	39
2.4	Chemical structure of V70 and radical formation mechanisms for azo polymerization initiators and peroxides. Azo polymerization initiators decompose with heat or light, forming nitrogen gas and carbon radicals that can then polymerize with vinyl monomers to form a polymer. Peroxides form R-CO <sub>2</sub> which immediately decomposes to CO <sub>2</sub> and an alkyl radical that forms a polymer chain through addition reactions. . . . .	41

- 3.1 Synthetic scheme of mPOC syntheses. POC was prepared by polycondensation of 1,8-octanediol (blue) and citric acid (black) and subsequent ring opening polymerization to attach glycidyl methacrylate groups (red). mPOC and mPOC-xHA were prepared following the formulations outlined in Table 3.1 by mixing powder V70, EDAB, and HA chemical components with ethanol into the polymer. Mixtures were injected into steel molds and allowed to cure overnight at 37°C. . . . . 45
- 3.2  $^1\text{H}$  NMR of POC (A) as compared to mPOC (B) with molecular structure inlays of both and electrospray ionization (ESI) data for POC (C) and mPOC(D). Peaks associated with glycidyl methacrylate are seen at 1.89, 2.67, 3.24, 3.96, 4.45, 5.68, and 6.07 ppm in the mPOC spectrum.  $^1\text{H}$  NMR spectrum of mPOC and POC were recorded using an automated Au400 spectrometer at ambient temperature, using DMSO-d6 as a solvent. Spectra were integrated by normalizing the citric acid region (2.78 ppm) to 4.00. For ESI, peak intensity corresponds to the relative number of macromolecules produced during ESI whereas the peak number corresponds to the molecular weight of the macromolecule. Structures of macromolecules verified through ESI are noted in Figure 3.3. ESI additionally verifies that methacrylate groups attach to POC (D) as noted by the increase in molecular weights corresponding to an attachment of methacrylate groups. . . . . 50
- 3.3 Chemical structures and exact masses of POC and mPOC as verified in ESI data (Figure 3.2C-D). Citric acid units are noted in black, 1,8-octanediol units in blue, and glycidyl methacrylate units in red. . . . . 52
- 3.4 FT-IR of POC (A) and mPOC-xHA (B) shows growth of peaks associated with hydrogen phosphate at  $470\text{ cm}^{-1}$  indicating presence of hydroxyapatite (HA). Peaks at  $1717\text{ cm}^{-1}$  represent the C=O bonds of carbonyl groups,  $1164\text{ cm}^{-1}$  for C-O-R bonds of ester groups, and  $1027\text{ cm}^{-1}$  for C-OH stretching. . . . . 53
- 3.5 Heat evolution during polymerization for mPOC, mPOC-xHA, and PMMA composites over time. Data points were acquired via a K-type thermocouple inserted into a Teflon Exothermic Heat Mold (ASTM F451-08). PMMA and mPOC maximum temperatures fall above the temperature threshold for the onset of thermal tissue necrosis, whereas addition of HA lowers the overall polymerization temperature. This is hypothesized to be due either to the decreased amount of polymer used in the mPOC-xHA composites, or HA suppressing the heat generated during polymerization. . . . . 54

- 3.6 Representative rheological characterization of mPOC (A) as compared to mPOC-20HA (B), mPOC-40HA (C), and mPOC-60 (D) confirms that all formulations maintain thermoresponsive behavior. Increasing HA amount in mPOC results in decreased time until gel point occurs. Data was acquired using a Modular Compact Rheometer 302e with a 20 mm parallel plate. Temperature was held at 37°C while a time sweep at an oscillatory frequency of 10 rad/s and magnitude of 0.5% strain was applied. The gel point is characterized by an increase of storage modulus ( $G'$ ) over loss modulus ( $G''$ ). . . . . 55
- 4.1 (A) Cell cytotoxicity to extracts after 24 hours of exposure. MC3T3 cells were seeded at a density of 10,000 cells per well and maintained in culture for 24 hours before being exposed to composite extracts (n of 4). Composite extracts were collected after 3 days of incubation in complete medium at 37°C. After 24 hours of exposure, an MTT assay was performed to determine viability of cells. mPOC-60HA performed best and was equivalent to the viability seen in the control group (complete media). (B) Cell proliferation on composite scaffolds over 1, 3, and 7 days. MC3T3 cells were seeded at 6,000 cells/well directly onto sterilized composite scaffolds (n of 4). A CCK8 assay was performed at days 1, 3, and 7 to assess cell proliferation over time. All composites present an initial decrease in cell proliferation at 24 hours, likely due to attachment issues to the scaffolds during seeding. Subsequent days for mPOC-xHA and PMMA show that cells proliferate over time. (C) LIVE/DEAD staining of cell proliferation on composite scaffolds at 1- and 7-days post seeding. Cell response was poor on mPOC scaffolds at both 1 and 7 days, whereas all other groups show visible, live (green) cell attachment. Some scaffold staining can be seen in the mPOC-40HA 1-day sample (red). By 7 days, cells have spread into and across all mPOC-xHA scaffolds. . . . . 66

- 4.2 (A) Scanning electron microscopy (SEM) images of composite surfaces with (7 Day) and without cell attachment. Scale bars are in white in the lower left-hand corner of individual images and denote 100  $\mu\text{m}$ . Clear cell attachment can be seen on mPOC-xHA composite surfaces, especially within and over the pores present on the surface. Pores in mPOC and mPOC-xHA form due to the release of nitrogen gas during free radical polymerization of azo initiators. PMMA surfaces show sheets of cell coverage, reminiscent of a fibrous encapsulation response commonly seen in a foreign body reaction. (B) Colour SEM image of mPOC-40HA surface after 7 days of cell attachment. Cells (light green) and nuclei (dark green) are seen spreading across the composite surface (dark blue) and across pores. Salt deposits (pink) are from residual media. It is hypothesized that cell proliferation (orange) is occurring along stretched cells. Scale bar (white) in lower right-hand corner corresponds to 10  $\mu\text{m}$ . (C) Colour SEM image of mPOC-20HA surface after 7 days of cell attachment. Cells (light green) and nuclei (dark green) are seen spreading across the composite surface (blue). Microvilli (pink) from cells act to stretch across surfaces and assist in cell movement. Scale bar (white) in lower right-hand corner corresponds to 1  $\mu\text{m}$ . . . . . 69
- 5.1 Representative Masson's Trichrome (MT) images from *in vivo* subcutaneous injection study of the sample-tissue interface. mPOC-xHA injections show collagen infiltration (green) at both 1 day and 4 weeks, whereas mPOC samples show thin tissue around the injection site at 1 day and a large immune response (dark red/purple) at 4 weeks. PMMA samples show a thin subcutaneous tissue region around samples at day 1, due in part to difficulty during sectioning. PMMA at 4 weeks shows a distinct collagenous capsule around the implant, indicative of the fibrous encapsulation seen as part of the body's foreign body response. Alternatively, mPOC-xHA shows integration of collagen into the material itself and has broken off parts of the material as seen in mPOC-60HA. Initial images are scaled at 100  $\mu\text{m}$  (white) and inset images at 20  $\mu\text{m}$  (black) whereas the sample position is indicated by yellow arrow. . . . . 79

- 5.2 Immunohistochemistry staining for CD68 (A) and  $\alpha$ -SMA-CD31 co-stain (B). (A) CD68 (stained red) has an apparent higher density of positively stained cells at the interface between the tissue and material (material position noted by green arrows). Some staining of the material occurred in mPOC-xHA containing polymers, but otherwise the presence of CD68 positive cells visibly decreased at the 4-week time point for mPOC-xHA polymers and PMMA. mPOC at 4 weeks shows a large increase in CD68 expression. (B) Vessels (stained red/brown) can be clearly seen within the tissue-material connective tissue interface of mPOC and mPOC-xHA composite polymers (black arrows) whereas minimal vessel presence can be seen in the thin interface of PMMA samples. Analysis for (C) CD68 and (D)  $\alpha$ -SMA-CD31 immunohistochemistry staining where  $*p < 0.05$  and  $**p < 0.01$ . (C) CD68 positive staining was analyzed within the subcutaneous tissue region where the polymers were injected. The percent of CD68 expressed is normalized to the total amount of cells present within the subcutaneous region. mPOC-xHA and PMMA composites show significantly decreased expression of CD68 by the 4-week time point, with mPOC-60HA and PMMA presenting similar data. (D) Number of vessels per  $\text{mm}^2$  was analyzed within the connective tissue region of the material-tissue interface. mPOC-60HA has significantly increased vessel density compared to mPOC-40HA, potentially due to the increased presence of HA. . . . . 80
- 6.1 Sawbones® individual composite L3 vertebrae with 10 pounds per cubic foot (0.16 g/cc) density solid foam cancellous- polyurethane core (product #3429-3-2). Dimensions are a) 48 mm, b) 35 mm, and c) 11 mm. Pedicle height is 16 mm. . . . . 97
- 6.2 Flowchart of the necessary experiments and data required for FDA approval of a substantially equivalent Class II Device. . . . . 100
- A.1  $^1\text{H}$  NMR spectra of mPOC synthesized with imidazole. Imidazole (inset structure) is not completely removed from the mPOC after synthesis and purification as seen by the highlighted (blue) peaks present at 7.73 and 7.16 ppm. These aromatic groups are unnecessary within the purified mPOC structure, thus further purification steps and a reworking of the mPOC synthesis were pursued to obtain an optimized mPOC. . . . . 113



- A.2 <sup>1</sup>H NMR spectra of POC washed in THF or ethanol. During the original synthesis of POC, the polymer is dissolved in ethanol before distilling the polymer in DI water. While the use of ethanol in this step does not impact the use of POC for further applications, it can affect further synthesis steps for mPOC. As such, ethanol was replaced by THF as THF is the primary solvent used during mPOC synthesis, resulting in distinct peaks at 3.59 and 1.75 ppm for the POC-THF workup. Ethanol peaks can be seen at 3.44 and 1.05 ppm. . . . . 114
- A.3 <sup>1</sup>H NMR spectra of mPOC with either imidazole or DMAP used as the ring-opening catalyst during mPOC synthesis. <sup>1</sup>H NMR spectra of both imidazole mPOC and DMAP mPOC are similar, except for the presence of aromatic groups associated with imidazole at 7.73 ppm and DMAP at 8.20 and 7.05 ppm. Using DMAP was hypothesized to increase the efficiency of attachment of methacrylate groups to the POC structure, potentially decreasing the amount of synthesis time. . 115
- A.4 <sup>1</sup>H NMR spectra of mPOC with DMAP used as the ring-opening catalyst during synthesis carried out for 24, 72, or 168 hours. It was hypothesized that letting the synthesis run for extended periods of time would increase the amount of methacrylate groups added to the POC structure. The change in synthesis times was also hypothesized to have effects on the mechanics and cytotoxicity of cured mPOC composites. Of note, the <sup>1</sup>H NMR spectra shows distinct separation of the peaks associated with citric acid (blue highlight) which may indicate that the hydrogen atoms are in more stable environments after 72 hours of synthesis. These data also show that further synthesis past 72 hours is unnecessary, as the <sup>1</sup>H NMR spectra between 72 and 168 hours are nearly identical. . . . . 116
- A.5 ESI data for mPOC synthesized with (A) imidazole for 6 hours, (B) DMAP for 6 hours, (C) DMAP for 24 hours, and (D) DMAP for 72 hours. Trace amounts of imidazole and DMAP can be seen in the 6-hour syntheses (A-B), noted by the molecular weights of 353.2 Daltons and 265.1 Daltons. Synthesis over 24 hours eliminates these trace compounds and greatly increases the size, occurrence, and variety of mPOC macromolecules (C). Synthesis over 72 hours (D) shows that one distinct structure of mPOC is likely to occur over other structures, namely a tri-1,8-octanediol – tri-citric acid – tri-glycidyl methacrylate (E). Moving forward from this data, mPOC synthesis time was increased from 6 hours to 24 hours for all subsequent polymer syntheses. . . . . 117

- A.6  $^1\text{H}$  NMR spectra of mPOC using non-distilled THF and distilled THF as a polymer solvent. It was noted that BHT, a trace component of THF, was found in the  $^1\text{H}$  NMR spectra of mPOC. In an effort to purify mPOC as much as possible, THF was distilled and used as an alternative solvent during mPOC synthesis. Using distilled THF showed a reduction of BHT within the  $^1\text{H}$  NMR spectra (blue highlight) noted at 1.36 ppm. . . . . 118
- A.7 ESI data for mPOC ran through chromatography with non-distilled THF (A) and distilled THF (B). The occurrence of macromolecules differs slightly between these samples, with non-distilled THF (A) resulting in primarily a 1034.53 Dalton macromolecule (C) and distilled THF (B) resulting in primarily an 892.47 Dalton macromolecule (C). Sodium adducts are noted within the ESI spectrum by an increase in macromolecule size of 23 Daltons. . . . . 119
- A.8 ESI data for a new molar synthesis of POC (A) and mPOC (B). Typical molar ratio between 1,8-octanediol and citric acid are 1:1. This figure instead shows ESI data for a 1.2:1 ratio, which aimed to attach more 1,8-octanediol groups to the overall macromolecule structure. (A) POC ESI data shows primarily a tri-1,8-octanediol – di-citric acid structure weighing 750.40 Daltons (C). Sodium adducts are noted within this spectrum by an increase in macromolecule size of 23 Daltons. (B) Primary structure of mPOC is a tri-1,8-octanediol – tri-citric acid – diglycidyl methacrylate weighing 1207.95 Daltons (C). Increasing the amount of 1,8-octanediol compared to citric acid did increase the likelihood of POC macromolecules containing more units of 1,8-octanediol, but this was not seen in mPOC structures. Adjusting the ratio may have more precedent in POC applications over mPOC applications. . . . . 120

- A.9 (A) *In vitro* cell cytotoxicity study comparing mPOC composites cured with no solvent, ethyl acetate as the solvent, or ethanol as the solvent. L929 murine fibroblasts (passage 7) were seeded onto 96-well plates at 10,000 cells/well and allowed to attach and grow for 24 hours. Cells were exposed to various extract concentrations and allowed to incubate over 24 hours, then an MTT assay was performed to determine viability. Viability decreases for all groups as the extract concentration increases, though ethanol samples performed the best. Ethanol was chosen as the solvent utilized in mPOC polymerization moving forward. (B) *In vitro* cell cytotoxicity study comparing mPOC composites cured at various time points. L929 murine fibroblasts (passage 7) were seeded onto 96-well plates at 10,000 cells/well and allowed to attach and grow for 24 hours. Cells were exposed to various extract concentrations and allowed to incubate over 24 hours, then an MTT assay was performed to determine viability. Viability remains above minimum viability levels (above 80%) for all extract concentrations and cure times. . . . . 121
- A.10 (A) Molecular structures for simvastatin, lovastatin, and pravastatin. (B) *In vitro* cell cytotoxicity study comparing statins at various concentrations. L929 murine fibroblasts (passage 7) were seeded onto 96-well plates at 10,000 cells/well and allowed to attach and grow for 24 hours. Cells were exposed to various statin concentrations and allowed to incubate over 24 hours, then an MTT assay was performed to determine viability. Cytotoxicity is noted in both simvastatin and lovastatin at 10  $\mu\text{M}$ . This concentration was not further pursued. . . . . 125
- A.11 *In vitro* cell cytotoxicity study comparing statins at various concentrations and with various cell types. (A) HUVECs (passage 4) were seeded onto 96-well plates at 3,000 cells/well and allowed to attach and grow for 24 hours. Cells were exposed to various statin concentrations and allowed to incubate over 24 hours and 72 hours, then an MTT assay was performed to determine viability where  $*p < 0.05$ . Pravastatin presented a significant decrease in cell viability at day 3, so concentrations between 0 and 0.1  $\mu\text{M}$  were chosen for an additional cell viability study in HUVECs. (B) hMSCs (passage 1) were seeded onto 96-well plates at 5,000 cells/well and allowed to attach and grow for 24 hours. Cells were exposed to various statin concentrations and allowed to incubate over 24 hours and 72 hours, then an MTT assay was performed to determine viability where  $*p < 0.05$ . (C) Comparison of statins at concentrations between 0 and 0.1  $\mu\text{M}$ . HUVECs (passage 4) were seeded onto 96-well plates at 3,000 cells/well and allowed to attach and grow for 24 hours. Cells were exposed to various statin concentrations and allowed to incubate over 24 hours and 72 hours, then an MTT assay was performed to determine viability where  $*p < 0.05$ . Given all statins and concentrations fell above 80% viability, concentrations of up to 0.1  $\mu\text{M}$  were utilized for osteogenic cell studies. . . . . 127

- A.12 (A) Alkaline Phosphatase (ALP) expression at 5 and 10 days for control groups and statin experimental groups. Statistical significance between 5 and 10 days for each group are represented where  $*p < 0.05$  and  $**p < 0.01$ . Statins groups show statistically equivalent ALP expression at 10 days compared to negative controls, indicating that the statins do not promote early osteogenic expression. (B) ALP standard curve to determine ALP activity where  $y=4,375,468.57x-72,316.14$  and  $R^2=0.98$  for the fit linear regression. (C) Alizarin red staining of hMSCs after 21 days exposure to either simvastatin, lovastatin, or pravastatin of various concentrations. No calcium deposits are seen in any experimental group, whereas positive cells that were cultured in osteogenic media contain calcium deposits (red). Cell density remains consistent between groups. Scale bar inset is 100  $\mu\text{m}$ . . . . . 128
- A.13 *In vitro* cell cytotoxicity study for various concentrations of chemical components and free radical polymerization initiators. L929 murine fibroblasts (passage 7) were seeded onto 96-well plates at 6000 cells/well and allowed to attach and grow for 24 hours. Each chemical component was mixed into media at concentrations of 0.1, 0.5, 1, 5, and 10  $\mu\text{M}$ , filtered, and applied to cells for a 24-hour period following ISO 10993. Media was then aspirated, and 1mg/mL MTT solution was added into wells and allowed to react for 4 hours. MTT solution was removed, particulates were dissolved in DMSO to produce a colour change, and plates were read at 570nm. Viability is calculated as the average absorbance of experimental groups divided by the average absorbance of control groups, multiplied by 100 to obtain a percentage. . . . . 129
- A.14 (A) Immunohistochemistry staining for osteopontin (OPN) and (B) quantitative analysis. (A) OPN (red) was qualitatively noted at a higher occurrence in mPOC-60HA samples, verified through quantitative analysis (B) where OPN expression in mPOC-60HA is statistically significant compared to other experimental groups. Additional, extended *in vivo* models should be carried out in a bone defect model to verify the expression of bone marker cells in response to mPOC-xHA composites over controls. Scale bars are set at 100  $\mu\text{m}$  and  $**p < 0.01$ . . . . . 131

## LIST OF TABLES

2.1	Management options for vertebral compression fractures including the type of medical intervention, its treatments, and its disadvantages. . . . .	33
2.2	Chemical Components of PMMA . . . . .	36
2.3	Kyphon Activos 10 Chemical Composition . . . . .	37
3.1	Summary of Formulation Compositions . . . . .	46
3.2	Doughing Time, Maximum Temperature, and Setting Time . . . . .	53
3.3	Comparative statistical significance ( $*p < 0.05$ and $**p < 0.01$ against mPOC) for rheological characterization (Figure 3.5) . . . . .	56
3.4	Summary of mechanical, swelling, and mass loss characteristics of mPOC, mPOC-xHA, and PMMA. . . . .	56
3.5	Comparative statistical significance ( $*p < 0.05$ and $**p < 0.01$ ) for compressive strength data (Table 3.4). . . . .	57
4.1	pH of extracts over 72 hours for cell cytotoxicity study (Figure 4.1) . . . . .	67
4.2	Comparative statistical significance ( $*p < 0.05$ and $**p < 0.01$ ) for cell cytotoxicity data (Figure 4.1). . . . .	67
4.3	Comparative statistical significance ( $*p < 0.05$ and $**p < 0.01$ ) for cell proliferation data. No statistical significance was observed for mPOC or mPOC-40HA in subtable (b) and are thus not reported. . . . .	68

5.1	Comparative statistical analysis of CD68 expression in positively stained cells using student's t-test to compare pairs of means where $*p < 0.05$ and $**p < 0.01$ . No statistical significance was observed between groups at the 1-day time point in (a) and is thus not reported. . . . .	81
5.2	Comparative statistical analysis of vessel data using student's t-test to compare pairs of means. Statistical comparison of number of vessels per $\text{mm}^2$ between different material composites where $*p < 0.05$ . . . . .	82
6.1	RIPA Solution Composition . . . . .	88
6.2	Quote from Innoved Institute, LLC for Osteoporotic Vertebrae . . . . .	96
A.1	Summary of mechanical characteristics of various synthesis conditions for mPOC. Statistical significance is not calculated for this table given that the n number differs between groups. . . . .	112
A.2	Comparative statistical analysis of <i>in vitro</i> cell cytotoxicity for different solvents used in mPOC polymerization using student's t-test to compare pairs of means where $*p < 0.05$ and $**p < 0.01$ . . . . .	122
A.3	Comparative statistical analysis of <i>in vitro</i> cell cytotoxicity for cure times for mPOC polymerization using student's t-test to compare pairs of means where $*p < 0.05$ and $**p < 0.01$ . 12.5% and 48-Hr tables showed no significance between groups and are thus not reported. . . . .	123
A.4	Comparative statistical analysis of <i>in vitro</i> cell cytotoxicity for statins (Figure SA.10B) at different concentrations using student's t-test to compare pairs of means where $*p < 0.05$ and $**p < 0.01$ . Pravastatin did not have any statistical significance between groups and is thus not reported here. . . . .	126
A.5	Comparative statistical analysis of <i>in vitro</i> cell cytotoxicity for various concentrations of chemical components and free radical polymerization initiators using student's t-test to compare pairs of means where $*p < 0.05$ and $**p < 0.01$ . No statistical significance was seen for (a) 0.1 and 0.5 $\mu\text{M}$ or (b) V70, GMA, and EDAB so are not reported here. . . . .	130

## CHAPTER 1

### OVERVIEW

#### 1.1 Motivation

Reconstructive surgery at the musculoskeletal level is, and will always, pose a prevalent need. Whether this need arises from simple injury, more complex prognoses, or standard aging modalities, biomaterials that effectively treat and stabilize said injuries are necessary. The goal of most approved biomaterials for musculoskeletal applications aim to treat injuries by offering a permanent implant that replaces damaged sections or fixes them together, allowing the body to naturally heal the injury with a stable support. Throughout the field of biomaterials, new disciplines have emerged in the forms of tissue engineering and regenerative engineering, which revolves around designing functional biomaterials that replaces, regenerates, and restores tissue function<sup>5,6</sup>.

The concept and eventual goal of this thesis came about from a trip to the Museum of Science and Industry (MSI). I had started my second year and had been posed with the task of figuring out how the polymer that is addressed in my work could be effectively used as an alternative method to sutures in rotator cuff surgeries. I was less than thrilled about this, mostly because I believed the mechanics of the polymer would not be effective under tensile stress. But the MSI has this amazing section on the human body, and within it a section on the field of biomaterials. There I saw the use of bone cement to treat a fractured vertebra, and it clicked that I could use my polymer in this compressive system.

Injuries involving the vertebrae can be treated a number of ways, none of which are incredibly ideal. The ones involving surgical intervention leave patients with permanent implants. The

driving force of my work was to develop an alternative bone cement that would mimic one of the standard treatments for vertebral body fractures but offer the benefits of regeneration. Therefore, a bone cement that offers stability, minimizes inflammation, and slowly degrades and promotes regeneration was developed.

## 1.2 Thesis Outline

Chapter 2 provides an overview of bone remodeling, what happens when remodeling goes awry, and the medical interventions used to treat fractures that occur in the vertebrae. The history of bone cements and the clinical use of PMMA is presented leading into the precedent of using POC as a base for developing an alternative bone cement. Chapter 3 explores the chemistry and characterization of mPOC and its composites. We show successful methacrylation of POC into a thermoresponsive polymer compatible with the setting times and mechanical needs of standard bone cements. Chapter 4 utilizes the lessons learned from Chapter 3 and tests the materials in a murine bone cell line. The use of HA at higher percentages in the polymer network show better cell cytotoxicity, proliferation, and attachment responses, so composites containing 40 and 60% HA were chosen as the best variants to pursue. In Chapter 5 we perform an *in vivo* experiment to show that HA improves the foreign body response to levels comparable to the clinical standard, PMMA. Chapter 6 discusses the significance of this work as well as future experiments and directions. The Appendices address the large amount of tinkering required to make this project as successful as possible. This work provides an exciting polymer system with a novel polymerization reaction that mimics standard PMMA reaction mechanics, but with good handling characteristics, tunable mechanics, and equivalent biocompatibility for use as an alternative bone cement for orthopedic applications.



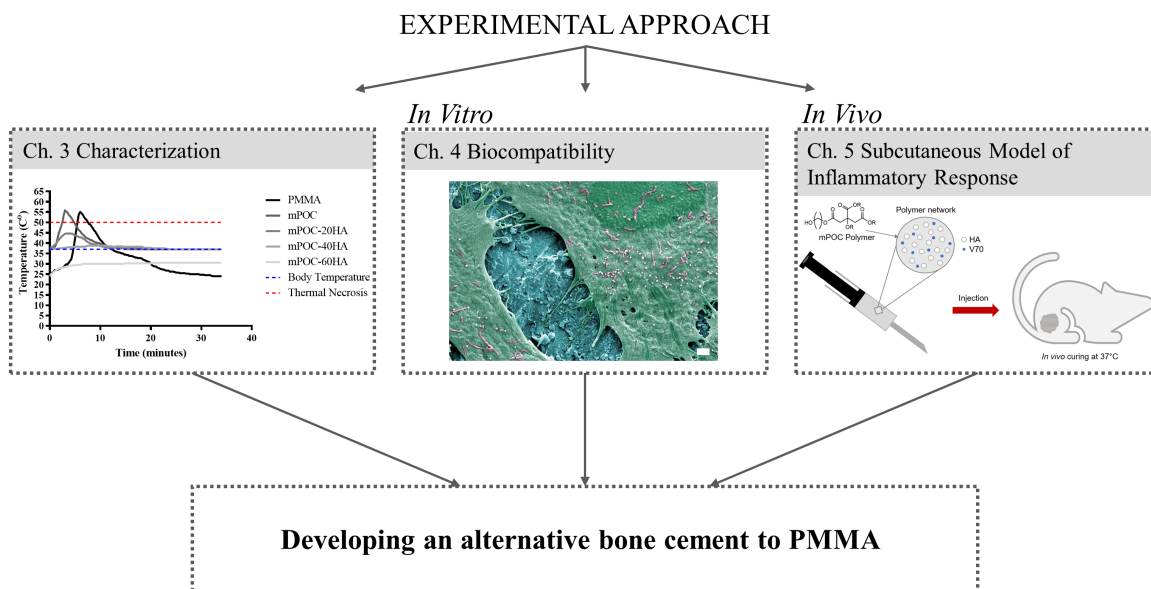


Figure 1.1: Schematic of the thesis outline.

### 1.3 Specific Aims

*Aim 1. To engineer an injectable, heat responsive CBB. a) Investigate three HA concentrations of mPOC on their heat evolution, setting times, rheology, mechanics, swelling, and degradation. (b) confirm all mPOC composites maintain cell viability, proliferation, and attachment compared to the clinical control PMMA.*

*Aim 2. Evaluate mPOC-composite capacity to reduce inflammation in a rat model. Select the optimum variants from Aim 1 and conduct a pilot experiment to assess the inflammatory response in a rat model, following by histological and immunohistochemical staining.*

## CHAPTER 2

### BACKGROUND

#### 2.1 Bone

##### 2.1.1 Bone Remodeling

Bone is a highly vascularized and innervated organ that is largely made up of proteins and minerals. The organic matrix is composed of around 90% Type I collagen and 5% citrate, providing tensile strength and elasticity to the structure. The inorganic component of bone is primarily made up of hydroxyapatite (HA),  $\text{Ca}_5(\text{PO}_4)_3(\text{OH})$  or  $\text{Ca}_{10}(\text{PO}_4)_6(\text{OH})_2$ , the mineral form of calcium apatite resulting in up to 50% by volume and 70% by weight of bone in the body<sup>7</sup>. Additionally, many cell types, blood vessels, small molecules, and cytokines make up, maintain, and regenerate each type of bone tissue, classified as either cortical or trabecular bone. Cortical bone is dense, highly mineralized tissue found on the periphery of bone that is necessary for the structural integrity of bone. Trabecular bone conversely is highly porous and found on the interior of bone, providing elasticity and a plethora of other cells and parts needed for bone functions such as acid/base regulation and calcium homeostasis<sup>8</sup>. Importantly, there are 4 cell types that help mediate bone remodeling: structural bone lining cells and osteocytes, bone-forming osteoblasts, and bone-resorbing osteoclasts. The balance between osteoblasts and osteoclasts determines the overturn of old bone into new and is an important factor in various bone-related diseases.

Bone remodeling as a whole happens in three stages: resorption, reversal, and formation. Supporting these stages are the osteocytes and bone lining cells. Osteocytes are differentiated cells derived from osteoblasts that have become encased in the mineral matrix of bone. Bone lining

cells communicate with the osteocytes to promote the differentiation of hematopoietic stem cells into osteoclasts, which initiates the first stage of bone remodeling<sup>9</sup>. During resorption, which takes place over 10 days, osteoclasts dissolve the mineralized portion of bone by secreting hydrochloric acid and then degrade the protein portion of the bony matrix by secreting proteolytic enzymes<sup>10</sup>. Following resorption, the reversal phase oversees macrophage-like cells preparing the surface for new osteoblasts. During formation, osteoblast precursors are recruited from mesenchymal stem cells (MSCs) to proliferate and differentiate into osteoblasts which actively secrete nonmineralized osteoid at the location of newly formed bone. This osteoid matrix is made up of type 1 collagen, which will mineralize as osteoblasts, convert to osteocytes, or go through apoptosis<sup>8,11,12</sup>.

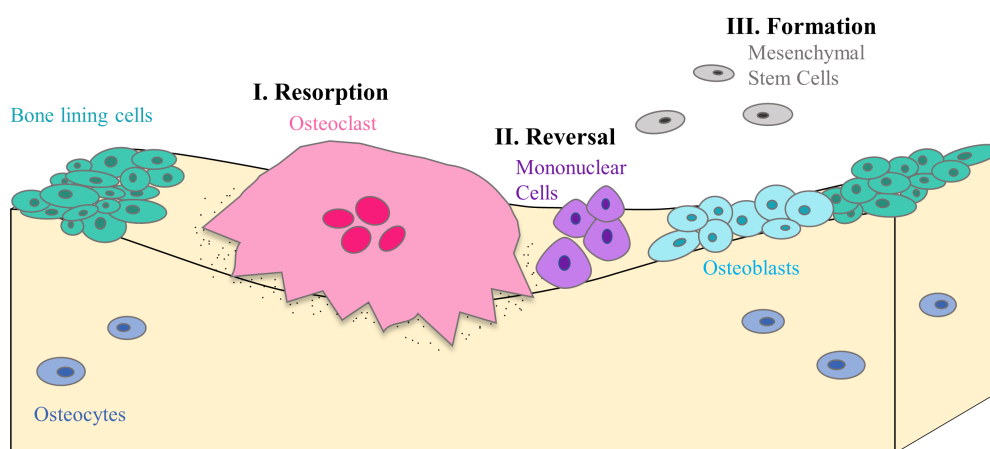


Figure 2.1: The three stages of bone remodeling: resorption, reversal, and formation. During resorption, osteoclasts dissolve the bone matrix by secreting hydrochloric acid. Reversal oversees mononuclear cells preparing the exposed surface for new osteoblasts. Lastly, osteoblast precursors are recruited and differentiated into osteoblasts to form new bone during formation.

Typically, bone remodeling is an equivalent exchange between osteoclasts and osteoblasts.

Where one dissolves bone, the other lays down new bone so that the structure maintains the same near constant size, volume, and strength. One of the most common bone diseases, osteoporosis, results from an imbalance between this resorption and formation. Due to excessive bone resorption, which can be caused by a number of physiological occurrences such as lack of estrogen, calcium deficiency, and changing biochemical pathways, the bone matrix becomes weakened resulting in an increased risk of bone fractures. This loss of bone mineral density occurs throughout the body, though this thesis is framed around the bone that makes up the vertebral column.

### **2.1.2 Fractures and Medical Interventions**

Osteoporosis is the most common condition associated with vertebral compression fractures (VCFs), with 30-50% of individuals over 50 affected resulting in an annual occurrence of 1.5 million VCFs and an annual cost of 750 million dollars<sup>13-15</sup>. These VCFs are typically compression fractures or wedge fractures that are characterized by the collapse of a vertebral body segment. Up to 75% of these fractures are found in the thoracolumbar junction with an additional 30% present in the L2-L5 region<sup>16</sup>. Presence of a VCF is commonly associated with an increased risk of future fractures, especially in adjoining vertebral segments<sup>17</sup>. These fractures additionally can cause sudden back pain and loss of function, and if left unmanaged could result in chronic pain, chronic spinal deformity leading to kyphosis, loss of mobility, pulmonary and gastrointestinal complications, and depression<sup>18-20</sup>. Management options for VCFs include nonsurgical management, spinal fusion, vertebroplasty (VP), and kyphoplasty (KP). Nonsurgical management involves pain medication, bracing, and physical therapy, with issues arising in the forms of cardiac complications, deep vein thrombosis, and urinary tract infections. Spinal fusion involves bone grafting of either autografts (a patient's own bone), allografts (donor bone), or synthetic options with additional plates, screws, and rods to fuse vertebrae together. This requires an open surgery in the area around the spinal

cord which can result in complications of infection, nerve damage, and pseudarthrosis. VP and KP are similar procedures that involve injecting bone cement into a fractured vertebrae to stabilize it. Complications from this can include infection, additional fractures over time, and cement leakage<sup>21</sup>. While all options are available and up to a patient's decision, VP showed a statistically significant reduction of both morbidity and mortality compared to nonsurgical management. The current use of the nondegradable bone cement poly (methyl methacrylate) (PMMA) in VP/KP presents an exciting opportunity to address the development of alternative, degradable bone cements for ideal VCF treatment<sup>22</sup>.

Table 2.1: Management options for vertebral compression fractures including the type of medical intervention, its treatments, and its disadvantages.

<b>Medical Intervention</b>	<b>Treatment</b>	<b>Disadvantages</b>
Nonsurgical Management	Pain medication, bracing, physical therapy	Cardiac complications, deep vein thrombosis, urinary tract infections
Spinal Fusion	Bone grafting (autograft, allograft, or synthetic) to fuse vertebrae with plate, screw, and rod fixation	Infection, nerve damage, pseudarthrosis, decreased mobility
Vertebroplasty/Kypoplasty	Injection of bone cement into vertebrae	Infection, additional fractures, cement leakage

### 2.1.3 Bone Cement

PMMA is one of the earliest bone cements and was produced in 1936 by happy occurrence upon noting that mixing PMMA powder with its monomer methyl methacrylate (MMA) created a dough that was moldable and easily manipulated<sup>23</sup>. Since then, many bone cements have been developed and tested both *in vitro* and *in vivo* to pursue various properties necessary for different bone tissue engineering applications. For VCFs requiring VP/KP, bone cements ideally have good handling

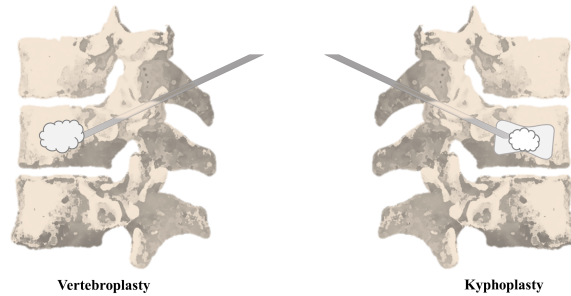


Figure 2.2: Schematic for vertebroplasty (VP) and kyphoplasty (KP). VP involves directly injecting bone cement into a fractured vertebral segment to stabilize the fracture. KP begins by introducing a balloon catheter into the fractured vertebrae, expanding the balloon to the vertebrae's original height, and then filling the created cavity with bone cement.

characteristics, are easily injectable, have low curing temperatures, have high radiopacity, have mechanical properties similar to native bone upon setting, are nontoxic, and present excellent biocompatibility, osteoconductivity, osteoinductivity, and bioactivity<sup>24</sup>. Bone cements loosely fall into two categories, acrylic-based cements and biodegradable cements, which will be expanded upon here and in the following section addressing PMMA (an acrylic-based cement).

Biodegradable cements are commonly based around bioactive ceramics and bioactive glasses due to their similarity in composition to the mineral phase of bone. Calcium phosphate was initially studied during the 1980s regarding its solubility but was found to produce HA as a product and was capable of self-setting<sup>25</sup>. This led to approval by the FDA during the following decade for use in craniofacial defects and bone fractures<sup>26,27</sup>. Calcium phosphate cements (CPCs) can be composed of a variety of calcium-based components with popular options being HA, tricalcium phosphate (TCP,  $\text{Ca}_3(\text{PO}_4)_2$ ), and dicalcium phosphate dihydrate (DCPD,  $\text{CaHPO}_4 \cdot 2\text{H}_2\text{O}$ ), and are distinguished by their end hydration products: apatite or brushite<sup>28</sup>. Commercially available

options include Norian SRS (a brushite CPC) and BoneSource (an apatite CPC) which are used for craniofacial applications. Unfortunately, CPCs have inferior injectability, short setting times, low mechanical strengths, and run the risk of forming biofilms, limiting their use as bone cements for VP/KP<sup>29</sup>. In the case of Norian XR, a radiopaque, injectable bone cement intended for VP/KP that has since been discontinued, escape of this CPC cement into the surrounding blood stream caused immediate clotting in the lungs and heart leading to death<sup>30</sup>.

Therefore, polymeric materials have been more recently popularized when designing biodegradable cements. The skeletal system has differing mechanical necessities depending on whether the bones are under compressive, tensile, or rotational forces, so polymeric materials with synthetically tunable structures can specifically be created for each individual system. For example, as demonstrated in this work, the synthesis and introduction of composite materials can be modified to address mechanical requirements, as well as the other many requirements needed for ideal bone cements. Research has primarily expanded upon utilizing PMMA given its FDA approval, with clinically available cements for VP/KP including KyphX HV-R, Kyphon Activos 10, and Symphony VR Radiopaque<sup>24</sup>. While these products have been approved for use, PMMA as a base component poses many potential issues as discussed next.

## **2.2 PMMA**

PMMA is an acrylic-based cement that was initially used during the 1950s in dentistry as a cement or grout to enhance implant fixation. Later it was utilized in total hip replacement to secure the acetabular and femoral components of an implant to bone and distribute the mechanical forces accordingly throughout the implant interface<sup>31</sup>. Use of PMMA was approved by the FDA in the 1970s for use in hip and knee prosthetic fixation. Clinically used PMMA is formed by mixing a powdered MMA styrene co-polymer and a liquid MMA monomer together, which allows the

liquid monomer to polymerize around the pre-polymerized powder to form the hardened PMMA. Other chemical components found in PMMA commercially are listed in Table 2.2. Mixing the liquid and powder monomer components of PMMA together will initiate a physical change resulting in a tacky paste. The addition of benzoyl peroxide and subsequent accelerators allows the PMMA to form at room temperature via peroxide-based free radical polymerization, a polymerization method by which the polymer forms by a successive addition of free radical building blocks via cleavage of carbon double-bonds to single bonds<sup>32,33</sup>.

Table 2.2: Chemical Components of PMMA

<b>Component</b>	<b>Role</b>
<i>Powder Components</i>	
PMMA	Polymer Frame
Zirconium dioxide/Barium sulphate	Radiopacifiers
Gentamycin	Antibiotic
<i>Liquid Components</i>	
MMA	Monomer
N,N-dimethyl-p-toluidine (DMPT)	Accelerator
Benzoyl Peroxide	Initiator
Hydroquinone	Stabilizer/Inhibitor

Adapted from Webb et. al.<sup>3</sup>

PMMA polymerization is a highly exothermic reaction, producing heat *in vivo* up to 56°C and in some cases up to 90°C<sup>34</sup>. This high temperature output is one of the inherent disadvantages of PMMA. Not only does the onset of tissue necrosis initiate at sustained temperatures above 50°C, but the extreme temperature cases could also potentially volatilize unreacted monomers, creating pockets of unreacted MMA monomers within the polymer network that could lead to mechanical failure<sup>32</sup>. Additionally PMMA lacks direct adhesion to and degradation within the bone cavity, eliminating any regeneration of the surrounding bone or removal of the material overtime



Table 2.3: Kyphon Activos 10 Chemical Composition

<b>Component</b>	<b>Amount</b>
<i>Powder Components</i>	
PMMA	64.4%
Barium sulphate	25%
Hydroxyapatite	10%
Benzoyl Peroxide	0.6%
<i>Liquid Components</i>	
MMA	97.6%
N,N-dimethyl-p-toluidine (DMPT)	2.4%
Hydroquinone	20 ppm

Adapted from Kyphon Activos 10 (Medtronic) User Manual

and creating a weak tissue/material interface that could result in fracture<sup>35</sup>. Cement leakage after application can infiltrate the adjacent tissue or enter into the circulatory system (similar to the case of Norian XR) causing systemic toxicity or potentially fatal pulmonary or cardiac embolisms<sup>2,36-38</sup>. PMMA also has a higher compressive strength compared to native bone, resulting in non-uniform load distributions between surfaces that in part has resulted in the failure of KP procedures and fractures of both the cement/bone interface and adjacent vertebrae within a minimum of 3 months when utilizing PMMA<sup>39-41</sup>. Given that PMMA is the only clinically available bone cement for orthopedic applications and its many inherent issues, there is a need for alternative bone cements with improved handling, biocompatibility, and mechanical characteristics.

Recently, additive materials have been incorporated into PMMA to lower this high exothermic potential, while additionally addressing its disadvantageous bioactivity and mechanical mismatch. Nanocomposite materials containing chitosan and graphene oxide have been found to lower the polymerization temperature of PMMA by 10°C, gelatin modified PMMA has shown reduced compressive mechanical properties, and HA modified PMMA has shown modular mechanics while decreasing exothermic temperatures<sup>42-45</sup>. While incorporating additives into PMMA may adjust

its polymerization reaction, ultimate compressive characteristics, and biological integration, the redesign of bone cements as a whole to more closely match physiological bone may be more advantageous.

### **2.3 Citrate-Based Biomaterials**

Citrate-based biomaterials (CBBs) have shown promise for bone tissue engineering applications due to its incorporation of citric acid and HA within its polymer network<sup>4,46</sup>. The chemical derivative of citric acid, citrate, comprises about 5% of the organic material of bone but was also revealed to play a key role in bone remodeling. Through nuclear magnetic resonance (NMR) spectroscopy, it was revealed that strongly bound citrate molecules stabilize the thickness of apatite nanocrystals towards ideal resorption rates and mechanical properties<sup>7,47</sup>. Citrate also was found to elevate metabolic activity of cellular energy to increase alkaline phosphatase production in early-stage osteogenic differentiation of human MSCs via citrate-specific membrane transporters<sup>48</sup>. The chemical structure of citric acid alone offers available pendant carboxyl and hydroxyl moieties that are ideal for integrating functionality into the polymer network. Incorporating HA, a large component of the mineral phase of bone, into the polymer matrix offers additional osteogenic attributes including biocompatibility, bioactivity, osteoconduction, osteointegration, and osteoinduction<sup>7,49</sup>.

The Ameer group has previously reported on the synthesis and characterization of poly(1,8-octanediol-co-citrate) (POC), a CBB that has been shown to have anti-inflammatory and antimicrobial characteristics<sup>50</sup>. POC created a framework for creating many composite materials used in tissue engineering applications such as cardiovascular, bone, muscle, cartilage, skin, nerve, and spinal cord applications<sup>46,51-55</sup>. Fortunately, POC has extensive research into its orthopedic applications, with POC being combined with HA, TCP, silica, and gallium bioglass<sup>46,56,57</sup>. These examples showcase POC's ability to be modified for a variety of needs, offering great precedent to

use it for a bone cement application.

POC is prepared via a polycondensation reaction in which equimolar amounts of citric acid and 1,8-octanediol are combined which can later be cured into a network of degradable ester crosslinks through thermal polycondensation<sup>58,59</sup>. The chemical structure of a monomer unit of POC is shown in Figure 2.3. Recently, the CBB Citregen™ has been fabricated into orthopedic fixation devices cleared for use in patients by the U. S. Food and Drug Administration (FDA) and is the first thermoset bioresorbable polymer for clinically used implantable devices<sup>4,60</sup>. While these POC and POC-HA composites have exciting characteristics for orthopedic tissue engineering, their previous iterations don't cover the requirements needed for a successful bone cement. As such, the POC prepolymer can be functionalized with vinyl or acrylate groups to create a secondary crosslinking mechanism that uses radical polymerization to form a solid<sup>59</sup>. We propose incorporating this additional synthesis step to introduce a chemical uniquely able to carry out the free radical polymerization step featured in PMMA polymerization.

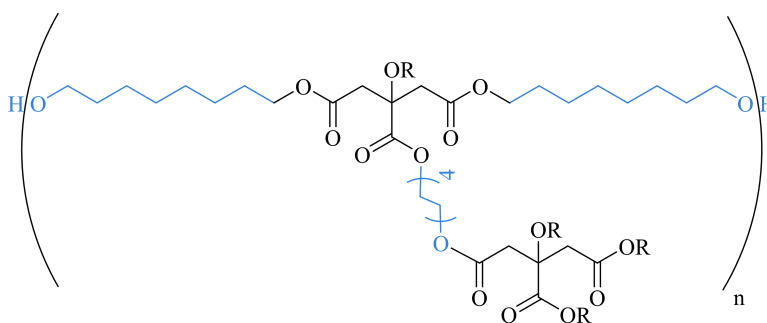


Figure 2.3: Chemical structure of a monomer unit of POC. Citrate moieties (black) confer antioxidant activity and are linked by 1,8-octanediol (blue).

## 2.4 V70

V70, 2,2'-azobis(4-methoxy-2,4-dimethylvaleronitrile), is an azo-based initiator that forms nitrogen gas and two carbon radicals when activated<sup>61</sup>. Where PMMA free radical polymerization is initiated through near immediate peroxide polymerization of benzoyl peroxide, producing CO<sub>2</sub> and oxygen radicals, V70 begins its azo polymerization upon reaching a temperature or light threshold. Since the bone cement would be actively used in an area not exposed to light, the temperature threshold to induce polymerization is key when choosing an azo compound. V70 interestingly has a temperature threshold of 30°C, slightly below the normal body temperature of 37°C. Integration of V70 into the polymer network of POC-HA would thus allow it to initiate polymerization once injected into the body.

Being able to integrate V70 into the polymer network of POC requires an additional synthesis step after the polycondensation of citric acid and 1,8-octanediol. This is due to the azo polymerization being based around access to vinyl bonds. Looking back at PMMA, the methacrylate group within its chemical network is what allows benzoyl peroxide to begin polymerization. Thus, incorporation of methacrylate groups into POC would add in the necessary vinyl groups. As such, we incorporated a ring opening compound, imidazole, and glycidyl methacrylate into a second synthesis step to attach methacrylate groups to POC. This resulted in a methacrylated POC, or mPOC. At this stage, mixing V70, HA, and the accelerator ethyl-4-(dimethylamino) benzoate (EDAB) into mPOC resulted in an injectable, thermoresponsive polymer that quickly cures at 37°C, a promising step towards developing an alternative bone cement. This polymer is further characterized, tested, and optimized within this thesis.



the concentration of local calcium ions to activate the proliferation of osteoblasts and promote the growth and differentiation of human mesenchymal stem cells toward an osteogenic line<sup>63</sup>. Incorporation of HA into polymeric scaffolds have seen success by combining the osteoconductive and osteoinductive HA into more mechanically stiff materials to promote osteoblast migration, attachment, and proliferation on scaffolds. The combination of both HA and citric acid, key components of natural bone, into the polymer developed and characterized in this thesis provided the necessary basis for a successful bone cement for orthopedic applications. Interestingly, HA had a significant effect on both the *in vitro* and *in vivo* response to scaffolds, as will be explored in Chapters 4 and 5.

## **CHAPTER 3**

### **POC SYNTHESIS AND CHARACTERIZATION**

#### **3.1 Objective**

Here, we will introduce the synthesis of mPOC as well as its composites where mPOC-xHA represents mPOC-20HA, mPOC-40HA, and mPOC-60HA. We will detail the chemistry and formulations used to prepare these materials and the characterization we used to confirm its intended product. Finally, we will present that these materials can maintain thermoresponsive, degradative, and consistent mechanical properties throughout all formulations.

#### **3.2 Experimental Section**

##### **3.2.1 Materials**

All chemicals were purchased from Sigma-Aldrich (St. Louis, MO) and used without further purification except when indicated otherwise. Kyphon Activos 10 bone cement (Medtronic, Memphis, TN) was acquired and utilized as a PMMA clinical standard of care reference.

##### **3.2.2 Synthesis Scheme of mPOC**

POC was prepared by polycondensation as reported in Yang et. al.<sup>50</sup>. Briefly, equimolar amounts of 1,8-octanediol and citric acid were combined in a round bottom flask and melted together under nitrogen atmosphere at 165°C with stirring at 100rpm for 20 minutes. The temperature was then decreased to 140°C and continued to mix for 72 minutes to obtain POC pre-polymer. Once cooled, the pre-polymer was dissolved in 50 mL of tetrahydrofuran (THF), poured into 500 mL of actively

vortexed Milli-Q water, and allowed to settle over one hour after vortex was removed. The supernatant was removed, the purified POC was poured into a separate bottle container, frozen at  $-80^{\circ}\text{C}$  for 30 minutes, and then lyophilized overnight.

POC was methacrylated by dissolving 66 g of POC in 540 mL of THF. After dissolution, the mixture was transferred to a round bottom flask where 2448 mg of imidazole was added, followed by drop-wise addition of 53.3 mL of glycidyl methacrylate. The mixture was stirred for 24 hours at  $60^{\circ}\text{C}$  with stirring at 500rpm. To enhance purification of mPOC, the polymer was run through liquid chromatography to strip off any unreacted monomers or aromatic groups from the bulk polymer structure. Briefly, silica gel was added to a funnel and covered with a filter under vacuum. Distilled THF was run through the setup, then the mPOC polymer, then distilled THF until 800-1000 mL of solvent was reached. The excess solvent was removed through rotary evaporation at  $30^{\circ}\text{C}$  on medium speed. The resulting mPOC was washed in a series of 10% ethanol-deionized (DI) water solutions, leached in DI water overnight, washed in a series of DI water solutions, frozen at  $-80^{\circ}\text{C}$  for 30 minutes, lyophilized overnight, and stored at  $-20^{\circ}\text{C}$ .

Cured mPOC and mPOC-xHA composites were achieved by sequentially mixing ethanol, ethyl 4-dimethylaminobenzoate (EDAB), HA nanopowder ( $<200\text{nm}$ ), and V70 with a vortex mixer to ensure even distribution. Weight percentages of components used to make the bulk material are featured in Table 3.1. Specifically, ethanol and EDAB were vortexed together until homogenous. Then V70 was added to mPOC and mixed, followed by addition of the ethanol/EDAB mixture, then HA to create the bulk polymer. Composites were either injected into a steel mold and allowed to cure at  $37^{\circ}\text{C}$  overnight or placed in a  $4^{\circ}\text{C}$  fridge until needed. Free radical polymerization was achieved once the polymer composites reached  $30^{\circ}\text{C}$ .



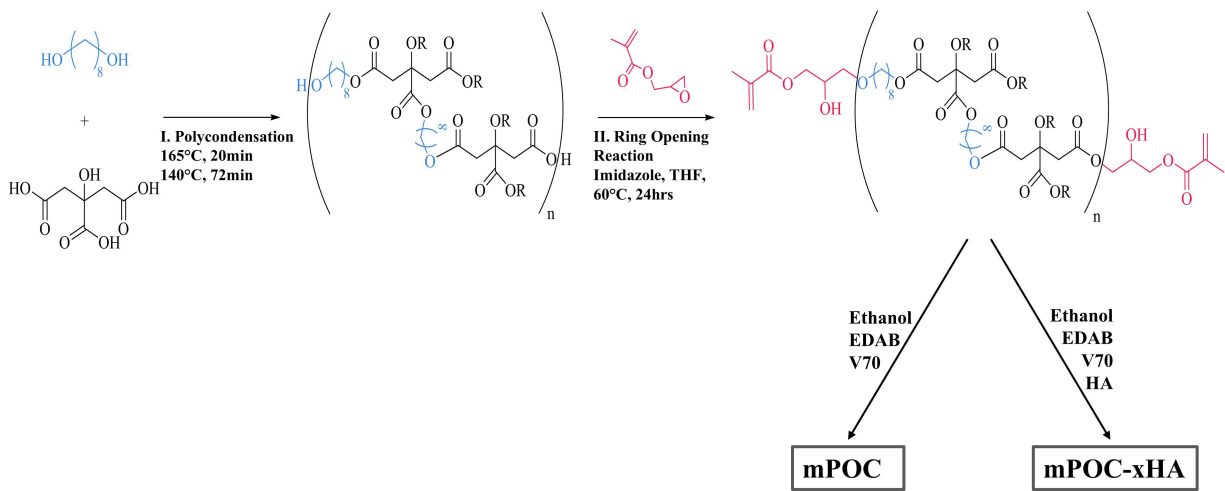


Figure 3.1: Synthetic scheme of mPOC syntheses. POC was prepared by polycondensation of 1,8-octanediol (blue) and citric acid (black) and subsequent ring opening polymerization to attach glycidyl methacrylate groups (red). mPOC and mPOC-xHA were prepared following the formulations outlined in Table 3.1 by mixing powder V70, EDAB, and HA chemical components with ethanol into the polymer. Mixtures were injected into steel molds and allowed to cure overnight at 37°C.

### 3.2.3 Nuclear Magnetic Resonance (NMR)

POC and mPOC spectra were confirmed using an Au400 nuclear magnetic resonance spectrometer (NMR, Agilent, Santa Clara, CA) at ambient temperature. 10-15 mg of each sample were first dissolved in 700 mL deuterated dimethyl sulfoxide (DMSO-d<sub>6</sub>) and run through NMR, then 100 µl of deuterium oxide (D<sub>2</sub>O, heavy water) was added and re-run through NMR. D<sub>2</sub>O allows exchangeable protons to exchange with the deuterium in D<sub>2</sub>O, which results in those protons disappearing from the NMR structure. DMSO-d<sub>6</sub> alone was used as a control reference.

### 3.2.4 Electrospray Ionization (ESI)

Potential chemical structures of POC and mPOC were verified through electrospray ionization (ESI, amaZon SL, Bruker, Billerica, MA). POC and mPOC polymers were prepared by dissolution

Table 3.1: Summary of Formulation Compositions

Formulation	Initiator wt. % (V70)	Accelerator wt. % (EDAB)	Hydroxyapatite wt. %	Ethanol wt. %
mPOC	1	2	0	5
mPOC-20HA	1	2	20	5
mPOC-40HA	2	2	40	5
mPOC-60HA	2	2	60	5

in methanol.

### 3.2.5 Fourier-Transform Infrared Spectroscopy (FT-IR)

HA integration into mPOC composites was confirmed using Fourier transform infrared (FT-IR, Nicolet Nexus 870 Spectrometer, Thermo Scientific, Waltham, MA) transmission spectra, recorded in attenuated total reflectance mode by accumulation of 32 scans with a resolution of  $8\text{ cm}^{-1}$ . Samples were prepared by cutting 1 mm discs from cured 12 mm tall, 6 mm diameter polymer composite columns.

### 3.2.6 Doughing and Setting Times

Doughing and setting times were recorded following ASTM F451-08. For doughing times, a timer was started at the onset of mixing the powder and liquid components of each material. All material doughing times (mPOC, mPOC-HA composites, and PMMA, n of 2) were recorded at  $23^{\circ}\text{C}$  with additional doughing times for mPOC and mPOC-HA composites recorded at  $37^{\circ}\text{C}$  given the thermal initiation of V70 around  $30^{\circ}\text{C}$ . Each material was probed with the clean region of a powder free lavender nitrile glove (Kimberly-Clark, Ref: 52818, Lot: BYO3332122) beginning at 1.5 minutes and repeated every 15 seconds until the material separated cleanly from the glove. Doughing times are reported to the nearest 15 seconds.

Setting times (n of 2) were determined from the continuous time versus temperature recording

noted in the thermal reaction characterization method. Setting time is denoted by Equation (1):

$$T_{\text{set}} = \frac{T_{\text{max}} + T_{\text{amb}}}{2} \quad (3.1)$$

Where  $T_{\text{max}}$  is the maximum temperature in °C and  $T_{\text{amb}}$  is the ambient temperature initially recorded within 1 minute of doughing time (approximately  $23 \pm 1^\circ\text{C}$  for PMMA and mPOC-60HA samples and  $37 \pm 1^\circ\text{C}$  for mPOC, mPOC-20HA, and mPOC-40HA samples). Setting times are reported to the nearest 5 seconds.

### 3.2.7 Thermal Reaction

The exothermic temperature of mPOC and mPOC-xHA during free radical polymerization was measured with a Thermocouple Data Logger (OMEGA Engineering, Stamford, CT) following ASTM F451-08. A K-type thermocouple was inserted into each material within one minute of its doughing time. PMMA samples were recorded at  $23^\circ\text{C}$  and allowed to return to its baseline temperature whereas mPOC and mPOC-HA composites were held at and returned to  $37^\circ\text{C}$ . The maximum temperatures are reported to the nearest  $1^\circ\text{C}$ .

### 3.2.8 Rheology

The gel point of mPOC and mPOC-xHA composites was measured using a Modular Compact Rheometer 302e (Anton Paar, Ashland, VA) with a 20 mm parallel plate (#999860) and solvent trap cover to minimize sample evaporation. The thermosetting mixtures were placed in a disposable aluminum dish attached to the temperature-controlled plate. The parallel plate was lowered until the measurement gap was 1 mm. The starting temperature of the materials was  $20^\circ\text{C}$  and the temperature of the Peltier plate was  $37^\circ\text{C}$ . The oscillatory program consisting of a time sweep at an oscillatory frequency of 10 rad/s and magnitude of 0.5% strain was used to monitor the viscosity

as the composites cured. The gel point was characterized by an increase of storage modulus ( $G'$ ) over loss modulus ( $G''$ ).

### 3.2.9 Swelling and Mass Loss

Swelling of mPOC and mPOC-xHA composites was assessed by incubating 12 mm tall, 6 mm diameter column samples in phosphate buffered saline (PBS) at 37°C for 24 hours. Samples were removed, blotted, weighed ( $W_{wet}$ ), and lyophilized for 72 hours to remove excess solvent. Samples were then weighed ( $W_{dry}$ ) and the swelling ratio was calculated using Equation 2:

$$\text{Swelling} = \frac{W_{wet}}{W_{dry}} \quad (3.2)$$

Mass loss of mPOC and mPOC-xHA composites was assessed by comparing the initial mass ( $W_0$ ) with the mass measured at a given time point ( $W_t$ ). Composites were incubated in PBS at 37°C for 14 days. At each time point, composites were removed, blotted, and weighed. After 14 days composites were additionally lyophilized and then weighed. Mass loss was calculated using Equation 3:

$$\text{Mass loss \%} = \frac{W_0 - W_t}{W_0} \cdot 100 \quad (3.3)$$

### 3.2.10 Mechanical Compression

The mechanical properties of mPOC and mPOC-xHA composites were determined using an MTS/Sintech 20/G universal testing machine (Eden Prairie, MN) with a 100 kN load cell. The compression tests were performed in accordance with the protocols described in ASTM F451-08. Briefly, 12 mm tall, 6 mm diameter cylindrical composites (n of 5) were compressed at a rate of 20 mm/minute.

The failure load was determined by the load at 2.0% offset along the deformation axis for PMMA samples and by the point of fracture for mPOC and mPOC-xHA composites after correcting for the compliance of the testing machine. Compressive strength was calculated as the failure load divided by the specimen cross sectional area and is reported to the nearest 1 MPa.

### **3.2.11 Statistical Analysis**

Statistical analysis was performed with Microsoft Excel software and GraphPad Prism 7.0 (GraphPad Software Ind., La Jolla, CA). Student's t-test was used to compare pairs of means and analysis of variance (ANOVA) with Bonferroni post-hoc analysis was used to compare means between multiple treatments. A p-value of 0.05 or less was considered to be statistically significant.

## **3.3 Results**

### **3.3.1 Characterization of POC**

Methacrylation of POC was confirmed by <sup>1</sup>H-NMR. Peaks present for mPOC at 6.06/5.72ppm, 4.47/4.45ppm, 3.95/3.91ppm, 3.26/3.24ppm, and 1.90ppm correspond to the peaks present in glycidyl methacrylate. The range of peaks in the region from 2.63-2.90ppm (peaks labeled 10 and 12) correspond primarily to the methylene protons from citric acid and potentially glycidyl methacrylate, which should have visible peaks at 2.81/2.86ppm. This may be due to the ring opening of glycidyl methacrylate and subsequent attachment to the bulk chemical structure during methacrylation. Peaks 1 through 8 are assigned to protons from 1,8-octanediol.

Ranges of potential POC and mPOC chemical structures and masses were verified through ESI. ESI is a technique used in mass spectrometry to produce ions using electrospray in which a high voltage is applied to a liquid to create an aerosol. This aerosol contains ions of macromolecules which are recorded as a mass value. This can then be used to determine the potential

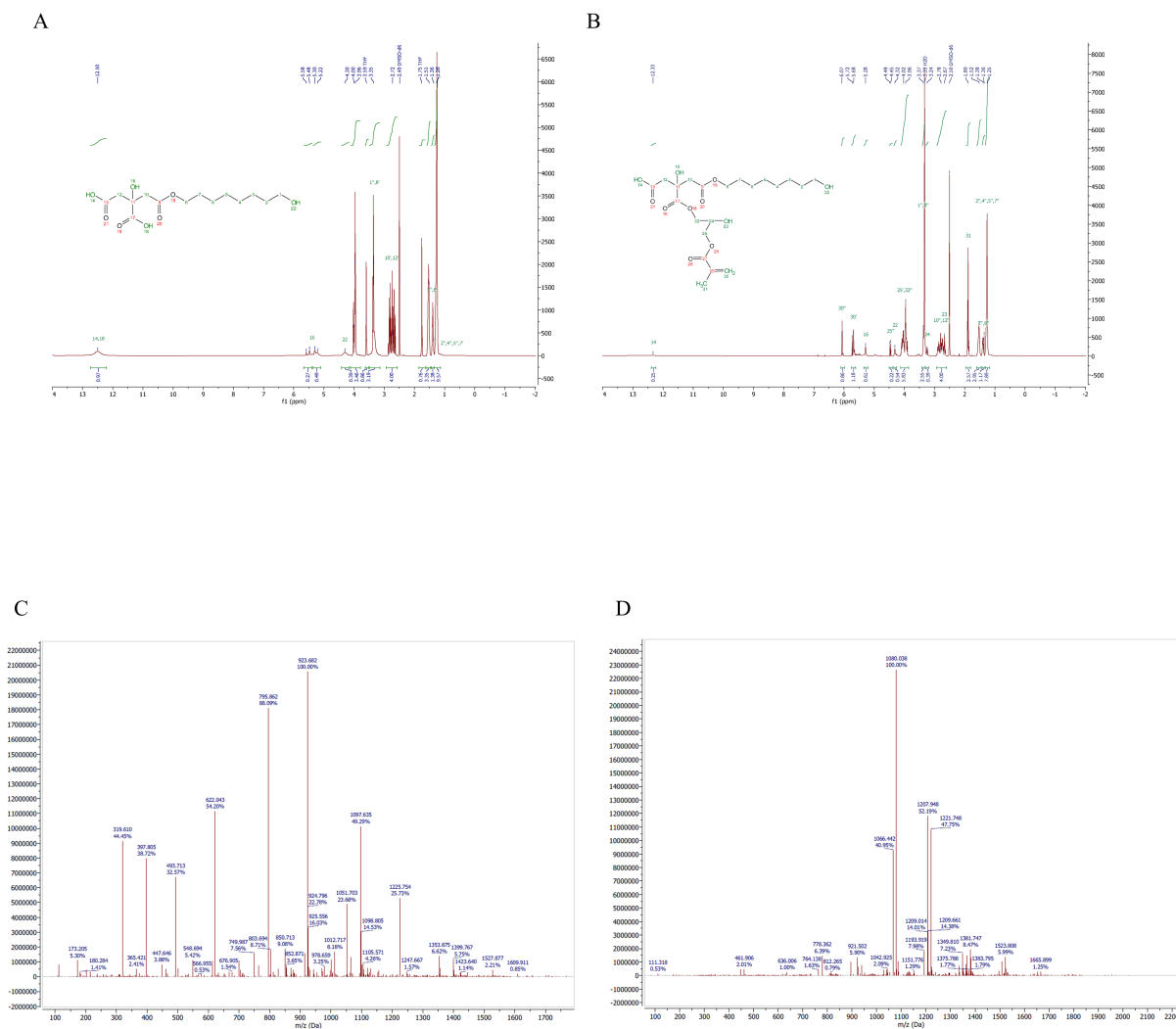


Figure 3.2:  $^1\text{H}$  NMR of POC (A) as compared to mPOC (B) with molecular structure inlays of both and electrospray ionization (ESI) data for POC (C) and mPOC(D). Peaks associated with glycidyl methacrylate are seen at 1.89, 2.67, 3.24, 3.96, 4.45, 5.68, and 6.07 ppm in the mPOC spectrum.  $^1\text{H}$  NMR spectrum of mPOC and POC were recorded using an automated Au400 spectrometer at ambient temperature, using DMSO- $d_6$  as a solvent. Spectra were integrated by normalizing the citric acid region (2.78 ppm) to 4.00. For ESI, peak intensity corresponds to the relative number of macromolecules produced during ESI whereas the peak number corresponds to the molecular weight of the macromolecule. Structures of macromolecules verified through ESI are noted in Figure 3.3. ESI additionally verifies that methacrylate groups attach to POC (D) as noted by the increase in molecular weights corresponding to an attachment of methacrylate groups.

chemical structures of the macromolecule. The signature peaks of 1,8-octanediol – citric acid, di-1,8-octanediol – citric acid, and di-1,8-octanediol – di-citric acid were easily identifiable, confirming the successful polycondensation of POC. Peaks of glycidyl methacrylate – tri-1,8-octanediol – di-citric acid and di-glycidyl methacrylate – tri-1,8-octanediol – di-citric acid were also identified, confirming methacrylation of mPOC. In the spectrum, major peaks were considered to make up most of the chemical structures present in the bulk polymers. As with any synthesis, the degree of integration varies resulting in a range of chemical structures. As such, the majority full monomer of mPOC appears have an exact mass of 1034.53 g/mol.

FT-IR characterization of mPOC-xHA shows successful integration of HA into the polymer network. The presence of the peak at  $1600\text{ cm}^{-1}$  in the mPOC spectrum corresponds to the methacrylate alkene, an indication of successful methacrylation of POC. Additionally, the peaks present at  $1000\text{-}1100\text{ cm}^{-1}$  and  $560\text{-}600\text{ cm}^{-1}$  represent the presence of  $(\text{PO}_4)^{-3}$  in mPOC-xHA composites, which are absent from the mPOC spectrum.

Doughing and setting times were variably affected by the addition of HA. Interestingly, mPOC-60HA composites cured at both  $23^\circ\text{C}$  and  $37^\circ\text{C}$  within a short amount of time from each other. All mPOC and mPOC-xHA formulations eventually reached the doughing phase at  $23^\circ\text{C}$  around 6 hours into the experiment. Conversely, mPOC, mPOC-20HA, and mPOC-40HA composites reached the doughing phase significantly sooner when incubated at  $37^\circ\text{C}$  (26, 34, and 25:15 minutes respectively) with mPOC-20HA composites requiring longer doughing times than mPOC alone. Conversely, mPOC-40HA and mPOC-60HA reached their doughing stages (25:15 and 14 minutes) before what was observed in mPOC (26 minutes). Compared to PMMA (12 minutes,  $23^\circ\text{C}$ ), the increased doughing times of mPOC, mPOC-20HA, and mPOC-40HA may prove advantageous in terms of handling and preparation of the cement. Once reaching the doughing stage, setting times quickly followed for each formulation resulting in times of 125, 100, 180, and 75

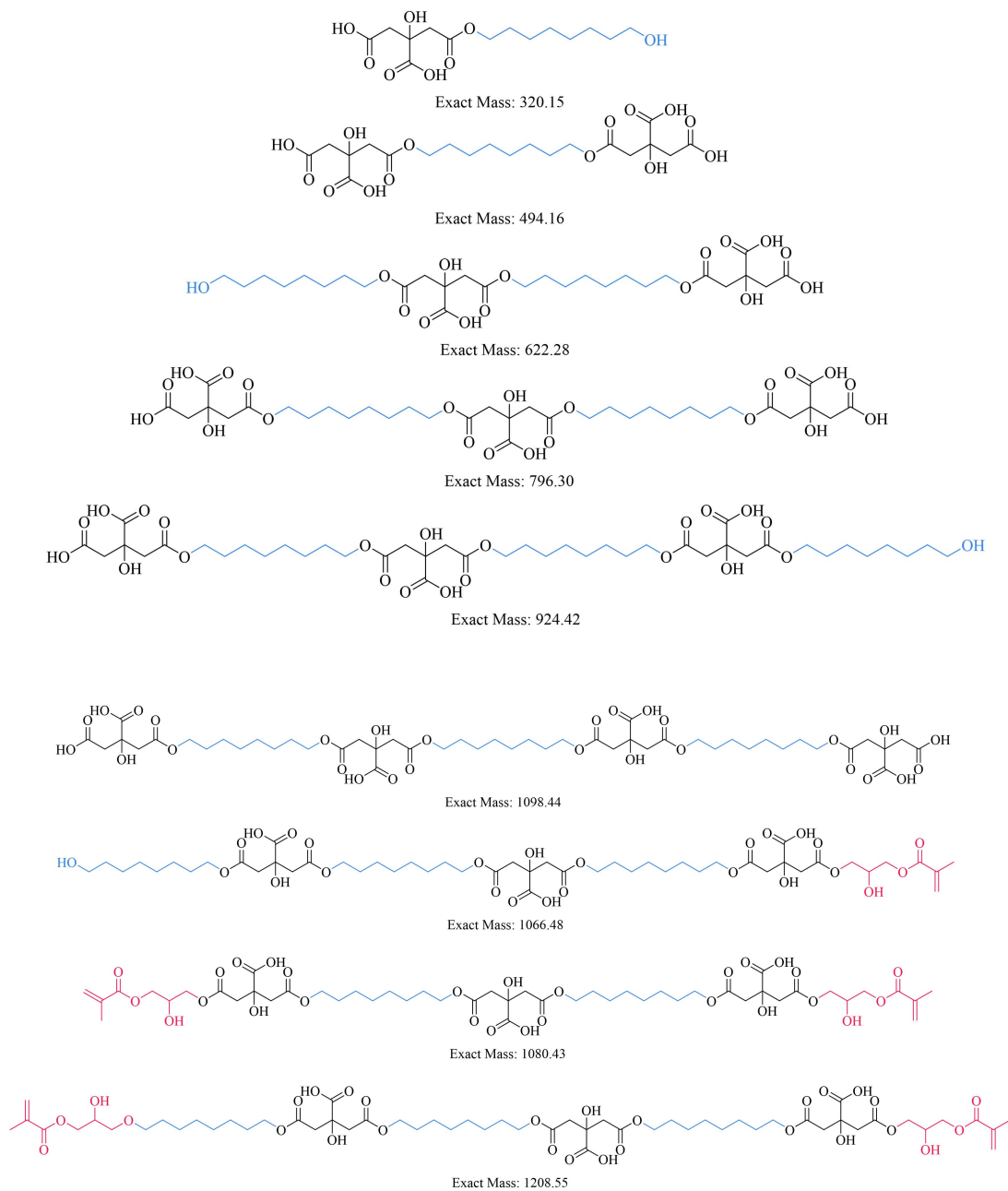


Figure 3.3: Chemical structures and exact masses of POC and mPOC as verified in ESI data (Figure 3.2C-D). Citric acid units are noted in black, 1,8-octanediol units in blue, and glycidyl methacrylate units in red.



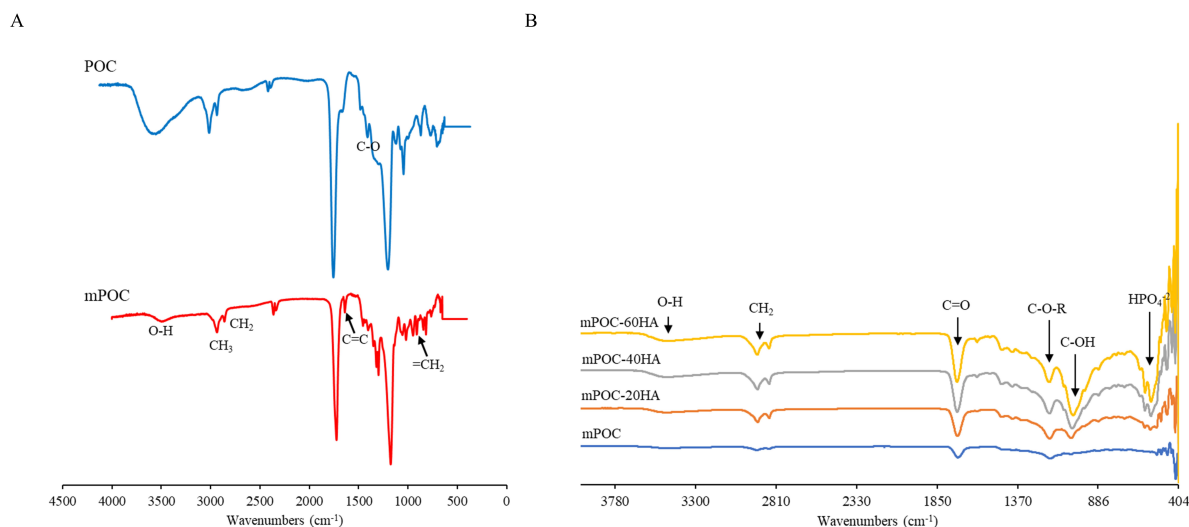


Figure 3.4: FT-IR of POC (A) and mPOC-xHA (B) shows growth of peaks associated with hydrogen phosphate at  $470\text{ cm}^{-1}$  indicating presence of hydroxyapatite (HA). Peaks at  $1717\text{ cm}^{-1}$  represent the C=O bonds of carbonyl groups,  $1164\text{ cm}^{-1}$  for C-O-R bonds of ester groups, and  $1027\text{ cm}^{-1}$  for C-OH stretching.

seconds to set for mPOC, mPOC-20HA, mPOC-40HA, and mPOC-60HA.

Table 3.2: Doughing Time, Maximum Temperature, and Setting Time

Formulation	Doughing Time at 23°C (minutes)	Doughing Time at 37°C (minutes)	Maximum Temperature (°C)	Setting Time (seconds)
mPOC	360	26	$56 \pm 1$	$125 \pm 5$
mPOC-20HA	360	$34 \pm 15$	$45 \pm 1$	$100 \pm 25$
mPOC-40HA	360	$25 : 15 \pm 15$	$39 \pm 0$	$180 \pm 25$
mPOC-60HA	$17 : 15 \pm 15$	$14 \pm 15$	$30 \pm 0$	$75 \pm 20$
PMMA	12	N/A	$55 \pm 3$	$290 \pm 5$

Incorporating HA into mPOC-xHA composites significantly decreased the maximum temperature during free radical polymerization as the percentage of HA went up. The clinical control PMMA was tested along with mPOC and mPOC-xHA composites. PMMA and mPOC were sim-

ilar, recording an average of 55°C and 56°C respectively. mPOC-xHA were recorded as 45°C, 39°C, and 30°C for 20, 40, and 60 percent formulations. mPOC-60HA remained consistently around 30°C, within the range of thermal initiation of V70.

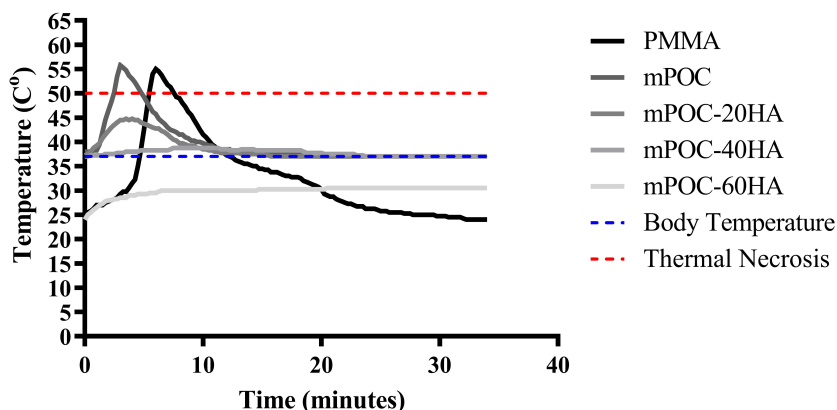


Figure 3.5: Heat evolution during polymerization for mPOC, mPOC-xHA, and PMMA composites over time. Data points were acquired via a K-type thermocouple inserted into a Teflon Exothermic Heat Mold (ASTM F451-08). PMMA and mPOC maximum temperatures fall above the temperature threshold for the onset of thermal tissue necrosis, whereas addition of HA lowers the overall polymerization temperature. This is hypothesized to be due either to the decreased amount of polymer used in the mPOC-xHA composites, or HA suppressing the heat generated during polymerization.

### 3.3.2 Rheology

After performing rheology, we find that each of the 4 formulations initiate free radical polymerization via V70 azo-based initiation at 37°C. The results show that as the HA content increases in each formulation, the time until gel point decreases. These gel points occur at 33.4, 24.9, 10.6, and 2.00 minutes for mPOC, mPOC-20HA, mPOC-40HA, and mPOC-60HA respectively. It is hypothesized that the decrease in time as HA content increases is due to the reduced mPOC-polymer component. Since there is less polymer present, it takes less time for the entirety of the cement to

polymerize.

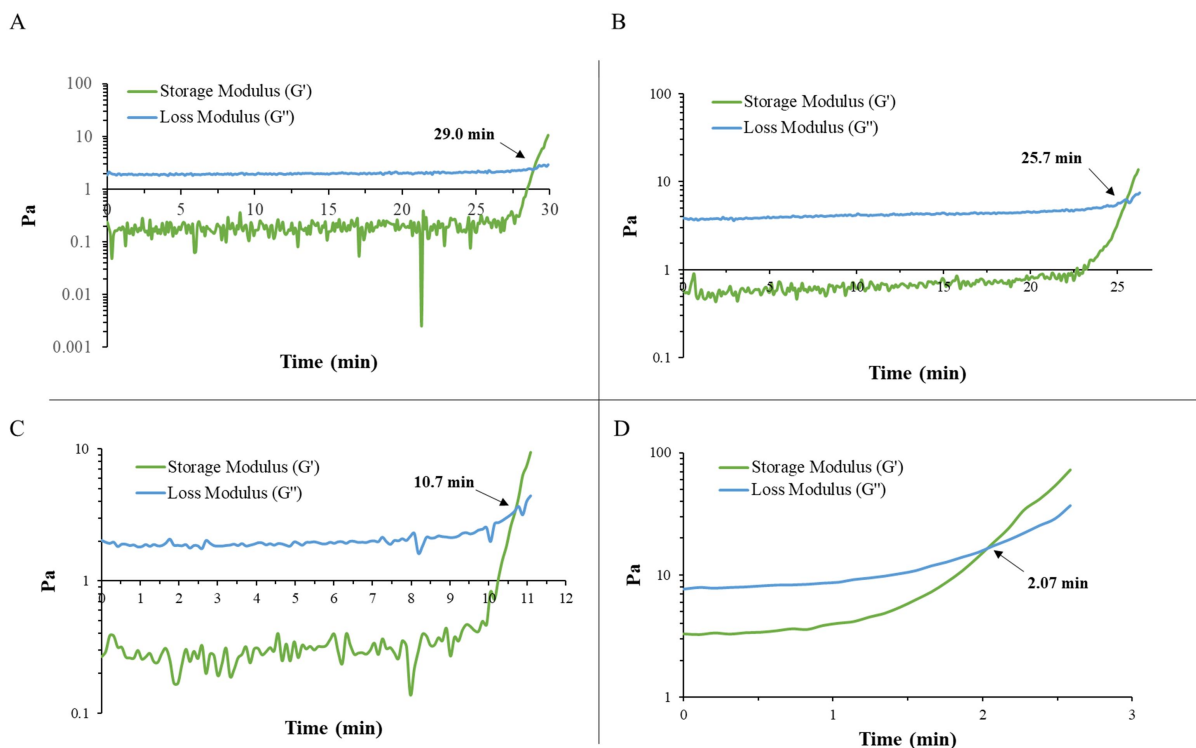


Figure 3.6: Representative rheological characterization of mPOC (A) as compared to mPOC-20HA (B), mPOC-40HA (C), and mPOC-60 (D) confirms that all formulations maintain thermoresponsive behavior. Increasing HA amount in mPOC results in decreased time until gel point occurs. Data was acquired using a Modular Compact Rheometer 302e with a 20 mm parallel plate. Temperature was held at 37°C while a time sweep at an oscillatory frequency of 10 rad/s and magnitude of 0.5% strain was applied. The gel point is characterized by an increase of storage modulus ( $G'$ ) over loss modulus ( $G''$ ).

For swelling and mass loss studies we find that increasing the amount of HA results in an apparent decrease in swelling and increase in mass loss. It can be observed that mPOC alone swells but does not hydrolyze as quickly as composites containing HA. It is hypothesized that HA potentially disrupts the polymer network during free radical polymerization creating a structure for easy infiltration of solvent. The decreased swelling of mPOC-xHA may be due to HA stabilizing

Table 3.3: Comparative statistical significance ( $*p < 0.05$  and  $**p < 0.01$  against mPOC) for rheological characterization (Figure 3.5)

<b>Formulation</b>	<b>Gel Point (minutes)</b>
mPOC	$33.4 \pm 10.3$
mPOC-20HA	$24.9 \pm 0.727$
mPOC-40HA	$10.6 \pm 0.690^*$
mPOC-60HA	$2.00 \pm 0.215^{**}$

the structure overall. It is hypothesized that HA remains in a stable state and orientation whereas mPOC takes on water and swells. The slow degradation and minimal swelling of mPOC-xHA may allow for integration of natural bone into the composites during remodeling. These properties are assisted by the design of mPOC-xHA, which contains both citric acid and HA that are naturally involved in apatite formation and bone remodeling<sup>47</sup>.

Table 3.4: Summary of mechanical, swelling, and mass loss characteristics of mPOC, mPOC-xHA, and PMMA.

<b>Formulation</b>	<b>Compressive Strength (MPa)</b>	<b>Swelling Ratio</b>	<b>Mass loss (%)</b>
mPOC	$18 \pm 7^{**}$	$1.06 \pm 0.00119$	$1.78 \pm 0.770$
mPOC-20HA	$19 \pm 2^{**}$	$1.05 \pm 0.00567$	$2.32 \pm 0.352$
mPOC-40HA	$35 \pm 3^{**}$	$1.04 \pm 0.000757^{**}$	$3.07 \pm 0.367^*$
mPOC-60HA	$25 \pm 4^{**}$	$1.03 \pm 0.00180^{**}$	$4.63 \pm 0.228^{**}$
PMMA	$48 \pm 3$	-	-

$**p < 0.01$  compared against PMMA clinical standard of care reference for ultimate compressive strength data

$*p < 0.05$  and  $**p < 0.01$  compared against mPOC for swelling and mass loss data

Table 3.5: Comparative statistical significance ( $*p < 0.05$  and  $**p < 0.01$ ) for compressive strength data (Table 3.4).

	mPOC	mPOC-20HA	mPOC-40HA	mPOC-60HA	PMMA
mPOC	-		**		**
mPOC-20HA		-	**	*	**
mPOC-40HA	**	**	-	**	**
mPOC-60HA		*	**	-	**
PMMA	**	**	**	**	-

### 3.3.3 Mechanical Compression

Mechanical compression of mPOC, mPOC-xHA, and PMMA show distinct differences given each formulation makeup. Including HA up to 40% of the total formulation increased the compressive strength of composites, whereas 60% composites decreased in compressive strength compared to 40% formulations. PMMA exhibited the highest compressive strength (48 MPa), significantly exceeding that of mPOC (18 MPa) and mPOC-xHA (19 MPa, 35 MPa, and 25 MPa for 20, 40, and 60HA). Where PMMA has a standard, controlled formulation, mPOC-xHA composites could allow for a modular framework. Different amounts of HA could be included into the polymer to closely match the mechanics of the necessary bone system, seamlessly integrating the bone cement into the body and reducing the chance of additional adjacent fractures.

## 3.4 Discussion

These data convey that we can successfully modify POC with methacrylate groups, allowing for further modification by way of thermoresponsive initiators. Notably, the addition of HA into the polymer formulations enhances the temperature output, gelling kinetics, and mechanics of this alternative bone cement providing a modular platform for specific orthopedic applications. The temperature output is of note as PMMA and mPOC produce temperatures that surpass the temper-

ature threshold for the onset of tissue necrosis (50°C). HA significantly decreases this temperature well below that threshold. The decrease in temperature as the HA percentage increased is hypothesized to be due to the decreasing amount of available polymerizable polymer. The reduced amount of polymer may produce the same reaction and heat generation, but since less of it is present it doesn't compound on itself and generate more heat. The HA included may also act as a protective physical mechanism to help suppress the heat generation as polymerization progresses. Szymanowski and coworkers saw similar results when comparing PMMA-based cements with the addition of HA micro- and nanoparticles<sup>64</sup>. They observed that an increased weight percentage of microparticle HA of up to 21% within the polymer matrix resulted in decreased polymerization temperatures. Notably, nanoparticle HA did not affect the polymerization temperature within their scaffolds. They propose that this is due to the availability of monomers trapped between HA particles; the larger microparticles limited interaction of monomers during polymerization, leading to an increased time for complete polymerization whereas nanoparticles did not limit this access at all. Conversely, nanoparticle HA seems to have a more pronounced effect on the exothermic characteristics of V70 mediated polymerization of mPOC, which may in part be explained by differences in molecular structures between PMMA and mPOC but would need to be verified by testing both micro- and nano-particle HA within this given polymer system.

mPOC-60HA was able to polymerize at both 23°C and 37°C. This is thought in part to be due to the reduced amount of polymer present in the composite (31% of the total mass) and any introduction of heat into the material as it is being mixed, either from heat produced from friction between HA and the polymer or from user/environmental heat, that would initiate V70. For the composites cured at 37°C, mPOC-20HA required a longer doughing time than mPOC alone, which follows similar trends found when testing various weight percentages of HA (0, 5, 10, and 15%) in PMMA<sup>44</sup>.

The gelling characteristics are also ideal as the materials can be kept below body temperature during handling (and ideally below 23°C given the ability of mPOC-60HA to polymerize at 23°C), whereas PMMA will polymerize upon mixing<sup>65</sup>. Inclusion of the thermal initiator V70 has advantage over similar self-setting polymeric bone cements such as PMMA due to its extended working time below physiological temperatures. Whereas PMMA-based cements rapidly initiate curing upon mixing resulting in working times between 10-20 minutes, our mPOC-20HA and mPOC-40HA composites remain in the liquid-phase below 30°C due to the temperature activation range of V70<sup>35</sup>. Self-setting materials that do not rely on benzoyl peroxide as an initiator also face similar working time windows, with amorphous magnesium phosphate/polyvinyl alcohol scaffolds curing within 10-15 minutes, poly propylene fumarate (PPF)-based cements curing within 5 minutes, and calcium sulfate/hydroxypropyl methylcellulose scaffolds curing within 12-21 minutes<sup>66-68</sup>. The increased working time of V70-based scaffolds allows them to be tailored to a patient's need, stored as a ready-to-use mixture under cold conditions, and brought up to temperature in a controlled environment for precise application. V70 allows mPOC-HA composites to begin polymerization at 37°C, with the time to transition into a solid matrix determined by the amount of HA introduced into the polymer matrix. Rheological assessment indicated that increasing the amount of HA from 20 to 60% into the mPOC-HA composites translates to significantly decreased curing times with reported average gel points being 33.4 minutes, 24.9 minutes, 10.6 minutes, and 2.00 minutes for mPOC, mPOC-20HA, mPOC-40HA, and mPOC-60HA respectively. The polymerization of the mPOC matrix may be facilitated due to the decreasing amount of polymer present. Additionally, it has been proposed that fillers that interact weakly within a polymer structure may inhibit reactive sites and reduce polymerization as seen with colloidal silica fillers in gels<sup>69-71</sup>. Since the increased HA reduced the overall polymerization time and impacted the gelation kinetics, it is thought that the HA interacts physically within the polymer network by way of coordinate bonds

between the carbonyl group and calcium from HA, and acts as a filler over any potential chemical interactions<sup>72</sup>. Being able to adequately control the viscosity and polymerization of the mPOC-HA composites during injection into a bone-void such as a vertebral segment may lower both the risk of cement extrusion into the spinal canal and adjacent musculature and escape of methylmethacrylate monomers as seen in the use of PMMA<sup>73</sup>.

Mechanical compression data suggests that the dispersion of HA within the polymer network likely describes the differences between mPOC, mPOC-20HA, and mPOC-40HA composites, as HA integrates within the microstructure to enhance compressive characteristics. Decreased compressive mechanics of mPOC-60HA could potentially be due to poor integration of the polymer network between and around HA particles, leading to pockets of unmixed polymer or due to the change in the pore structure formed as V70 polymerizes and releases nitrogen gas. The increase and then decrease in compressive mechanics between mPOC-40HA and mPOC-60HA may also be explained simply by surpassing the ideal packing level. Nanoparticles have been shown to improve the microstructure of concretes by filling the pores within the cement to increase its packing level, providing increased mechanics as the nanoparticle percentage increases<sup>74,75</sup>. William and coworkers similarly found that compressive strength in explanted vertebral bodies treated with PMMA and PMMA supplemented with HA decreased in groups treated with the 1g:3g (PMMA:HA) group compared to the 1g:1g and 1g:2g groups<sup>76</sup>. While the compressive mechanics of mPOC-40HA are promising, additional tensile testing would need to be evaluated as increasing HA concentration has been shown to decrease tensile and bending characteristics<sup>44</sup>. In terms of VP/KP applications, the vertebrae are primarily made up of trabecular bone which typically varies in strength from 0.1-30 MPa<sup>77</sup>. Additionally, osteoporotic vertebrae can be 20-30% weaker depending on the progression of the disease<sup>78</sup>. The mechanical compression data presented in this chapter shows that the compressive strength of PMMA (48 MPa) exceeds 1.5 times the typical strength of trabecu-



lar bone whereas mPOC, mPOC-20HA, and mPOC-60HA formulations fall within this range of typical vertebral trabecular bone, with mPOC-40HA falling slightly above this range.

### **3.5 Conclusion**

The work here sets up the studies presented in Chapters 4 and 5 which explore the biocompatibility of the polymer composites both *in vitro* and *in vivo*. It is essential that we were able to perform the characterization experiments featured in this chapter to ensure that we could successfully mimic a clinically relevant bone cement to more faithfully study and test a potential alternative. Excitingly, the developed bone cement already achieves several key characteristics that surpass the VP/KP clinical control PMMA tested alongside our composites. The modularity of the polymer itself underscores the inherent capacity of mPOC to be combined with a wide variety of chemical compounds, ceramics, and other natural materials to further match native bone.

## CHAPTER 4

### IN VITRO STUDIES OF CELLULAR RESPONSE

#### 4.1 Objective

Herein, we investigate the biocompatibility of the formulations prepared and characterized in Chapter 3 and ultimately choose the best variants to conduct a subsequent *in vivo* study. To do so, we culture MC3T3s in regular  $\alpha$ -MEM media, expose them either directly or indirectly to the formulated composites and clinical control, and evaluate their response both qualitatively and quantitatively to determine their susceptibility to each scaffold.

#### 4.2 Experimental Section

##### 4.2.1 Culture of Undifferentiated Cells

Murine pre-osteoblast MC3T3-E1 Subclone 14 (ATCC, Manassas, VA) cells were used for all studies in this work. MC3T3 cells were cultured in alpha Minimum Essential Medium ( $\alpha$ -MEM) supplemented with 10% fetal bovine serum (FBS) and 1% 10x penicillin-streptomycin. All MC3T3 cells used in these studies were at passage 12 or below. Cells were cultured at 37°C and 5% carbon dioxide (CO<sub>2</sub>).

##### 4.2.2 Cytotoxicity (MTT) Assay

MC3T3 cells were seeded onto sterile 96-well plates (10,000 cells/well) and maintained in culture for 24 hours to form a semi-confluent monolayer. Extracts of mPOC, mPOC-xHA, and PMMA were obtained by incubating cylindrical specimens (6 mm in diameter and 1 mm in height) in

complete medium for 72 hours at 37°C (ratio of medium to composites determined by calculating the total surface area of samples divided by 3 cm<sup>2</sup>). The pH of extract media was observed at 24, 48, and 72 hours. 100 µL of extracts were applied to cells (n of 4 per experimental extract/control) for 24 hours with the morphology of the cells checked with a light microscope before and after extract application.

After 24 hours, MTT solution was prepared from fresh MTT powder by dissolution in complete medium at a concentration of 1 mg/mL. The solution was sterilized by sterile filtration using syringe filters (pore size 0.2 µm). Extract medium was aspirated from wells and MTT solution (50 µL/well) was added. The plate was incubated at 37°C for 4 hours, then MTT solution was removed and 100 µL of DMSO was added to each well. After mixing, the contents of the wells were transferred to a fresh plate and the formazan formation was determined by detecting the absorption at 570 nm (reference 650 nm). The viability was calculated using the following equation, where OD<sub>570e</sub> is the mean value of the measured optical density (OD) of the various extract concentrations of the test sample and OD<sub>570b</sub> is the mean value of the measured OD of the positive controls (cells not exposed to extract).

$$\text{Viability \%} = \frac{100 \cdot OD_{570e}}{OD_{570b}} \quad (4.1)$$

#### 4.2.3 Proliferation (CCK8) Assay

Composite scaffold samples (6 mm diameter, 1 mm tall) consisting of mPOC, mPOC-xHA, and PMMA were sterilized by soaking in 70% ethanol for 30 minutes and then exposure to UV light for 1 hour. Samples were then washed and leached in PBS until a stable pH (7.4) was reached. MC3T3 cells were then seeded onto sterilized samples (n of 4) at 6000 cells/well and maintained in culture for up to 7 days.

For testing, media was aspirated from wells, a 10% Cell Counting Kit 8 (CCK8) (Dojindo Molecular Technologies, Inc., Rockville, MD) solution was prepared in media, and 110  $\mu\text{L}$  was added to wells. The solution was allowed to incubate for 4 hours, then removed from wells and read at an absorbance of 450 nm. Cell number was determined using a standard curve.

#### **4.2.4 LIVE/DEAD Assay**

LIVE/DEAD staining was performed in parallel with proliferation studies. Calcein AM was used as an indicator of live cells and ethidium homodimer-1 was used as an indicator of dead cells (Thermo Fisher Scientific, Waltham, MA). The staining solution was prepared by adding 2  $\mu\text{L}$  of calcein AM and ethidium homodimer-1 to 1 mL of  $\alpha$ -MEM media, scaling as necessary to the total amount needed. Scaffolds (n of 3) were transferred to a 12 well plate and enough staining solution was added to cover the samples. Samples were left to incubate in the dark at 37°C for 30 minutes, flipped over (scaffolds are opaque), and then imaged on a Nikon Eclipse TE-2000U fluorescence microscope. 2-3 images were taken per sample to qualitatively visualize cell status, attachment, and orientation.

#### **4.2.5 Scanning Electron Microscopy (SEM) Imaging**

SEM imaging was performed in parallel with proliferation and LIVE/DEAD studies. Samples were transferred to a 12 well plate, washed in sterile PBS, and fixed in 4% paraformaldehyde for 24 hours. Samples were then dehydrated in a series of ascending ethanol solutions: 50% for 10 minutes, 70% for 10 minutes, 80% for 10 minutes, 90% for 10 minutes, and 100% for 10 minutes. Samples were then exposed to hexamethyldisiloxane (HMDS) and further dried under vacuum.

Once dried, samples were sputter coated in 8 nm of gold/palladium and imaged at 5 kV on an EPIC SEM JEOL JSM-700FLV. Surfaces of control samples and cell attachment/morphology of

tested samples were imaged at a series of magnifications (60x, 200x, 500x, 1000x, and 5000x) for qualitative assessment.

#### **4.2.6 Statistical Analysis**

Statistical analysis was performed with Microsoft Excel software and GraphPad Prism 7.0 (GraphPad Software Ind., La Jolla, CA). Student's t-test was used to compare pairs of means and ANOVA with Bonferroni post-hoc analysis was used to compare means between multiple treatments. A p-value of 0.05 or less was considered to be statistically significant.

### **4.3 Results**

#### **4.3.1 HA increases cell viability**

According to the MTT assay, incorporation of HA into mPOC significantly improves viability in MC3T3 cells. Composites containing 60% HA present the best viability, equivalent to the control wells that contained cells exposed to regular media. The cellular response to PMMA is not statistically significant from mPOC-60HA but does fare better than mPOC-40HA. Readings for pH indicated that mPOC-60HA extract media remained equivalent to the pH reading for the control media (6.8), whereas other samples began decreasing the pH: 6.6 for PMMA, 6.4 for mPOC-40HA, 5.9 for mPOC-20HA, and 5.2 for mPOC.

#### **4.3.2 HA increases cell proliferation**

CCK8 data shows that HA improves proliferation of MC3T3 cells over time for all mPOC-xHA composites. Initially all tested samples lose cells, either to cell death or poor scaffold attachment, as seen by the noticeable reduction in cell number from the cell seeding state (6000 cells). All HA formulated samples and PMMA rebound after the initial cell loss compared to mPOC, which

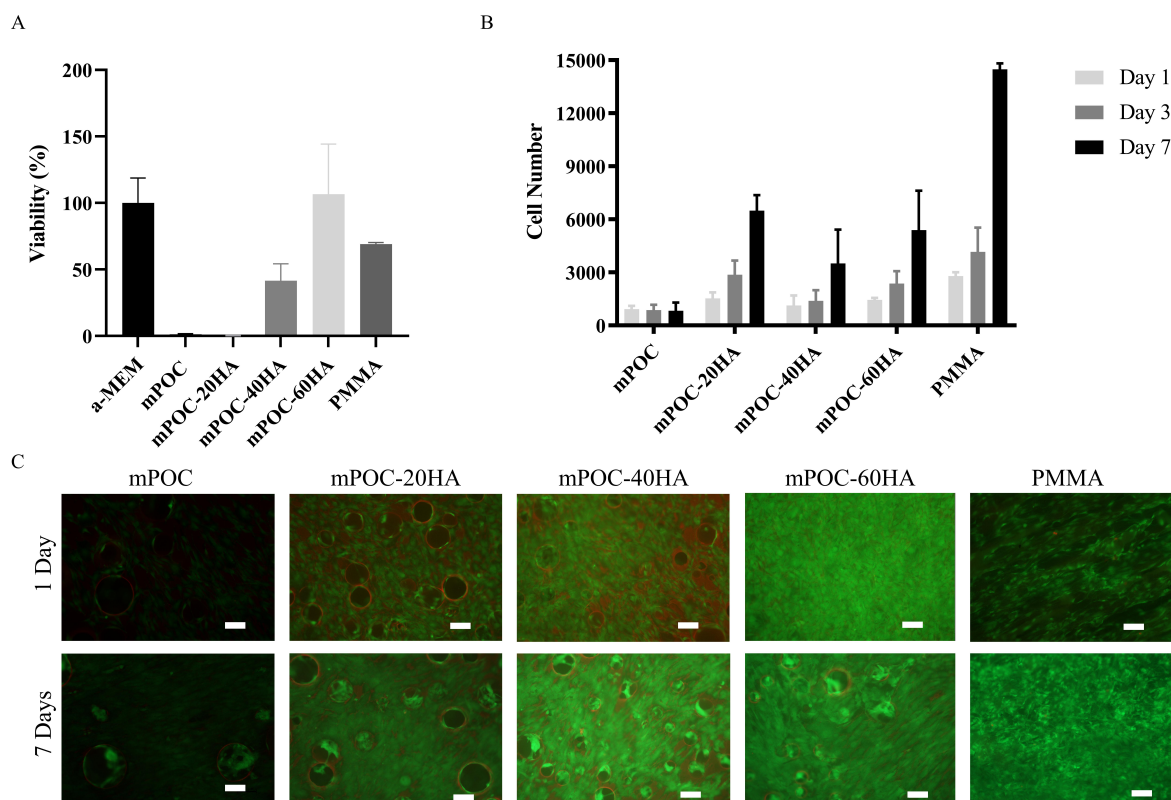


Figure 4.1: (A) Cell cytotoxicity to extracts after 24 hours of exposure. MC3T3 cells were seeded at a density of 10,000 cells per well and maintained in culture for 24 hours before being exposed to composite extracts (n of 4). Composite extracts were collected after 3 days of incubation in complete medium at 37°C. After 24 hours of exposure, an MTT assay was performed to determine viability of cells. mPOC-60HA performed best and was equivalent to the viability seen in the control group (complete media). (B) Cell proliferation on composite scaffolds over 1, 3, and 7 days. MC3T3 cells were seeded at 6,000 cells/well directly onto sterilized composite scaffolds (n of 4). A CCK8 assay was performed at days 1, 3, and 7 to assess cell proliferation over time. All composites present an initial decrease in cell proliferation at 24 hours, likely due to attachment issues to the scaffolds during seeding. Subsequent days for mPOC-xHA and PMMA show that cells proliferate over time. (C) LIVE/DEAD staining of cell proliferation on composite scaffolds at 1- and 7-days post seeding. Cell response was poor on mPOC scaffolds at both 1 and 7 days, whereas all other groups show visible, live (green) cell attachment. Some scaffold staining can be seen in the mPOC-40HA 1-day sample (red). By 7 days, cells have spread into and across all mPOC-xHA scaffolds.

Table 4.1: pH of extracts over 72 hours for cell cytotoxicity study (Figure 4.1)

Experimental Group	pH: 0h	24h	48h	72h
$\alpha$ -MEM	6.8	6.8	6.8	6.8
mPOC	6.8	5.7	5.6	5.2
mPOC-20HA	6.8	6.0	6.0	5.9
mPOC-40HA	6.8	6.4	6.4	6.4
mPOC-60HA	6.8	6.8	6.8	6.8
PMMA	6.8	6.6	6.6	6.6

Table 4.2: Comparative statistical significance ( $*p < 0.05$  and  $**p < 0.01$ ) for cell cytotoxicity data (Figure 4.1).

	$\alpha$ -MEM	mPOC	mPOC-20HA	mPOC-40HA	mPOC-60HA	PMMA
$\alpha$ -MEM	-	**	**	**		*
mPOC	**	-	*	**	**	**
mPOC-20HA	**	*	-	**	**	**
mPOC-40HA	**	**	**	-	*	**
mPOC-60HA		**	**	*	-	
PMMA	*	**	**	**		-

maintains its cell number without proliferation. LIVE/DEAD imaging shows that the cells attached to each sample surface are alive. SEM images show sparse cellular attachment for mPOC, cell attachment and spreading onto the surface and pores of mPOC-xHA, and complete, overlapping coverage and spreading of cells onto PMMA at 7 days. Cell coverage over pores increases in mPOC-xHA composites as the percentage of HA within the formulation increases.

#### 4.4 Discussion

Our results show that HA is necessary for successful biocompatibility in mPOC-based composites. This design choice is especially relevant, as bone cements cannot be further leached or modified once used as they are directly applied into a bone defect. Previously reported POC-based composites for orthopedic applications would ideally be molded and then leached before application into

Table 4.3: Comparative statistical significance ( $*p < 0.05$  and  $**p < 0.01$ ) for cell proliferation data. No statistical significance was observed for mPOC or mPOC-40HA in subtable (b) and are thus not reported.

Day 1	mPOC	mPOC-20HA	mPOC-40HA	mPOC-60HA	PMMA
mPOC	-	*		**	**
mPOC-20HA	*	-			**
mPOC-40HA			-		**
mPOC-60HA	**			-	
PMMA	**	**	**	**	-

Day 3	mPOC	mPOC-20HA	mPOC-40HA	mPOC-60HA	PMMA
mPOC	-	**		**	**
mPOC-20HA	**	-	*		
mPOC-40HA		*	-		*
mPOC-60HA	**			-	
PMMA	**		*		-

Day 7	mPOC	mPOC-20HA	mPOC-40HA	mPOC-60HA	PMMA
mPOC	-	**	*	**	**
mPOC-20HA	**	-	*		**
mPOC-40HA	*	*	-		**
mPOC-60HA	**			-	**
PMMA	**	**	**	**	-

(a) Statistical comparison of cell number between different material surfaces on the same day.

mPOC-20HA	Day 1	Day 3	Day 7
Day 1	-	*	**
Day 3	*	-	**
Day 7	**	**	-

mPOC-60HA	Day 1	Day 3	Day 7
Day 1	-	*	*
Day 3	*	-	*
Day 7	*	*	-

PMMA	Day 1	Day 3	Day 7
Day 1	-		**
Day 3		-	**
Day 7	**	**	-

(b) Statistical comparison of cell number between the same material on different days.



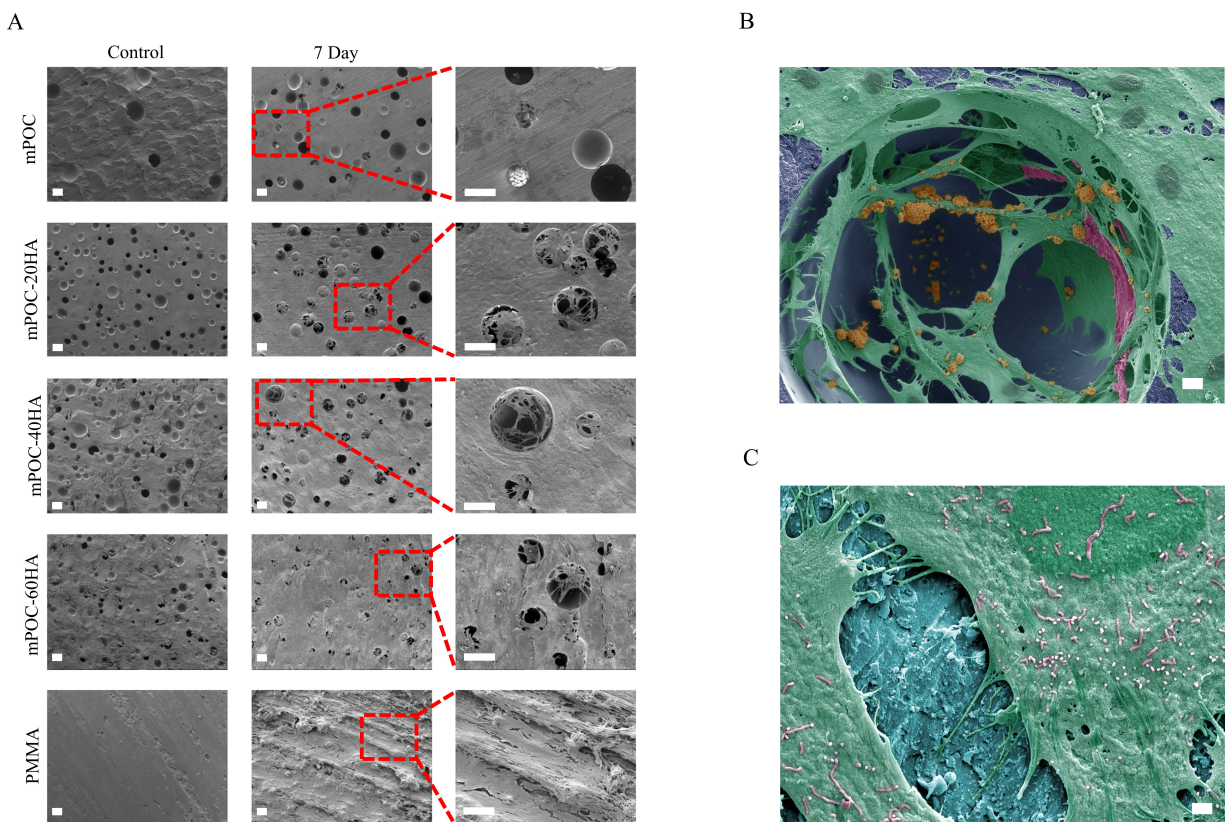


Figure 4.2: (A) Scanning electron microscopy (SEM) images of composite surfaces with (7 Day) and without cell attachment. Scale bars are in white in the lower left-hand corner of individual images and denote  $100\ \mu\text{m}$ . Clear cell attachment can be seen on mPOC-xHA composite surfaces, especially within and over the pores present on the surface. Pores in mPOC and mPOC-xHA form due to the release of nitrogen gas during free radical polymerization of azo initiators. PMMA surfaces show sheets of cell coverage, reminiscent of a fibrous encapsulation response commonly seen in a foreign body reaction. (B) Colour SEM image of mPOC-40HA surface after 7 days of cell attachment. Cells (light green) and nuclei (dark green) are seen spreading across the composite surface (dark blue) and across pores. Salt deposits (pink) are from residual media. It is hypothesized that cell proliferation (orange) is occurring along stretched cells. Scale bar (white) in lower right-hand corner corresponds to  $10\ \mu\text{m}$ . (C) Colour SEM image of mPOC-20HA surface after 7 days of cell attachment. Cells (light green) and nuclei (dark green) are seen spreading across the composite surface (blue). Microvilli (pink) from cells act to stretch across surfaces and assist in cell movement. Scale bar (white) in lower right-hand corner corresponds to  $1\ \mu\text{m}$ .

defects such as those pertaining to the craniofacial region. Qui et. al. reported similar qualitative cytotoxicity effects of POC to cells over a 3- and 14-day period<sup>46</sup>. POC alone scaffolds show minimal to no cell attachment and spreading, whereas POC-HA scaffolds with varying amounts of HA show visible attachment, spreading, and proliferation. Quantitative analysis of cellular biocompatibility is lacking in this paper and most papers involving POC given the overall poor response to the material. The debut paper on POC does compare MTT data for human aortic smooth muscle cells seeded onto POC or PLLA but does not address the cell viability for either<sup>50</sup>. Subsequent papers tend to present visual data of cell attachment and spreading<sup>51</sup>.

To elaborate on the method used for cell cytotoxicity, MTT is a tetrazolium dye that is reduced to an insoluble formazan by NADPH-dependent cellular oxidoreductase enzymes, meaning that the more MTT that is reduced the more living cells are present. This is qualitatively noted by a colour change of yellow to purple and is quantitatively collected through an absorbance reading. The data collected within this experiment clearly shows that mPOC and mPOC-20HA have little to no cell viability, indicating that the exposure to fresh extract media almost immediately caused cell death. This is due to the acidic media that was collected from mPOC and mPOC-20HA, which is hypothesized to release acidic monomers of citric acid from the surface of the scaffolds. Conversely, mPOC-40HA and mPOC-60HA present better cytotoxicity due to the increased amount of HA. HA has been shown to buffer the release of acidic monomers, with increasing HA concentrations correlating to increased pH levels in leaching media<sup>79,80</sup>. Ma et. al. explicitly explored the cytocompatibility of the monomers making up POC, citric acid and 1,8-octanediol<sup>81</sup>. Both citric acid and 1,8-octanediol had drastic cytotoxic effects on 3T3 cells at concentrations above 2 mg/mL, though interestingly citric acid concentrations of up to 7 mg/mL could be applied to human mesenchymal stem cells (hMSCs) without impacting cell viability negatively. The choice of utilizing MC3T3 cells in this study may have resulted in negative results for the mPOC and mPOC-20HA

samples, but we focus here both on choosing the best, most compatible material before moving forward with *in vivo* testing and for comparison to PMMA. For that reason, mPOC-20HA will not be pursued in the following *in vivo* studies.

The CCK8 data again reinforces that HA is necessary for the health and proliferation of MC3T3 cells. Surprisingly, the mPOC-20HA samples hold up to other mPOC-xHA samples, counter to the results shown in the MTT data. The cell attachment and spreading seen from SEM images show that mPOC does not support attachment or proliferation, potentially due to the acidic surface or unreacted monomer interaction of citric acid or 1,8-octanediol. The introduction of HA greatly enhances cell attachment and spreading, with noticeable pore coverage as the amount of HA incorporation is increased. PMMA shows a completely covered surface which is reminiscent of a foreign body response (FBR). Layers of cells are visible on the surface of PMMA which mimics the protein adsorption, matrix deposition, and fibrous encapsulation of FBR.

The enhanced cellular response to scaffolds containing HA may be due to a number of mechanisms directly related to HA. As noted, increased amounts of HA stabilizes the pH of scaffolds, providing a neutral environment for cell survival and attachment. Additionally, cell survival and adhesion are highly regulated by the degree of protein adsorption onto scaffold surfaces<sup>82</sup>. HA has been shown to increase the adsorption capacity of proteins, which may explain the increased cellular proliferation over time of the mPOC-xHA scaffolds. Given HA's similarity to bone, the mPOC-xHA scaffolds may also attract proteins such as runt-related transcription factor 2 (RUNX2), which is associated with osteoblast differentiation. Long-term differentiation studies of the MC3T3 cells on mPOC-xHA scaffolds, as well as any bone-specific marker studies may further indicate HA's effect on upregulating these proteins.

## 4.5 Conclusion

The cellular response to new materials is paramount when deciding what will be successful at the *in vivo* and clinical level testing stages. Though some of the negative effects of POC and mPOC could be addressed by post-processing and leaching steps, it is the goal of this thesis to provide an alternative bone cement that mimics PMMA as closely as possible without its inherent difficulties. As such, it is very promising that the inclusion of HA in these preliminary cell studies was able to circumvent the non-ideal cellular responses associated with POC and mPOC. Moving forward, our goal is to test these bone cement formulations in a small animal model. We selected mPOC as a polymer control, mPOC-40HA and mPOC-60HA as our hypothesized best options, and PMMA as our clinical control to conduct an *in vivo* subcutaneous injection study in Sprague Dawley rats to assess biocompatibility.

## **CHAPTER 5**

### ***IN VIVO* MODEL FOR INFLAMMATORY EFFECT**

#### **5.1 Objective**

In selecting mPOC-40HA and -60HA composites as the best cell compatible bone cements, we aimed to test this compatibility in a subcutaneous model. This model allows us to test the biocompatibility of a given material by injecting it subcutaneously and evaluating the inflammatory response, degradation and bioresorbability, and the degree of integration into the surrounding tissues. If the material does not progress into a FBR and instead slowly integrates into the surrounding tissues, this is an indication that the material is biocompatible. This preliminary assessment of biocompatibility is often followed by a bone defect model that can assess the ability of the material to both recruit osteogenic cells and promote bone remodeling.

#### **5.2 Experimental Section**

##### **5.2.1 Rat Model and Preparation of Materials**

All animal procedures were performed in accordance with the Guide for the Care and Use of Laboratory Animals published by the National Institutes of Health (NIH)<sup>83</sup>. Procedures were approved by the Northwestern University Animal Care and Use Committee. Subcutaneous injections of each test group into the rat posterior were used to assess biocompatibility *in vivo*. Twenty male Sprague Dawley rats (175-200 g, Charles River Laboratories) were used for these studies – four rats per time point collected. All mPOC and mPOC-xHA components were sterilized with ethylene oxide gas, prepared under sterile conditions, and kept on ice before injection. Kyphon Activos 10

(Medtronic) PMMA bone cement was prepared immediately before subcutaneous injection. Rats were anesthetized with isoflurane (2-3% with oxygen), shaved, and sterilized with betadine and ethanol before subcutaneous injections of approximately 100  $\mu$ L of each test formulation – first PMMA in the upper left quadrant, mPOC in the upper right quadrant, mPOC-40HA in the lower left quadrant, and mPOC-60HA in the lower right quadrant. After each injection, the site was marked with a permanent marker for tracking purposes. The animals were sacrificed at 1 hour to determine adequate curing, 1 and 3 days to determine the acute inflammatory response, and 4 weeks to evaluate the chronic inflammatory response. For later animal time points, rats were housed in the Pancoe-NorthShore University Health System Life Sciences Pavilion and cared for in compliance with the regulations established by the Northwestern University Institutional Animal Care and Use Committee. Animals were examined for post-operative pain each day following injections and up to 10 days for the 4-week time point group. Signs of animal mobility, eating and drinking habits, changes in body weight, and appearance of surgical wounds were noted.

### **5.2.2 Tissue Processing**

Animals were euthanized by carbon dioxide inhalation and a secondary method of cervical dislocation. Skin samples containing the subcutaneous injections were removed and fixed using 4% paraformaldehyde in PBS solution for 24 hours. Samples were subsequently rinsed in 1x PBS multiple times to remove any residual paraformaldehyde. Half of the samples containing HA (mPOC-40HA, mPOC-60HA, and PMMA) were decalcified using 10% Ethylenediaminetetraacetic acid (EDTA) in DI water solution for 7 days, then rinsed with PBS multiple times to remove residual EDTA. Samples were dehydrated in a series of ascending ethanol solutions, cleared by xylene, and embedded in paraffin wax. 5-micron thick sections were cut and mounted onto slides by either myself for histological imaging and analysis, or the Pathology Core Facility at Northwestern Uni-

versity for immunohistochemical imaging. Sections were treated with xylene to remove paraffin and hydrated by a series of descending ethanol solutions and water.

### **5.2.3 Histological Assessment**

Hematoxylin and Eosin (H& E) and Masson's Trichrome (MT) staining were performed to observe histological characteristics of the samples. All time points were represented for these staining methods. For H& E, sections were incubated in hematoxylin for 5 minutes, washed in water for 5 minutes, then emerged in DI water, 70% ethanol, 80% ethanol, and 95% ethanol for 2-3 minutes each. Slides were then counterstained with eosin-Y for 1 minute and emerged in 100% ethanol and xylene for 2x5 minutes each. MT sections were incubated in Weigert's iron hematoxylin for 15 minutes, and counterstained with Solution A (0.5 g acid fuchsia, 0.5 g xylidine ponceau, 99 mL water, 1 mL glacial acetic acid) for 10 minutes, Solution B (1 g phosphomolybdic acid, 100 mL DI water) for 10 minutes, and Solution C (2 g light green SF yellowish, 2 mL glacial acetic acid, 100 mL DI water), washing between each step with DI water. After the last rinse, slides were immersed in 1% acetic acid solution for 2 minutes. Slides were then dehydrated in an ascending ethanol series and cleared with xylene for 2x5 minutes. All slides were mounted with Cytoseal and sealed with nail polish. Sections were visualized under light microscopy and imaged at 4x magnification (Cytation 5, BioTek Instruments, Winooski, VT) and 4x, 10x, 20x, and 40x magnification (Nikon Eclipse TE2000-U).

### **5.2.4 Immunohistochemistry Assessment**

Immunohistochemistry staining was prepared through the Mouse Histology and Pathology Core at Northwestern University. Time points represented in this data are for 1 day and 4 weeks. Slides were immersed into antigen retrieval buffer (pH 6.0, 10 mM Sodium citrate buffer, 0.05% Tween

20) at 110°C for 10 minutes in a pressure cooker then washed with PBS. Samples were blocked using a solution made of 5 mg/mL bovine serum albumin (BSA), 5% normal goat serum, and 1x PBS for 30 minutes. Slides were then either stained for CD68 or co-stained for  $\alpha$ -SMA and CD31.

For CD68, samples (n of 3) were incubated with primary antibody (Cell Signaling #CST97778) at a concentration of 1:200 in blocking buffer at 4°C overnight. Slides were then washed by PBS 3x5 minutes and incubated on the Biocare Intellipath Staining Platform with secondary antibody (Biocare Mach2 Rabbit HRP-Polymer (Biocare #RHRP520MM)) and DAB Chromogen Detection (DAKO #K3468) diluted in blocking buffer at room temperature for 30 minutes. Slides were washed by PBS 6x5 minutes, then mounted with anti-fade medium and sealed with nail polish.

For  $\alpha$ -SMA and CD31 co-stain (n of 3), samples were incubated with primary antibodies (abcam #ab5694 and Santa Cruz #sc-1506 for  $\alpha$ -SMA and CD31 respectively) at a concentration of 1:1000 in blocking buffer at 4°C overnight. Slides were then washed by PBS 3x5 minutes and incubated on the Biocare Intellipath Staining Platform with  $\alpha$ -SMA secondary antibody (Biocare Mach2 Rabbit HRP-Polymer (Biocare #RHRP520MM)) and brown chromogen DAB Chromogen Detection (DAKO #K3468) diluted in blocking buffer at room temperature for 30 minutes. Slides were washed by PBS 3x5 minutes and incubated with CD31 secondary antibody (Biotin-SP-AffiniPure Donkey anti-goat IgG (Jackson ImmunoResearch #705-065-147)), Strept-Avidin AP (Thermo Fisher #43-4322), and Warp Red Chromogen (Biocare #WR806) diluted in blocking buffer at room temperature for 30 minutes. Slides were washed by PBS 6x5 minutes, then mounted with anti-fade medium and sealed with nail polish.

The Pathology Core Facility at Northwestern University imaged slides at 40x using the Hamamatsu K.K. Nanozoomer 2.0 HT (Hamamatsu Photonics K.K., Hamamatsu, Shizuoka, Japan). Images were visualized and exported as JPEGs at a scale of 1600% using NDP.view2 software. The subcutaneous region of each section was analyzed using FIJI (Fiji Is Just ImageJ) for CD68



images. Specific steps taken to obtain results from FIJI are as follows: colour deconvolution for H&E was performed on each image, the default threshold was applied, binary watershed was performed, and particles ranging from 10-50 pixels were analyzed. The count, total area, average size, and percent area were acquired. The total area data is presented in this thesis. Number of vessels per mm<sup>2</sup> was analyzed for  $\alpha$ -SMA-CD31 images within the connective tissue region of the material-tissue interface.

### **5.2.5 Statistical Analysis**

Statistical analysis was performed with Microsoft Excel software and GraphPad Prism 7.0 (GraphPad Software Ind., La Jolla, CA). Student's t-test was used to compare pairs of means and ANOVA with Bonferroni post-hoc analysis was used to compare means between multiple treatments. A p-value of 0.05 or less was considered to be statistically significant.

## **5.3 Results**

### **5.3.1 HA reduces inflammatory response**

All tested bone cements were successfully injected subcutaneously into the backs of Sprague Dawley rats. mPOC alone did not cure as expected, potentially due to the lower body temperature of the rats. All other materials were easily identifiable by a hardened oblong spheroid underneath the subcutaneous skin tissue.

#### *5.3.1 Histology Imaging*

Tissue sections for 1 day time points show acute inflammatory responses to all tested materials. Sections for 4 weeks show an apparent large chronic response to the mPOC polymer as noted

by the large red/purple mass where the polymer is considered to be. mPOC-40HA and mPOC-60HA samples are seemingly integrating into the surrounding tissue with additional collagen fibers present as identified by the green, fibrous characteristics. PMMA images at 4 weeks presents a distinct dividing barrier of collagen and cells around the material.

### 5.3.1 Immunohistochemistry Imaging

Tissue sections were positive for CD68 in all subcutaneous injection sites. All materials were not significantly different from each other at 1 day. mPOC-40HA, mPOC-60HA, and PMMA presented significantly decreased amounts of CD68 positive cells between 1 day and 4-week time points. mPOC-60HA and PMMA were not significantly different at either time point from each other. Tissue sections were positive for  $\alpha$ -SMA-CD31 staining around all subcutaneous injection sites. There was a significant increase in vessel density for mPOC-60HA samples compared to mPOC-40HA.

## 5.4 Discussion

The results show that mPOC-xHA was successful at reducing the inflammatory response of mPOC and mimicking the *in vivo* characteristics of PMMA. At 4 weeks, mPOC-xHA composites show integration into the surrounding tissues whereas PMMA shows distinct fibrous encapsulation of the PMMA bone cement. This is a promising result as it reiterates that the mPOC-xHA bone cement can degrade and be broken down over time, avoiding the problems associated with PMMA such as mechanical instability due to fibrous encapsulation<sup>84</sup>.

The data from CD68 analysis is quite exciting as mPOC-60HA and PMMA show equivalent inflammatory responses at the tested time points. These results compounded with the tunable characteristics of mPOC-xHA offer initial proof that these materials could be pursued as an alternative

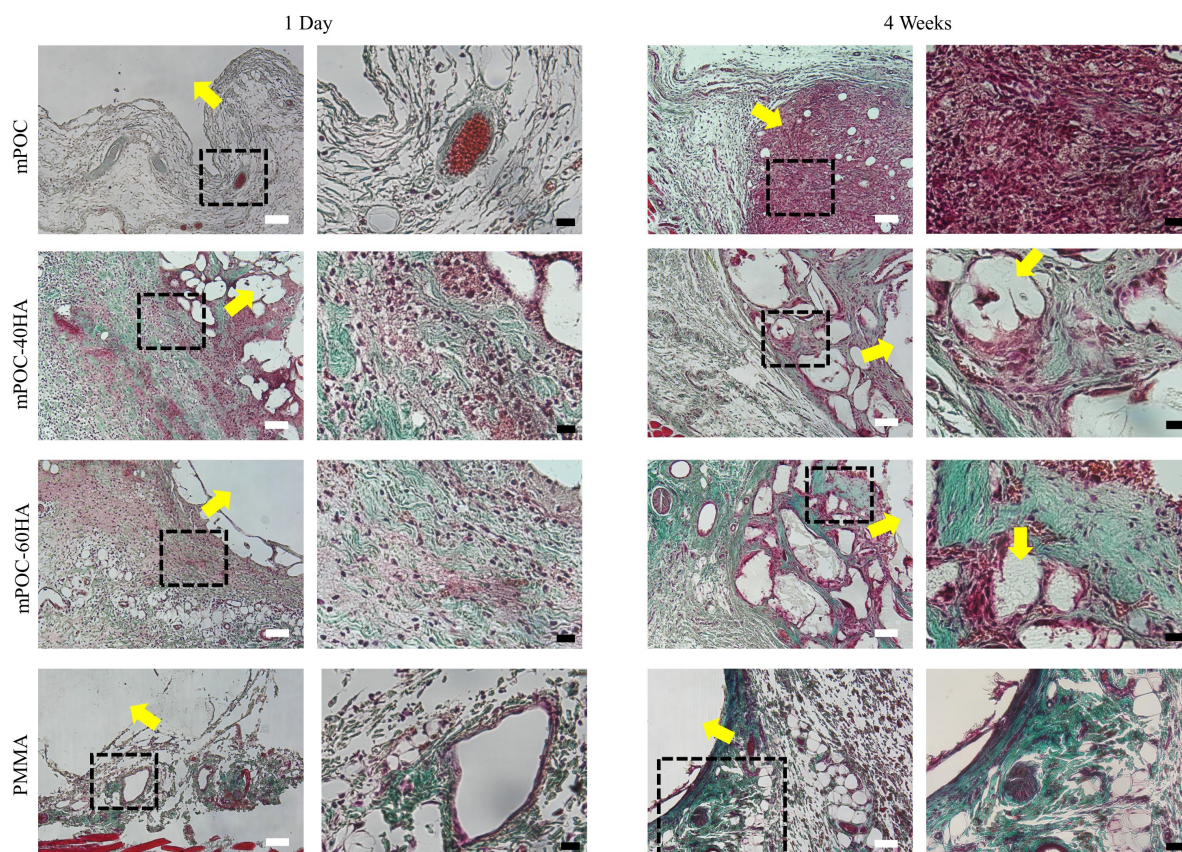


Figure 5.1: Representative Masson's Trichrome (MT) images from *in vivo* subcutaneous injection study of the sample-tissue interface. mPOC-xHA injections show collagen infiltration (green) at both 1 day and 4 weeks, whereas mPOC samples show thin tissue around the injection site at 1 day and a large immune response (dark red/purple) at 4 weeks. PMMA samples show a thin subcutaneous tissue region around samples at day 1, due in part to difficulty during sectioning. PMMA at 4 weeks shows a distinct collagenous capsule around the implant, indicative of the fibrous encapsulation seen as part of the body's foreign body response. Alternatively, mPOC-xHA shows integration of collagen into the material itself and has broken off parts of the material as seen in mPOC-60HA. Initial images are scaled at 100  $\mu\text{m}$  (white) and inset images at 20  $\mu\text{m}$  (black) whereas the sample position is indicated by yellow arrow.

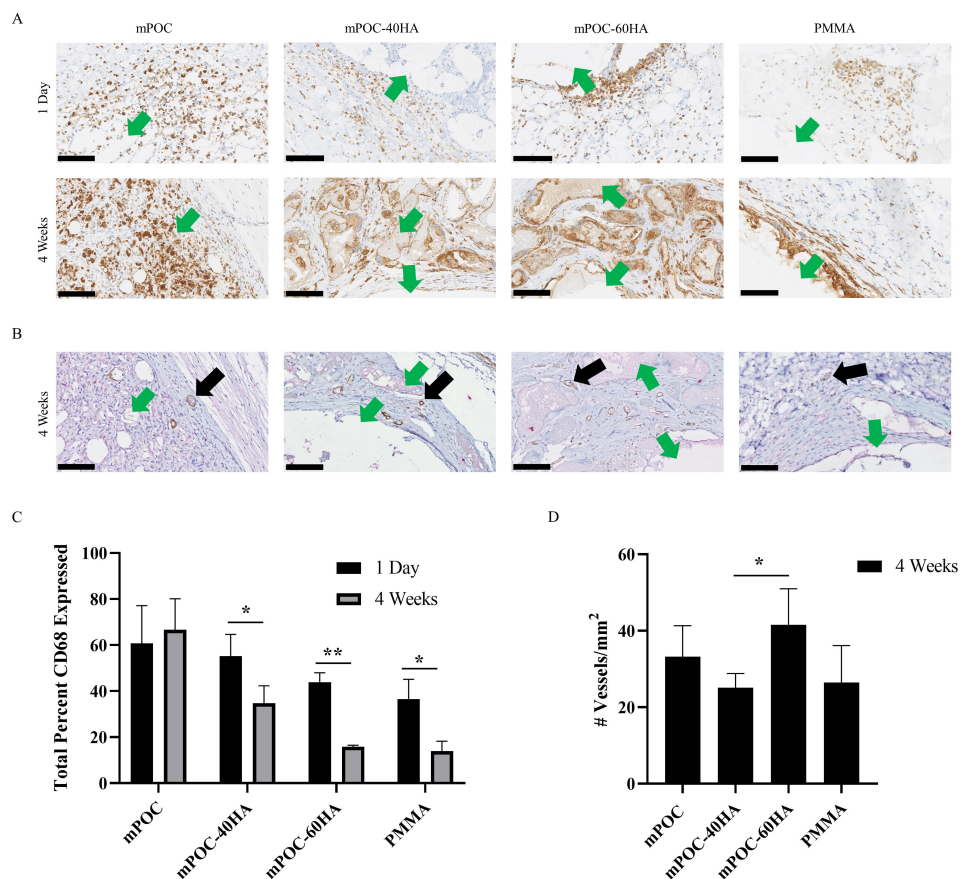


Figure 5.2: Immunohistochemistry staining for CD68 (A) and  $\alpha$ -SMA-CD31 co-stain (B). (A) CD68 (stained red) has an apparent higher density of positively stained cells at the interface between the tissue and material (material position noted by green arrows). Some staining of the material occurred in mPOC-xHA containing polymers, but otherwise the presence of CD68 positive cells visibly decreased at the 4-week time point for mPOC-xHA polymers and PMMA. mPOC at 4 weeks shows a large increase in CD68 expression. (B) Vessels (stained red/brown) can be clearly seen within the tissue-material connective tissue interface of mPOC and mPOC-xHA composite polymers (black arrows) whereas minimal vessel presence can be seen in the thin interface of PMMA samples. Analysis for (C) CD68 and (D)  $\alpha$ -SMA-CD31 immunohistochemistry staining where  $*p < 0.05$  and  $**p < 0.01$ . (C) CD68 positive staining was analyzed within the subcutaneous tissue region where the polymers were injected. The percent of CD68 expressed is normalized to the total amount of cells present within the subcutaneous region. mPOC-xHA and PMMA composites show significantly decreased expression of CD68 by the 4-week time point, with mPOC-60HA and PMMA presenting similar data. (D) Number of vessels per  $\text{mm}^2$  was analyzed within the connective tissue region of the material-tissue interface. mPOC-60HA has significantly increased vessel density compared to mPOC-40HA, potentially due to the increased presence of HA.

Table 5.1: Comparative statistical analysis of CD68 expression in positively stained cells using student's t-test to compare pairs of means where  $*p < 0.05$  and  $**p < 0.01$ . No statistical significance was observed between groups at the 1-day time point in (a) and is thus not reported.

<b>4 Weeks</b>	<b>mPOC</b>	<b>mPOC-40HA</b>	<b>mPOC-60HA</b>	<b>PMMA</b>
<b>mPOC</b>	-	*	**	**
<b>mPOC-40HA</b>	*	-	*	*
<b>mPOC-60HA</b>	**	*	-	
<b>PMMA</b>	**	*		-

(a) Statistical comparison of CD68 between different material composites.

<b>mPOC</b>	<b>1 Day</b>	<b>4 Weeks</b>
<b>1 Day</b>	-	
<b>4 Weeks</b>		-

<b>mPOC-40HA</b>	<b>1 Day</b>	<b>4 Weeks</b>
<b>1 Day</b>	-	*
<b>4 Weeks</b>	*	-

<b>mPOC-60HA</b>	<b>1 Day</b>	<b>4 Weeks</b>
<b>1 Day</b>	-	**
<b>4 Weeks</b>	**	-

<b>PMMA</b>	<b>1 Day</b>	<b>4 Weeks</b>
<b>1 Day</b>	-	*
<b>4 Weeks</b>	*	-

(b) Statistical comparison of CD68 between the same materials at different time points.

Table 5.2: Comparative statistical analysis of vessel data using student's t-test to compare pairs of means. Statistical comparison of number of vessels per mm<sup>2</sup> between different material composites where  $*p < 0.05$ .

4 Weeks	mPOC	mPOC-40HA	mPOC-60HA	PMMA
mPOC	-			
mPOC-40HA		-	*	
mPOC-60HA		*	-	
PMMA				-

bone cement to PMMA. As this *in vivo* study was preliminary, we only evaluated the inflammatory response of the materials up to 4 weeks. We will expand on future directions to advance the *in vivo* work in an orthopedic setting to assess the functionality of these polymers in enhancing bone remodeling over time in the following chapter. Data from the  $\alpha$ -SMA-CD31 analysis shows similar vessel development across all experimental cements, with a slight increase of vessel density in mPOC-60HA. Of qualitative note, the size and distribution of vessels within the connective tissue region are different between groups. mPOC-xHA shows vessel development between sections of polymer that have begun to break down and integrate into the surrounding tissues, whereas vessel development in PMMA is very minor within the thin connective tissue region. Comparing these interface images to that of the MT images, tissue response to PMMA shows a distinctly dense fibrous encapsulation of the material, potentially leaving little room for vessel development at this early time point. Again, further *in vivo* studies will need to be performed to better study the vessel development around the materials, especially within an orthopedic bone model.

HA incorporation into mPOC-xHA has a significant effect *in vivo*. Part of this may be due to the buffering effect HA has on the immediate environment surrounding the mPOC-xHA scaffolds, providing a neutralizing agent for the acidic products of mPOC. The increased capacity of HA to adsorb proteins onto its surface may also provide a platform to adsorb specific proteins relevant to wound healing and bone formation, such as RUNX2, osterix (Osx), and vascular endothelial

growth factors (VEGF)<sup>85</sup>. VEGF upregulation may correlate to the statistically significant difference in vessel density between mPOC-40HA and mPOC-60HA, but further studies would need to be performed to verify this.

## 5.5 Conclusion

Chapters 3, 4, and 5 show that mPOC-xHA may serve as an alternative, injectable bone cement for orthopedic applications. The novel use of V70 allows for composite curing at body temperature, avoiding the disadvantageous handling characteristics of PMMA. While many bone cements have been created and researched, the materials presented in these chapters combine the benefits of using antimicrobial and antioxidative CBBs, a key bone component (HA), and thermal initiators to create tunable, biocompatible biomaterials that avoid many of the mechanical failings of PMMA and CPCs. Moving forward these materials will be tested in both *ex vivo* and *in vivo* bone systems to further prove their use in orthopedic applications.

## CHAPTER 6

### THESIS SUMMARY AND OUTLOOK

#### 6.1 Summary of Thesis Work

The work presented in this thesis encompasses a subset of the orthopedic tissue engineering field that is in need of new, biodegradable materials. One of the key methods of introducing new materials onto the market, and thus making them clinically available, is to prove that a new material is substantially equivalent to a legally marketed material. In this case, this thesis developed a novel thermoresponsive, injectable bone cement that closely mimics the polymerization methods and biocompatibility of clinically available PMMA, while providing better handling characteristics, compressive mechanics, and degradability that could enhance its application and retention within patients.

While many bone cements have been marketed and developed over the years, these primarily are based upon PMMA and its composite formulations<sup>86</sup>. As such, these are polymer systems with liquid and powder components derived from PMMA powder, MMA liquid monomers, and the peroxide initiator benzoyl peroxide as seen from companies including Stryker, Medtronic, Johnson & Johnson, Merck, and Zimmer. Inquiries into how to modify PMMA into a more biocompatible material has resulted in studies incorporating HA, CPCs, bone particles, or bioglass into the powder component<sup>87-91</sup>. Though these methods can lead to more biocompatible materials, the initial handling characteristics of PMMA pose issues that can affect both the initial application of the material and post-surgical healing in patients. Our goal was to not only improve these handling characteristics and immediate patient recovery, but develop and provide a resorbable, biocompati-



ble bone cement for eventual use in procedures such as VP and KP.

Since the peroxide-based polymerization of PMMA was the main factor in determining its polymerization heat and curing time, modifying or replacing that aspect was of interest. Peroxide initiators such as benzoyl peroxide form free radicals upon immediate dissociation of a weak peroxy bond, which then interact with the carbon-carbon double bond of MMA to quickly initiate free radical polymerization. Instead, this thesis delves into using azo-based polymerization whose dissociation of its' azo-bond is dependent on temperature thresholds. This is a near novel utilization of azo-based initiators in orthopedic applications as azobisisobutyronitrile (AIBN) has previously been researched for its application in bone cement<sup>92</sup>. AIBN was not further studied as it was shown to be relatively equivalent to benzoyl peroxide in polymerizing acrylate-based cement. AIBN itself has a high temperature threshold of 65°C that would not be ideal for *in situ* curing capabilities. The novelty of this thesis relies instead on the use of a different azo-initiator, V70, that has a temperature threshold of 30°C, well within an achievable temperature for biological applications. As such, consideration of V70 and its polymerization mechanics was incorporated into the design of the final bone cement formulation, resulting in a methacrylated version of POC.

Specifically, we described the synthesis and characterization of four formulations of an injectable, thermoresponsive, citrate-based biomaterial that is suitable for orthopedic applications. These formulations, mPOC, mPOC-20HA, mPOC-40HA, and mPOC-60HA maintained injectability, thermoresponsive behavior at physiological temperatures, and mechanical compression properties within vertebral bone ranges. mPOC-40HA and mPOC-60HA were deemed the most biocompatible from *in vitro* studies and were used in a subcutaneous *in vivo* experiment to further address their inflammatory effect. *In vivo*, it was found that mPOC-60HA performed on par with the clinically available PMMA Kyphon Activos 10 when injected subcutaneously.

## 6.2 Future Work

This work primarily focused on the development and initial biocompatibility of the tested materials. Optimization of the tested materials should still be evaluated, as injectability of the materials for use in VP/KP is of key importance to this thesis. Adjusting the injectability towards a less viscous state would be obtainable by increasing the amount of solvent within the formulation. While keeping the material less viscous is ideal for its initial injectability, the material needs to also polymerize quickly once initiated to avoid any cement leakage during application. This curing property can be addressed by increasing the amount of initiator to induce a quicker polymerization. Given these design considerations, injectability should be addressed first with the subsequent materials characterization and *in vitro* studies performed in this thesis. After this point, several additional areas of investigation could benefit from future testing and analysis. These fall within directly addressing the orthopedic capabilities of the developed bone cements and would cover *in vitro*, *in vivo*, and *ex vivo* experiments and models.

### 6.2.1 Alkaline Phosphatase/Alizarin Red *In Vitro* Study

Although testing the biocompatibility of mPOC and mPOC-xHA composites is important at both the *in vitro* and *in vivo* level, this does not address the capability of the materials to induce bone formation and succeed on an orthopedic tissue engineering platform. Data included within the appendices indicate that expression of osteopontin (OPN), a marker for osteoblasts and important factor in inducing bone remodeling, was expressed at a significantly increased level in mPOC-60HA composites when compared to PMMA. While OPN is considered a marker relevant to bone remodeling, it could represent other cell line expression such as neutrophils, macrophages, T cells, and mast cells. Verifying that the *in vivo* results indicate the OPN expressed is relevant to bone

remodeling would require an *in vitro* study that identifies expression of additional bone markers, specifically alkaline phosphatase (ALP) and alizarin red. The experimental design, hypotheses, and analysis/discussion of expected results would be as follows.

ALP is an early marker for osteodifferentiation that is found on the surface of osteoblasts whereas late markers for osteodifferentiation can be identified by their expression of osteocalcin, osteopontin, and calcium deposition. To this effect, total ALP expression can be determined through an assay that allows ALP to catalyze alkaline buffer resulting in a detectable fluorescent signal, meaning the more ALP expressed the more fluorescent of a signal. Alizarin red staining is a method to detect calcium deposition or mineralization which is an important early-stage marker of matrix mineralization and a crucial step towards the formation of a calcified extracellular matrix. Free ionic calcium within a surface or cellular body will precipitate with addition of alizarin and stain red, indicating the amount of calcification occurring.

To prepare samples for ALP assays and alizarin red staining, 12 mm diameter and 1 mm tall composite samples must be prepared. Given the results obtained from the previous *in vitro* and *in vivo* studies, mPOC-40HA and mPOC-60HA will be evaluated along with PMMA as a clinical control. Samples should be molded in a stainless-steel mold at 37°C overnight, removed, and cut flat to 1 mm tall samples. Samples can then be transferred to a biological hood, sterilized in 70% ethanol for 2x30 minutes, and sterilized under UV light exposure on both sides for 15 minutes. Sterilized samples can then be placed (n of 3 for each time point of 7, 14, 17, and 21 days) into the bottom of a 24 well plate.

For ALP assay, MC3T3 cells should be seeded directly onto sterilized samples at 10,000 cells per 100  $\mu$ L and allowed to attach for 1 hour before adding additional non-osteogenic  $\alpha$ -MEM media to cover the samples. At each designated time point, samples are collected and immersed in a radioimmunoprecipitation assay (RIPA) buffer solution and are put through at least three

freeze/thaw cycles to rupture the cell membranes of cells attached to the samples. RIPA/cell solution can then be spun down to separate out any insoluble particles. To perform the ALP assay (BioRad Alkaline Phosphatase Assay Kit, Des Plaines, IL), para-nitrophenylphosphate (pNPP) solution is prepared by dissolving one pNPP tablet in 1 mL 5X diethanolamine buffer and 4 mL of DI water. 10  $\mu$ L of RIPA/cell solution and 90  $\mu$ L pNPP solution are then added into wells on a 96-well plate in duplicate for each sample. The solutions react protected from light for 30 minutes and then read on a plate reader at an absorbance of 405-420 nm. Mean absorbance of a blank standard is subtracted from all sample readings, duplicates are averaged, and the amount of para-nitrophenol (pNP) in each sample is determined utilizing a standard curve of pNPP concentrations. ALP expression is then determined using the equation:

$$ALP\ Activity(U/mL) = (B/(\Delta T * V)) * D \quad (6.1)$$

Where B is the amount of pNP in a sample well calculated from the standard curve ( $\mu$ mol), T is the reaction time in minutes (30 minutes), V is the original sample volume added into the reaction well in mL (0.01 mL), and D is the sample dilution factor (1). ALP expression over time can then be plotted using Excel.

Table 6.1: RIPA Solution Composition

<b>Component</b>	<b>Vendor</b>	<b>Amount</b>
Double Distilled Water	Bioworld	178 mL
Sodium Dodecyl Sulfate	Fisher Bioreagents	0.2 g
Sodium Chloride	Fisher Scientific	1.7532 g
Sodium Deoxycholate	Bioworld	10 mL
Triton X-100	Acros Organic	2 mL
Tris Hydrogen Chloride	Thermo Scientific	10 mL

Alizarin red staining can be performed in parallel with the ALP assay on day 21 following

an established protocol (PromoCell, Heidelberg, Germany). The staining solution is prepared by dissolving 2 g Alizarin Red S powder (Sigma-Aldrich, St. Louis, MO) in 90 mL DI water, adjusted with hydrochloric acid to reach a pH of 4.1-4.3, brought up to 100 mL total volume with DI water, and filtered. Cells/samples are washed with PBS and fixed in Saccomanno Fixation Solution (Morphisto, Offenbach, Germany) for 30 minutes. Samples are then aspirated, washed in DI water, aspirated, and exposed to the Alizarin Red S staining solution until covered. Samples are covered and incubated at room temperature for 10-15 minutes, washed in DI water, and then PBS is added to the samples. Mineralization can then be visualized under light microscopy with images processed with ImageJ and quantified via threshold intensity.

If bone specific OPN was indeed present in the *in vivo* results, it is hypothesized that the mPOC-60HA samples will show the highest ALP expression and mineralization. mPOC-40HA should also show some degree of both, though at a lesser level. This is hypothesized due to the presence of both citric acid and HA within the polymer network, both of which could potentially persuade MC3T3 cells toward their osteogenic line. PMMA is not expected to produce high levels of ALP or mineralization, though some may occur due to the small percentage of HA present in the Kyphon Activos 10 bone cement (10% HA). An even more indicative cell line to use in these experiments would be human mesenchymal stem cells, which can differentiate into a vast number of potential cell lines including myocytes, adipocytes, osteoblasts, neurons, and chondrocytes. Increased ALP expression and mineralization in this cell line would further verify the ability of mPOC-xHA composites to induce osteodifferentiation, recruit bone cells, and provide a framework for bone remodeling.

### **6.2.2 *In Vivo* Femoral Defect**

An important step in testing the efficacy of the bone cements presented in this thesis is to study its ability to integrate into natural bone tissue by way of some type of orthopedic bone defect model. Commonly, these models are performed in rabbits as they provide a large bone structure in what is considered a small animal model. Previously, Qui et. al. developed and tested a POC-HA composite for orthopedic implants within a rabbit femoral defect model, finding that after 6 weeks implantation the implants interfaced well with the surrounding bone with minimal inflammation, no encapsulation, and presence of mineralized chondrocytes adjacent to the implant indicating normal bone remodeling<sup>46</sup>. For our own purposes, we would prepare and test mPOC-40HA and mPOC-60HA bone cements within a similar femoral bone defect to determine their levels of integration, bone remodeling, and inflammatory effect, assessing which bone cement would be ideally used in a later VP/KP model against clinically relevant PMMA.

Specifically, nine New Zealand white rabbits (Covance, Kalamazoo, MI) weighing between 2.3 and 2.7 kg would be used to assess biocompatibility. Animal experiments would be carried out in compliance with a protocol approved by the Northwestern University's Animal Care and Use Committee (Chicago, IL). Rabbits would be anesthetized by ketamine (40 mg/kg intramuscularly) and xylazine (5.7 mg/kg intramuscularly), supplemented with isoflurane (1-2% inhalation). A 4.0 cm medial parapatellar arthrotomy, a standard technique to expose the knee joint, would be used to expose the medial femoral condyle. A 2.7 mm diameter, 4.0 mm deep bone defect would be created in the exposed right medial femoral condyle using a mosaicplasty harvester (Smith & Nephew, Memphis, TN). Liquid mPOC-40HA and mPOC-60HA would be injected into the defect and allowed to cure. An n of 3 rabbits would be used for each group (3 for control, 3 for mPOC-40HA, and 3 for mPOC-60HA). After all surgical procedures, the rabbits would be housed in the Pancoe-NorthShore University Health System Life Sciences Pavilion and cared for in compliance

with the regulations established by the Northwestern University Institutional Animal Care and Use Committee. Animals would be examined for post-operative pain each day following the procedure until day 10, and then each week to assess signs of animal mobility, eating and drinking habits, changes in body weight, and appearance of surgical wounds. Knees would be harvested at 6 weeks post injection with gross examination documented with a digital camera. Knee sections would be fixed in 10% neutral buffered formalin, sectioned at 5 mm, and either decalcified in 10% EDTA solution and stained for H& E or not decalcified and stained for von Kossa. Sections would be evaluated by standard light microscopy.

Sections stained for H&E should indicate a low level of inflammatory cells and lack of a fibrous capsule forming around the bone cement injection site. If the cement has begun to degrade, parts of the cement may be visibly broken off the main bone cement mass and seen integrating into the surrounding bone. Von Kossa staining is a method used to quantify mineralization of calcium in tissues. The interface between the bone cements and surrounding bone would ideally present the formation of new osteoids and mineralized chondrocytes, confirming the progression of normal bone remodeling and indicating that the bone cements would be integrating into this process. It is hypothesized that the mPOC-60HA bone cement would perform better than its mPOC-40HA counterpart due to the increased level of HA within the polymer network. The previous study by Qui et. al. utilized POC with 65% HA and showed very promising results in their *in vivo* model at 6 weeks, something that would ideally be shown for our own bone cements<sup>46</sup>. While this initial bone defect model would provide necessary information on how the bone cements behave in an orthopedic setting, they are still not being tested in a model that would mimic the orthopedic condition or surgical procedures addressed in the framework of this thesis. For that, an osteoporotic VP/KP model would be the most beneficial to further study.

### **6.2.3 *In Vivo* Osteoporotic VP/KP Model**

Inducing osteoporosis in animal models has been successfully done primarily in mouse and rat models by way of ovariectomy (OVX) in females. This significantly decreases the amount of estrogen, leading to increased bone resorption and, over time, decreased bone mineral density and the onset of osteoporosis<sup>93</sup>. These OVX models are useful in studying drugs and treatments for osteoporosis as well as for utilization in bone tissue engineering strategies. Since the bone cements presented in this thesis were developed and tested for the use in VP/KP, surgical procedures that are by far the most used in osteoporotic patients, performing a similar VP/KP model within an osteoporotic animal would present convincing evidence of the efficacy of these CBB bone cements.

Developing an animal around mice and/or rats presents some disadvantages due to their size and mobility method. Their size would make a vertebral defect procedure tricky as either the vertebrae would be too small to work with, or the amount of material used would be too small an amount to determine true bone remodeling. Additionally, these animals use all four limbs to mobilize which does not truly mimic the vertebral mechanics and stresses that are relevant to humans. Ideally, bi-pedal non-human primate models would be used, though these models would be expensive and time consuming to develop an osteoporotic model in. Instead, OVX has been successfully performed in female rabbits resulting in the development of osteoporosis within the range of 8 weeks to 6 months<sup>94,95</sup>. While these animals also utilize all four limbs for mobility, the lumbar vertebrae do undergo compressive, shear, and rotational stresses similarly seen in human vertebrae.

Specifically for this model and experiment, sixty 5-month-old female New Zealand white rabbits (Convance, Kalamazoo, MI) weighing between 3.2 and 3.5 kg would be used. Animal experiments would be carried out in compliance with a protocol approved by the Northwestern University's Animal Care and Use Committee (Chicago, IL). Rabbits would acclimate for two weeks



before OVX and sham procedures. The bone mineral density (BMD) of the lumbar spine would be measured using dual-energy X-ray one week before surgery. Fifty-four animals would undergo OVX (ovariectomy performed through the dorsal side) and six animals would undergo a sham surgery (normal procedure with no ovary removal). After all surgical procedures, the rabbits would be housed in the Pancoe-NorthShore University Health System Life Sciences Pavilion and cared for in compliance with the regulations established by the Northwestern University Institutional Animal Care and Use Committee. Animals would be examined for post-operative pain each day following the procedure until day 10, and then each week to assess signs of animal mobility, eating and drinking habits, changes in body weight, and appearance of surgical wounds. OVX animals would receive 0.6 mg/kg/day dexamethasone sodium phosphate intramuscularly after one week of OVX and up to 8 weeks. Sham animals would receive the same amount in saline. BMD would be measured again post-operatively at 4 and 8 weeks.

For VP/KP, animals would be randomly divided into three groups (n of 18): mPOC-60HA, Kyphon Activos 10 PMMA, and a control group. The mPOC-60HA and PMMA groups would undergo VP. Rabbits would be anesthetized and the L4 and L5 vertebral bodies would be identified and monitored under X-ray. A 14G bone marrow cannula would be inserted into the vertebrae at 1-2 mm and after reaching position would be filled with the appropriate bone cement (approximately 0.1-0.2 mL) and allowed to cure before having the cannula retract. Penicillin would be administered intramuscularly before surgery and three days after surgery to prevent infection. Animals would be housed in the Pancoe-NorthShore University Health System Life Sciences Pavilion, cared for in compliance with the regulations established by the Northwestern University Institutional Animal Care and Use Committee, and examined for post-operative pain, signs of animal mobility, eating and drinking habits, changes in body weight, and appearance of surgical wounds.

Rabbits would be euthanized at 4, 8, and 12 weeks and the L4 and L5 vertebral segments

removed and stripped of soft tissue. Vertebral samples would be scanned by micro-CT and reconstructed using a data analyzer under the same conditions. Histological samples would be acquired by fixing vertebral samples in 10% formalin and dehydrated in a series of ascending ethanol solutions. Samples would be embedded in PMMA, cut into 10-20  $\mu\text{m}$  sections using a diamond tissue microtome, and stained with methylene blue and basic fuchsin. Samples would be imaged using the Pathology Core Facility at Northwestern University, imaging slides at 40x using the Hamamatsu K.K. Nanozoomer 2.0 HT (Hamamatsu Photonics K.K., Hamamatsu, Shizuoka, Japan). Quantification of data would be determined in collaboration with the Pathology Core Facility but would involve assessing the tissue response at the bone-material interface, new bone quality, and bone ingrowth.

The model outlined above would offer important insight into the performance of mPOC-60HA and PMMA. Given the inherent disadvantages of PMMA that were addressed in Chapter 2, notably its high mechanical strength and inability to degrade, PMMA is hypothesized to primarily offer stability to the vertebra (though at a much higher value than the natural bone) and not promote any sufficient bone bonding or remodeling. On the other hand, mPOC-60HA is hypothesized to promote bone remodeling and more closely match the BMD of the osteoporotic vertebrae. Successful results from this study would elevate mPOC-60HA along its track to eventual human/clinical studies.

#### **6.2.4 *Ex Vivo* Vertebral Mechanics**

One of the most relevant experiments that can be performed to determine the compressive mechanics of the mPOC-xHA bone cements is to prepare an *ex vivo* mechanical compression study using osteoporotic human vertebrae or a bone foam substitute that closely mimics that of vertebrae. This was initially proposed, but due to available funding (and a lack of interest) it was quickly turned

down. For those interested in pursuing an *ex vivo* study, the vendors, quotes, and experimental designs are as follows.

Given expected results from the previously described *in vitro* and *in vivo* studies, it is hypothesized that the mPOC-60HA bone cements will perform the best compared to other composites. As such, mPOC-60HA and clinically relevant PMMA would be evaluated in an *ex vivo* study. Perry et. al. and Kim et. al. provide excellent experimental designs that would be closely followed for these experiments<sup>96,97</sup>. Ideally forty vertebral bodies within the T9 to L4 region would be harvested from osteoporotic cadaveric spines, cleaned of any excess soft tissue, and scanned by dual energy x-ray to determine BMD of specimens. Molds of the superior and inferior vertebral end plates would then be created using an epoxy filler (Bondo: Bondo Corp, Atlanta, GA) to create flat end plates that would distribute compressive mechanical forces evenly. Vertebral body volume can additionally be determined by Archimedean water displacement. For initial mechanical testing to establish a VCF, each vertebral body would be compressed at a rate of 0.5 mm per second using a hinged-plated device on an MTS/Sintech 20/G universal testing machine (Eden Prairie, MN) to create an anterior wedge fracture around 25% of the initial anterior height. Force and displacement data would be recorded.

Vertebral bodies would then be randomly assigned to one of three groups: mPOC-60HA, Kyphon Activos 10 PMMA, and a control (no cement). Kyphoplasty would be performed with a balloon tamp until initial vertebral height was achieved (KyphX bone tamp, Medtronic, Minneapolis, MN). Bone cements would be injected into the cancellous void to 25% volume fill and allowed to cure at 37°C for 24 hours. Samples would then be recompressed as before to obtain posttreatment data.

Osteoporotic cadaver bone could be acquired through Innoved Institute, LLC (Elk Grove Village, IL). They were previously contacted to determine a quote for all cadaver bones needed for

the experiment described above. This resource would be able to provide cleaned cadaver bones of a given region with the BMD determined in house, shipping to and from the experimental location, and the necessary medical waste materials. Alternatively, bone foam that mimics vertebral bodies could be acquired from Sawbones® (Vashon, WA). Sawbones® offers osteoporotic composite bone in a variety of bone types including L3 vertebrae. The developed osteoporotic composite bone has a thin cortical shell with a 10 pounds per cubic foot solid rigid polyurethane foam cancellous core that would be ideal for testing cement augmentation.

Table 6.2: Quote from Innoved Institute, LLC for Osteoporotic Vertebrae

<b>Component</b>	<b>Quantity</b>	<b>Rate (\$)</b>	<b>Amount (\$)</b>
Vertebral Bodies	40.00	350.00	14,000.00
Dual Energy X-Ray Absorptiometry (per scan)	6.00	200.00	1,200.00
Kit for Returning Specimens	1.00	40.00	40.00
IATA Compliant Large Packaging	1.00	92.00	92.00
Cremate/Returned Specimen (per lb)	100.00	2.85	285.00
Outbound Local Shipping (0-50 miles)	1.00	100.00	100.00
Return Local Shipping (0-50 miles)	1.00	100.00	100.00

It is hypothesized that both bone cement treatments will exceed the initial osteoporotic compressive mechanics. It is also hypothesized that PMMA will have a higher failure strength compared to mPOC-60HA composites as seen from initial mechanical compression data as presented in Chapter 3. mPOC-60HA would ideally more closely match the initial compressive mechanics of osteoporotic specimens. This study would have limitations given that it is not being performed directly in a clinical setting, but it would provide important information on how mPOC-60HA could perform in a clinical setting. If bone foam is used instead of osteoporotic cadaver bone, the results from that study may not be completely relevant as only the L3 vertebra could be tested instead of a range of lumbar and thoracic vertebrae, there would be little variance in BMD and structure, and the bone foam is a close approximation of natural bone. While the results would be insightful, and

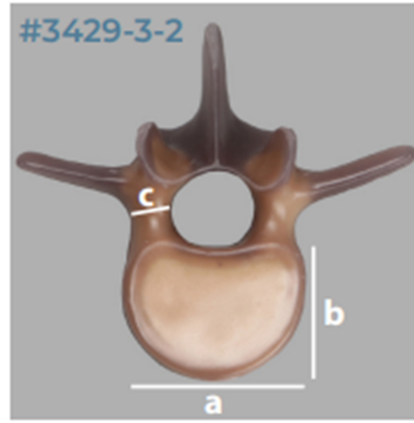


Figure 6.1: Sawbones® individual composite L3 vertebrae with 10 pounds per cubic foot (0.16 g/cc) density solid foam cancellous- polyurethane core (product #3429-3-2). Dimensions are a) 48 mm, b) 35 mm, and c) 11 mm. Pedicle height is 16 mm.

would cost less, the impact would be less valuable when compared to other similar experiments utilizing cadaver bone.

### 6.2.5 Research Necessary for FDA Approval

The pinnacle achievement of the work presented in this thesis would be to acquire FDA approval for use of mPOC-xHA as a bone cement. This material would likely be classified as a class II (special controls) medical device based on the current standard PMMA being classified as such as well as the recent 510(k) approval of Citregen™ and Citrelock™ from Acuitive Technologies<sup>98</sup>. mPOC-xHA would also likely follow similar testing requirements as those required for PMMA, given that they are both recognized as bone cements based off of “methylmethacrylate, polymethylmethacrylate, esters of methacrylic acid, or copolymers containing polymethylmethacrylate and polystyrene,” therefore making mPOC-xHA substantially equivalent to PMMA<sup>99</sup>. Specifically,

ASTM F451-16 regarding the Standard Specification for Acrylic Bone Cement, ASTM F983-86 regarding the Standard Practice for Permanent Marking of Orthopaedic Implant Components, and ASTM F565-04 regarding the Standard Practice for Care and Handling of Orthopedic Implants and Instruments should be followed when developing and testing mPOC-xHA<sup>100</sup>. Further research may need to be performed to address the biocompatibility of the chosen mPOC-xHA formulation following ISO-10993 for blood-contacting, long-term implanted devices. PMMA and mPOC-xHA cements should be compared for all physical and chemical characterizations of the cement; The mixing and application of the cement, working, and setting times following ASTM 451 and ISO 5833 should be addressed; The main components found in mPOC-xHA should be identified and quantified, with residual monomer levels and elution of monomers during mixing and after polymerization being determined via gas chromatography; The molecular weight should be established by gel permeation chromatography or solution viscosity measurements and the degree of polymerization should be determined; The HA morphology, size distribution, and dispersion should be addressed by SEM. Mechanical testing that should be addressed include several *in vitro* testing methods as described in ASTM F451-99 (Standard Specifications for Acrylic Bone Cement) which includes testing for modulus, fatigue, fracture toughness, fatigue crack propagation, flexural strength, compressive strength, shear strength, tensile strength, and creep compared to PMMA. The morphology of the fracture surface should be analyzed for porosity of the fractured surface and bulk material, dispersion of additives at the fractured surface, and failure analysis of the fractured surface. A description of variables including mixing, centrifugation, method of mixing, molding, machining, finishing effects, and aging/curing that may affect the *in vitro* data should also be included for PMMA and mPOC-xHA. A shelf-life should be established using an accelerated stability testing protocol that monitors the physical and mechanical properties of the cement as it progresses to its intended shelf-life. Finally, sterilization methods should be provided within a

summary outlining the type of sterilization method used and at what dose.

### **6.3 Significance and Outlook**

These proposed experiments and the results presented in this thesis provide an essential foundation for mPOC-xHA to be further tested and analyzed for use in orthopedic engineering. The ability for the bone cements to cure *in situ* without the disadvantages of PMMA is highly desired not only for its handling characteristics, but also its ability to integrate into and promote regeneration in surrounding tissues. Introducing an alternative bone cement based off of components already inherently contained within the bone matrix provides an advantageous material for many orthopedic tissue engineering applications.

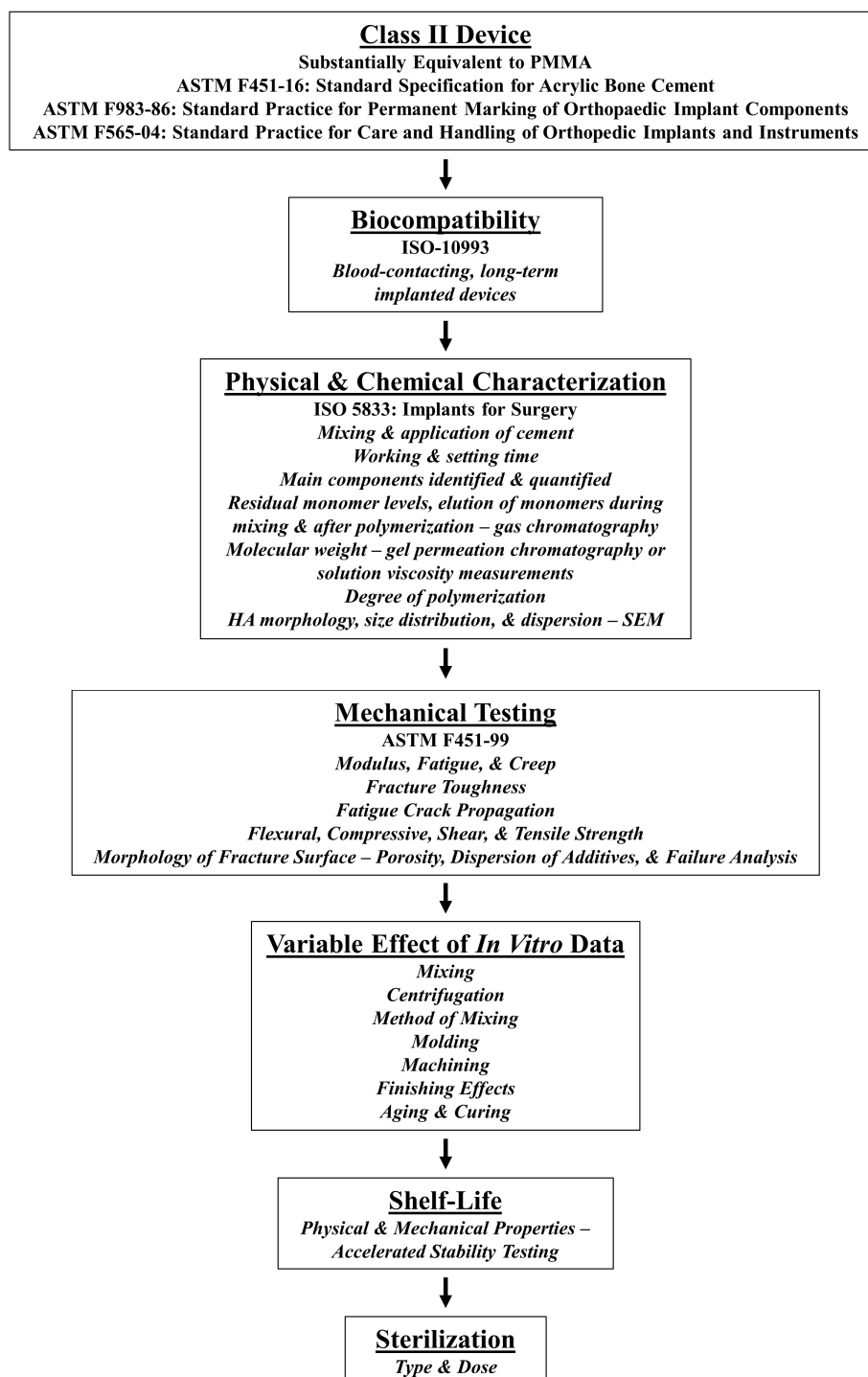


Figure 6.2: Flowchart of the necessary experiments and data required for FDA approval of a substantially equivalent Class II Device.



## REFERENCES

1. Vaishya, R., Chauhan, M. & Vaish, A. Bone cement. *Journal of Clinical Orthopaedics and Trauma* **4**, 157–163 (2013).
2. Kuhn, K.-D. in *The Well-Cemented Total Hip Arthroplasty: Theory and Practice* 52–59 (Springer Berlin Heidelberg, Berlin, Heidelberg, 2005). ISBN: 978-3-540-28924-1.
3. Webb, J. C. J. & Spencer, R. F. The role of polymethylmethacrylate bone cement in modern orthopaedic surgery. *The Journal of Bone and Joint Surgery. British volume* **89-B**, 851–857 (2007).
4. Wang, Y., Ameer, G., Sheppard, B. & Langer, R. A tough biodegradable elastomer. *Nature Biotechnology* **20**, 602–606 (2002).
5. Howard, D., Buttery, L. D., Shakesheff, K. M. & Roberts, S. J. Tissue engineering: strategies, stem cells and scaffolds. *Journal of Anatomy* **213**, 66–72 (2008).
6. Goldenberg, D., McLaughlin, C., Koduru, S. V. & Ravnic, D. J. Regenerative Engineering: Current Applications and Future Perspectives. *Frontiers in Surgery* **8** (2021).
7. Junqueira, L. C., Carneiro, J., Foltin, J., Lebowitz, H. & Boyle, P. J. in *Basic Histology, Text and Atlas* 10th, 144 (McGraw Hill Companies, 2003). ISBN: 978-0-07-137829-1.
8. Bilezikian, J., Raisz, L. & Rodan, G. in *Principles of bone biology* 2nd (Academic Press, San Diego, CA, 2002). ISBN: 9780080539607.
9. Matsuo, K. & Irie, N. Osteoclast–osteoblast communication. *Archives of Biochemistry and Biophysics* **473**. Highlight Issue: Bone Remodeling: Facts and Perspectives, 201–209 (2008).
10. Väänänen, H. K. & Laitala-Leinonen, T. Osteoclast lineage and function. *Archives of Biochemistry and Biophysics* **473**. Highlight Issue: Bone Remodeling: Facts and Perspectives, 132–138 (2008).
11. Toole, B. & Linsenmayer, T. Newer knowledge of skeletogenesis: Macromolecular transitions in the extracellular matrix. *Clinical Orthopaedics and Related Research* **129**, 258–278 (1977).

12. Franz-Odenaal, T. A., Hall, B. K. & Witten, P. E. Buried alive: How osteoblasts become osteocytes. *Developmental Dynamics* **235**, 176–190 (2006).
13. Ferrone, M. L. & Schoenfeld, A. J. in *Principles of Orthopedic Practice for Primary Care Providers* (eds Katz, J. N., Blauwet, C. A. & Schoenfeld, A. J.) 63–72 (Springer International Publishing, Cham, 2018). ISBN: 978-3-319-68661-5.
14. Ballane, G., Cauley, J., Luckey, M. & El-Hajj Fuleihan, G. Worldwide prevalence and incidence of osteoporotic vertebral fractures. *Osteoporosis International* **28**, 1531–1542 (2017).
15. Beall, D. P. *et al.* Prospective and Multicenter Evaluation of Outcomes for Quality of Life and Activities of Daily Living for Balloon Kyphoplasty in the Treatment of Vertebral Compression Fractures: The EVOLVE Trial. *Neurosurgery* **84**, 169–178 (2019).
16. Donnally III, C., DiPompeo, C. & Varacallo, M. in (StatPearls Publishing, 2022).
17. Lindsay, R. *et al.* Risk of New Vertebral Fracture in the Year Following a Fracture. *JAMA* **285**, 320–323 (2001).
18. Silverman, S. The clinical consequences of vertebral compression fracture. *Bone* **13**, S27–31 (1992).
19. McCarthy, J. & Davis, A. Diagnosis and Management of Vertebral Compression Fractures. *Am Fam Physician* **94**, 44–50 (2016).
20. Alexandru, D. & So, W. Evaluation and management of vertebral compression fractures. *Perm J.* **16**, 46–51 (2012).
21. Edidin, A. A., Ong, K. L., Lau, E. & Kurtz, S. M. Morbidity and Mortality After Vertebral Fractures. *Spine* **40**, 1228–1241 (2015).
22. Burton, A., Rhines, L. & Mendel, E. Vertebroplasty and kyphoplasty: a comprehensive review. *Neurosurg Focus* **18** (2005).
23. Donkerwolcke, M., Burny, F. & Muster, D. Tissues and bone adhesives—historical aspects. *Biomaterials* **19**, 1461–1466 (1998).
24. Lewis, G. Injectable bone cements for use in vertebroplasty and kyphoplasty: State-of-the-art review. *Journal of Biomedical Materials Research Part B: Applied Biomaterials* **76B**, 456–468 (2006).

25. Brown, W. in *Environmental phosphorus handbook* 203–239 (John Wiley and Sons, New York, 1973). ISBN: 9780471327790.
26. Friedman, C. D., Costantino, P. D., Takagi, S. & Chow, L. C. BoneSource™ hydroxyapatite cement: A novel biomaterial for craniofacial skeletal tissue engineering and reconstruction. *Journal of Biomedical Materials Research* **43**, 428–432 (1998).
27. Constantz, B. R. *et al.* Skeletal Repair by in Situ Formation of the Mineral Phase of Bone. *Science* **267**, 1796–1799 (1995).
28. He, Z. *et al.* Bone cements for percutaneous vertebroplasty and balloon kyphoplasty: Current status and future developments. *Journal of Orthopaedic Translation* **3**, 1–11 (2015).
29. Eliaz, N. & Metoki, N. Calcium Phosphate Bioceramics: A Review of Their History, Structure, Properties, Coating Technologies and Biomedical Applications. *Materials* **10** (2017).
30. Kimes, M. *Bad to the bone: A medical horror story* Last accessed April 2022. 2012.
31. Charnley, J. ANCHORAGE OF THE FEMORAL HEAD PROSTHESIS TO THE SHAFT OF THE FEMUR. *The Journal of Bone and Joint Surgery. British volume* **42-B**. PMID: 13855642, 28–30 (1960).
32. Hamajima, K. *et al.* The Effect of TBB, as an Initiator, on the Biological Compatibility of PMMA/MMA Bone Cement. *International Journal of Molecular Sciences* **21** (2020).
33. Lai, P., Chen, L., Chen, W. & Chu, I. Chemical and physical properties of bone cement for vertebroplasty. *Biomed J* **36**, 162–7 (2013).
34. Ratner, B., Hoffman, A., Schoen, F. & Lemons, J. *Biomaterials Science: An Introduction to Materials in Medicine* 3rd. ISBN: 9780080877808 (Academic Press, 2012).
35. Boger, A., Bohner, M., Heini, P., Verrier, S. & Schneider, E. Properties of an injectable low modulus PMMA bone cement for osteoporotic bone. *Journal of Biomedical Materials Research Part B: Applied Biomaterials* **86B**, 474–482 (2008).
36. Alekhin, M., Ter-Akopian, A., Abramov, A. & Skripnikova, A. [Intracardiac and Pulmonary Cement Embolism after Percutaneous Vertebroplasty]. *Kardiologiya* **59**, 92–96 (Apr. 2019).
37. Fadili Hassani, S. *et al.* Intracardiac cement embolism during percutaneous vertebroplasty: incidence, risk factors and clinical management. *European radiology* **29**, 663–673 (2019).

38. D'Errico, S., Niballi, S. & Bonuccelli, D. Fatal cardiac perforation and pulmonary embolism of leaked cement after percutaneous vertebroplasty. *Journal of Forensic and Legal Medicine* **63**, 48–51 (2019).
39. Ali, U., Karim, K. J. B. A. & Buang, N. A. A Review of the Properties and Applications of Poly (Methyl Methacrylate) (PMMA). *Polymer Reviews* **55**, 678–705. eprint: <https://doi.org/10.1080/15583724.2015.1031377> (2015).
40. Bokam, P. *et al.* Fracture behavior of cancellous bone and cancellous bone-PMMA bone cement interface: An experimental study using an integrated methodology (wedge splitting test and Heaviside-based digital image correlation). *Journal of the Mechanical Behavior of Biomedical Materials* **122**, 104663 (2021).
41. Rajah, G. *et al.* Predictors of delayed failure of structural kyphoplasty for pathological compression fractures in cancer patients. *Journal of Neurosurgery: Spine SPI* **23**, 228–232 (2015).
42. Tavakoli, M., Bakhtiari, S. S. E. & Karbasi, S. Incorporation of chitosan/graphene oxide nanocomposite in to the PMMA bone cement: Physical, mechanical and biological evaluation. *International Journal of Biological Macromolecules* **149**, 783–793 (2020).
43. Zheng, X. *et al.* Gelatin/gentamicin sulfate-modified PMMA bone cement with proper mechanical properties and high antibacterial ability. *Mater. Res. Express* **9** (2022).
44. Tham, D. Q. *et al.* PMMA Bone Cements Modified with Silane-Treated and PMMA-Grafted Hydroxyapatite Nanocrystals: Preparation and Characterization. *Polymers* **13** (2021).
45. Dubey, U., Kesarwani, S. & Verma, R. K. Incorporation of graphene nanoplatelets/hydroxyapatite in PMMA bone cement for characterization and enhanced mechanical properties of biopolymer composites. *Journal of Thermoplastic Composite Materials* **0**, 08927057221086833. eprint: <https://doi.org/10.1177/08927057221086833> (0).
46. Qiu, H., Yang, J., Kodali, P., Koh, J. & Ameer, G. A. A citric acid-based hydroxyapatite composite for orthopedic implants. *Biomaterials* **27**, 5845–5854 (2006).
47. Hu, Y.-Y., Rawal, A. & Schmidt-Rohr, K. Strongly bound citrate stabilizes the apatite nanocrystals in bone. *Proceedings of the National Academy of Sciences* **107**, 22425–22429 (2010).

48. Ma, C. *et al.* Citrate-based materials fuel human stem cells by metabonegenic regulation. *Proceedings of the National Academy of Sciences* **115**, E11741–E11750 (2018).
49. Kattimani, V. S., Kondaka, S. & Lingamaneni, K. P. Hydroxyapatite—Past, Present, and Future in Bone Regeneration. *Bone and Tissue Regeneration Insights* **7**, BTRI.S36138. eprint: <https://doi.org/10.4137/BTRI.S36138> (2016).
50. Yang, J., Webb, A. & Ameer, G. Novel Citric Acid-Based Biodegradable Elastomers for Tissue Engineering. *Advanced Materials* **16**, 511–516 (2004).
51. Yang, J., Webb, A. R., Pickerill, S. J., Hageman, G. & Ameer, G. A. Synthesis and evaluation of poly(diols citrate) biodegradable elastomers. *Biomaterials* **27**, 1889–1898 (2006).
52. Prabhakaran, M. P., Nair, A. S., Kai, D. & Ramakrishna, S. Electrospun composite scaffolds containing poly(octanediol-co-citrate) for cardiac tissue engineering. *Biopolymers* **97**, 529–538 (2012).
53. Zou, F., Sun, X. & Wang, X. Elastic, hydrophilic and biodegradable poly (1, 8-octanediol-co-citric acid)/polylactic acid nanofibrous membranes for potential wound dressing applications. *Polymer Degradation and Stability* **166**, 163–173 (2019).
54. Tran, R. T. *et al.* Synthesis and characterization of biomimetic citrate-based biodegradable composites. *Journal of Biomedical Materials Research Part A* **102**, 2521–2532 (2014).
55. Wang, C. *et al.* A bioactive injectable self-healing anti-inflammatory hydrogel with ultra-long extracellular vesicles release synergistically enhances motor functional recovery of spinal cord injury. *Bioactive Materials* **6**, 2523–2534 (2021).
56. Chen, F., Song, Z., Gao, L., Hong, H. & Liu, C. Hierarchically macroporous/mesoporous POC composite scaffolds with IBU-loaded hollow SiO<sub>2</sub> microspheres for repairing infected bone defects. *J. Mater. Chem. B* **4**, 4198–4205 (23 2016).
57. Zeimaran, E. *et al.* Fabrication and characterization of poly (octanediol citrate)/gallium-containing bioglass microcomposite scaffolds. *J Mater Sci* **50**, 1–13 (Jan. 2015).
58. Tran, R. T. *et al.* Synthesis and characterization of a biodegradable elastomer featuring a dual crosslinking mechanism. *Soft Matter* **6**, 2449–2461 (11 2010).
59. Tran, R. T., Yang, J. & Ameer, G. A. Citrate-Based Biomaterials and Their Applications in Regenerative Engineering. *Annual Review of Materials Research* **45**, 277–310 (2015).

60. Begun, C. *Acuitive Technologies Granted FDA 510(k) Clearance for CITREGEN(TM) CITRELOCK(TM) Tendon Interference Screw System* Last accessed June 2021. 2020.
61. Wako Pure Chemical Industries, L. *Azo polymerization initiators comprehensive catalog*
62. Wang, W. & Yeung, K. W. Bone grafts and biomaterials substitutes for bone defect repair: A review. *Bioactive Materials* **2**, 224–247 (2017).
63. Zhao, R. *et al.* Selective effect of hydroxyapatite nanoparticles on osteoporotic and healthy bone formation correlates with intracellular calcium homeostasis regulation. *Acta Biomaterialia* **59**, 338–350 (2017).
64. Sobczyk-Guzenda, A., Boniecka, P., Laska-Lesniewicz, A., Makowka, M. & Szymanowski, H. Micro- and Nanoparticulate Hydroxyapatite Powders as Fillers in Polyacrylate Bone Cement—A Comparative Study. *Materials* **13** (2020).
65. Funk, D., Nguyen, Q. & Swank, M. Polymethyl methacrylate cure time in simulated in vivo total knee arthroplasty versus in vitro conditions. *Journal Orthopedic Surgery Research* **16**, 629 (2021).
66. Jayabalan, M., Shalumon, K. & Mitha, M. Injectable biomaterials for minimally invasive orthopedic treatments. *Journal of Material Science: Material Medicine* **20**, 1379–1387 (6 2009).
67. Babaie, E., Lin, B., Goel, V. & Bhaduri, S. Evaluation of amorphous magnesium phosphate (AMP) based non-exothermic orthopedic cements. *Biomedical Materials* **11**, 055010 (2016).
68. Woo, K. M., Yu, B., Jung, H.-M. & Lee, Y.-K. Comparative evaluation of different crystal-structured calcium sulfates as bone-filling materials. *Journal of Biomedical Materials Research Part B: Applied Biomaterials* **91B**, 545–554 (2009).
69. Jiao, Y. *et al.* A rheological study of biodegradable injectable PEGMC/HA composite scaffolds. *Soft Matter* **8**, 1499–1507 (5 2012).
70. Chiou, B.-S., Raghavan, S. R. & Khan, S. A. Effect of Colloidal Fillers on the Cross-Linking of a UV-Curable Polymer: Gel Point Rheology and the WinterChambon Criterion. *Macromolecules* **34**, 4526–4533 (2001).

71. Raghavan, S. R. *et al.* Rheological study of crosslinking and gelation in chlorobutyl elastomer systems. *Polymer* **37**, 5869–5875 (1996).
72. Hughes, E. A., Parkes, A., Williams, R. L., Jenkins, M. J. & Grover, L. M. Formulation of a covalently bonded hydroxyapatite and poly(ether ether ketone) composite. *Journal of tissue engineering* **9** (2018).
73. Chen, Z. *et al.* What are risk factors for subsequent fracture after vertebral augmentation in patients with thoracolumbar osteoporotic vertebral fractures. *BMC Musculoskeletal Disorders* **22** (2021).
74. Li, W., Long, C., Tam, V. W., Poon, C.-S. & Hui Duan, W. Effects of nano-particles on failure process and microstructural properties of recycled aggregate concrete. *Construction and Building Materials* **142**, 42–50 (2017).
75. Mahmood, R. & Kockal, N. Nanoparticles used as an ingredient in different types of concrete. *SN Appl. Sci.* **3**, 529 (2021).
76. Komang-Agung, I. S., Hydravianto, L., Sindrawati, O. & William, P. S. Effect of Polymethylmethacrylate-Hydroxyapatite Composites on Callus Formation and Compressive Strength in Goat Vertebral Body. *Malaysian orthopaedic journal* **12** (2018).
77. Morgan, E. F., Unnikrisnan, G. U. & Hussein, A. I. Bone Mechanical Properties in Healthy and Diseased States. *Annual Review of Biomedical Engineering* **20**. PMID: 29865872, 119–143 (2018).
78. Cesar, R. *et al.* Axial compressive strength of human vertebrae trabecular bones classified as normal, osteopenic and osteoporotic by quantitative ultrasonometry of calcaneus. *Research on Biomedical Engineering* **33**, 91–96 (2017).
79. Lin, G., Cosimbescu, L., Karin, N. & Tarasevich, B. Injectable and thermosensitive PLGA-g-PEG hydrogels containing hydroxyapatite: preparation, characterization and in vitro release behavior. *Biomedical Materials* **7**, 024107 (2012).
80. Yan, J. *et al.* Injectable alginate/hydroxyapatite gel scaffold combined with gelatin microspheres for drug delivery and bone tissue engineering. *Materials Science and Engineering: C* **63**, 274–284 (2016).
81. Ma, C. *et al.* In vitro cytocompatibility evaluation of poly(octamethylene citrate) monomers toward their use in orthopedic regenerative engineering. *Bioactive Materials* **3**, 19–27 (2018).

82. Webster, T. J., Siegel, R. W. & Bizios, R. Osteoblast adhesion on nanophase ceramics. *Biomaterials* **20**, 1221–1227 (1999).
83. Council, N. R. *Guide for the Care and Use of Laboratory Animals* (The National Academies Press, Washington, DC, 1996).
84. Heikkilä, J., Aho, A., Kangasniemi, I. & Yli-Urpo, A. Polymethylmethacrylate composites: disturbed bone formation at the surface of bioactive glass and hydroxyapatite. *Biomaterials* **17**, 1755–1760 (1996).
85. Shi, H. *et al.* Hydroxyapatite Based Materials for Bone Tissue Engineering: A Brief and Comprehensive Introduction. *Crystals* **11** (2021).
86. Şerbetçi, K. & Hasirci, N. in, 241–386 (Oct. 2003). ISBN: 978-0-8247-4294-2.
87. Giunti, A., Moroni, A., Olmi, R. & Vicenzi, G. Composite acrylic cement with added hydroxyapatite: a study of the polymerization temperature. *Italian Journal of Orthopaedics and Traumatology* **9**, 369–375 (1983).
88. Castaldini, A. & Cavallini, A. Setting properties of bone cement with added synthetic hydroxyapatite. *Biomaterials* **6**, 55–60 (1985).
89. Park, H. C., Liu, Y. K. & Lakes, R. S. The Material Properties of Bone-Particle Impregnated PMMA. *Journal of Biomechanical Engineering* **108**, 141–148 (1986).
90. Yang, J.-M., Lu, C.-S., Hsu, Y.-G. & Shih, C.-H. Mechanical properties of acrylic bone cement containing PMMA-SiO<sub>2</sub> hybrid sol-gel material. *Journal of Biomedical Materials Research* **38**, 143–154 (1997).
91. Beruto, D. T., Botter, R. & Fini, M. The effect of water in inorganic microsponges of calcium phosphates on the porosity and permeability of composites made with polymethylmethacrylate. *Biomaterials* **23**, 2509–2517 (2002).
92. Yang, J.-M., You, J.-W., Chen, H.-L. & Shih, C.-H. Calorimetric characterization of the formation of acrylic type bone cements. *Journal of Biomedical Materials Research* **33**, 83–88 (1996).
93. Inada, M., Matsumoto, C. & Miyaura, C. [Animal models for bone and joint disease. Ovariectomized and orchidectomized animals]. *Clinical calcium* **21** **2**, 164–70 (2011).



94. Zhu, J. *et al.* Bioactive poly (methyl methacrylate) bone cement for the treatment of osteoporotic vertebral compression fractures. *Theranostics* **10**, 6544–6560 (2020).
95. Chen, J. *et al.* A novel injectable porous surface modified bioactive bone cement for vertebroplasty: an in vivo biomechanical and osteogenic study in a rabbit osteoporosis model. *American Journal of Translational Research* **7**, 548–57 (2015).
96. Perry, A. *et al.* Biomechanical evaluation of kyphoplasty with calcium sulfate cement in a cadaveric osteoporotic vertebral compression fracture model. *The Spine Journal* **5**, 489–493 (2005).
97. Kim, C. *et al.* Biomechanical evaluation of an injectable radiopaque polypropylene fumarate cement for kyphoplasty in a cadaveric osteoporotic vertebral compression fracture model. *Journal of Spinal Disorders and Techniques* **20**, 604–609 (2007).
98. *Citregen Tendon Interference Screw And Citrelock* Last accessed March 2022. 2020.
99. *Polymethylmethacrylate (PMMA) Bone Cement - Class II Special Controls Guidance Document for Industry and FDA* Last accessed March 2022. 2002.
100. *Product Classification for Orthopedic Bone Cements* Last accessed March 2022.
101. Oryan, A., Kamali, A. & Moshiri, A. Potential mechanisms and applications of statins on osteogenesis: Current modalities, conflicts and future directions. *Journal of Controlled Release* **215**, 12–24 (2015).
102. Shah, S. R., Werlang, C. A., Kasper, F. K. & Mikos, A. G. Novel applications of statins for bone regeneration. *National Science Review* **2**, 85–99 (2014).

**BODY HEAT-ACTIVATED POLYMER-MINERAL COMPOSITES FOR VERTEBRAL  
BODY FRACTURES**

Approved by:

Guillermo Ameer  
Biomedical Engineering  
*United States*

Evan Scott  
Biomedical Engineering  
*United States*

Shu Liu  
Biomedical Engineering  
*United States*

Jason Koh  
NorthShore University HealthSystem  
*United States*

Date Approved: May 27, 2022

## APPENDIX A

### APPENDIX

#### A.1 Adjusted POC Synthesis

Prior to use of mPOC in the above work, the synthesis of POC and mPOC was addressed. It was noticed within the NMR spectrums that POC and mPOC contained some unnecessary aromatic groups and residual compounds such as ethanol and THF that should not necessarily be present (Figure SA.1). First, POC was dissolved in THF instead of ethanol during the first day of synthesis which resulted in an elimination of the ethanol peaks seen in subsequent POC and mPOC NMR readings as well as increasing the yield of POC acquired for the next step of synthesis (Figure SA.2). Next, the catalyst used during the synthesis for mPOC (imidazole) was tested and compared to an alternative catalyst, 4-Dimethylaminopyridine (DMAP) (Figure SA.3). DMAP was hypothesized to be more efficient in attaching methacrylate groups to the POC polymer chain. It was initially noted that there were minimal methacrylate groups attaching to POC, meaning that monomer units of glycidyl methacrylate were floating within the POC polymer but not integrating into the structure. These free monomer units may have been causing the early cell cytotoxicity effects in early POC culture results. The switch to DMAP, as well as multiple washes of the polymer, may lessen the cytotoxicity. Time of synthesis of mPOC was increased from 6 hours to 24, 72, and 168 hours (1, 3, and 7 days) to determine if the level of methacrylation increased or had any effect on the polymer's mechanical compression characteristics (Figure SA.4). Methacrylation seemed to have increased while synthesizing for 24 hours, though additional days of synthesis resulted in weaker compressive mechanics. Through running ESI on DMAP and imidazole mPOC samples it

was noted that both fall within 750-1000 m/z (Figure SA.5). Most structures are octanediol-citric acid with either normal or transesterified glycidyl methacrylate attached to either octanediol or citric acid molecules. Chromatography was eventually used to strip out any unreacted monomer units and unreacted aromatic structures, as seen from the final synthesis presented in Chapter 3. The chromatography step was adjusted to only use distilled THF as it was found that trace amounts of butylated hydroxytoluene (BHT) appeared in the NMR spectrum when using non-distilled THF (Figures SA.6 and SA.7). To address the effect of monomer ratios on compressive mechanics, mPOC samples with a 1.2:1 octanediol: citric acid ratio was synthesized (Table A.1).

Table A.1: Summary of mechanical characteristics of various synthesis conditions for mPOC. Statistical significance is not calculated for this table given that the n number differs between groups.

<b>Formulation</b>	<b>Young's Modulus (MPa)</b>	<b>N</b>
6-Hr Synthesis mPOC-DMAP	49.3 ± 3.94	4
24-Hr Synthesis mPOC-DMAP	62.1 ± 10.3	4
72-Hr Synthesis mPOC-DMAP	190.1 ± 6.88	4
168-Hr Synthesis mPOC-DMAP	61.2	1
1.2:1 Octanediol: Citric Acid mPOC	48.6 ± 6.45	6

Initial mPOC polymerization involved ethyl acetate as the mixing solvent. This initial solvent was compared to ethanol, which is miscible in water, as it was hypothesized that ethanol may be a more cytocompatible solvent than ethyl acetate. L929 fibroblast cells were prepared and seeded at 10,000 cells per well in a 96 well plate following ISO 10993. Cells were exposed to various extract concentrations and allowed to incubate over 24 hours. It was found that the mPOC samples mixed with ethanol had better viability than those with no solvent or ethyl acetate as the solvent. Additional cell studies that included mPOC-xHA extracts with ethanol followed, reinforcing that switching to ethanol would be advantageous for cell survival. Cell cytotoxicity studies were also performed for 24-, 48-, and 72-hour crosslinked mPOC scaffolds as well as a 5% V70 (initiator)

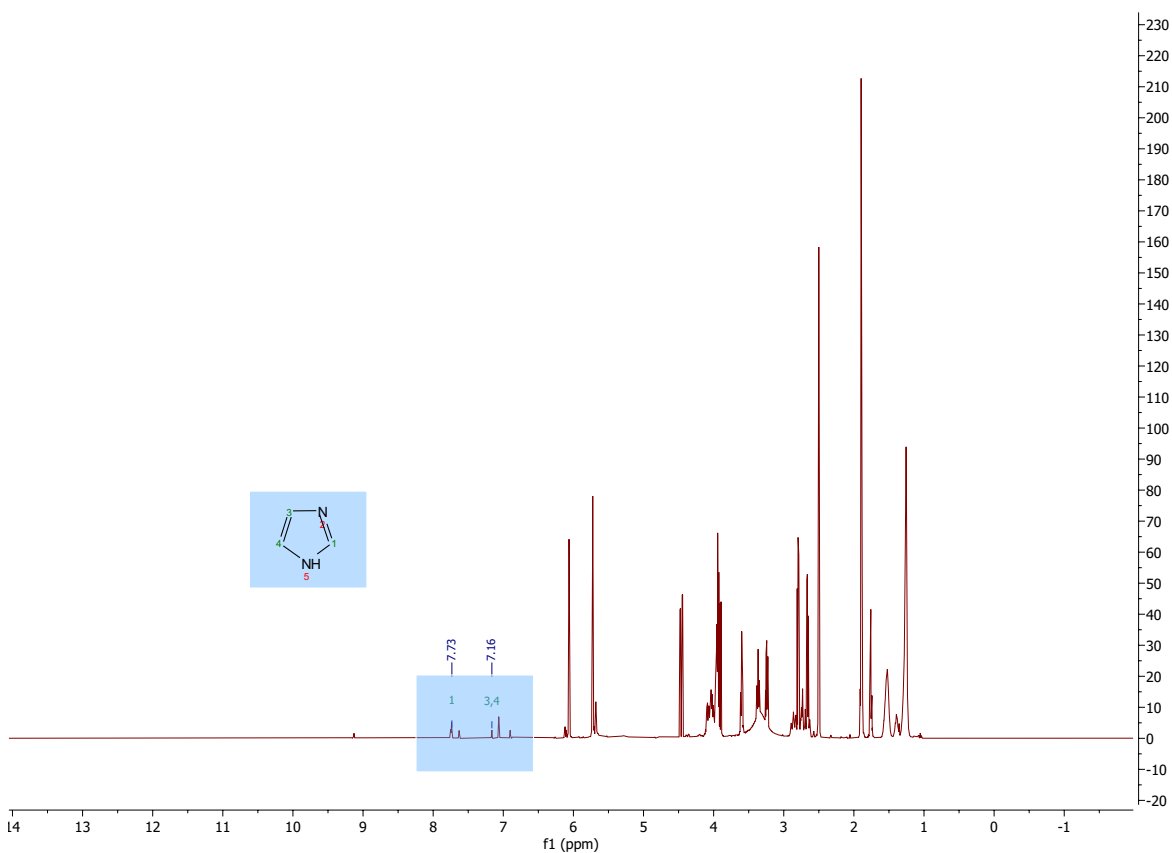


Figure S A.1:  $^1\text{H}$  NMR spectra of mPOC synthesized with imidazole. Imidazole (inset structure) is not completely removed from the mPOC after synthesis and purification as seen by the highlighted (blue) peaks present at 7.73 and 7.16 ppm. These aromatic groups are unnecessary within the purified mPOC structure, thus further purification steps and a reworking of the mPOC synthesis were pursued to obtain an optimized mPOC.

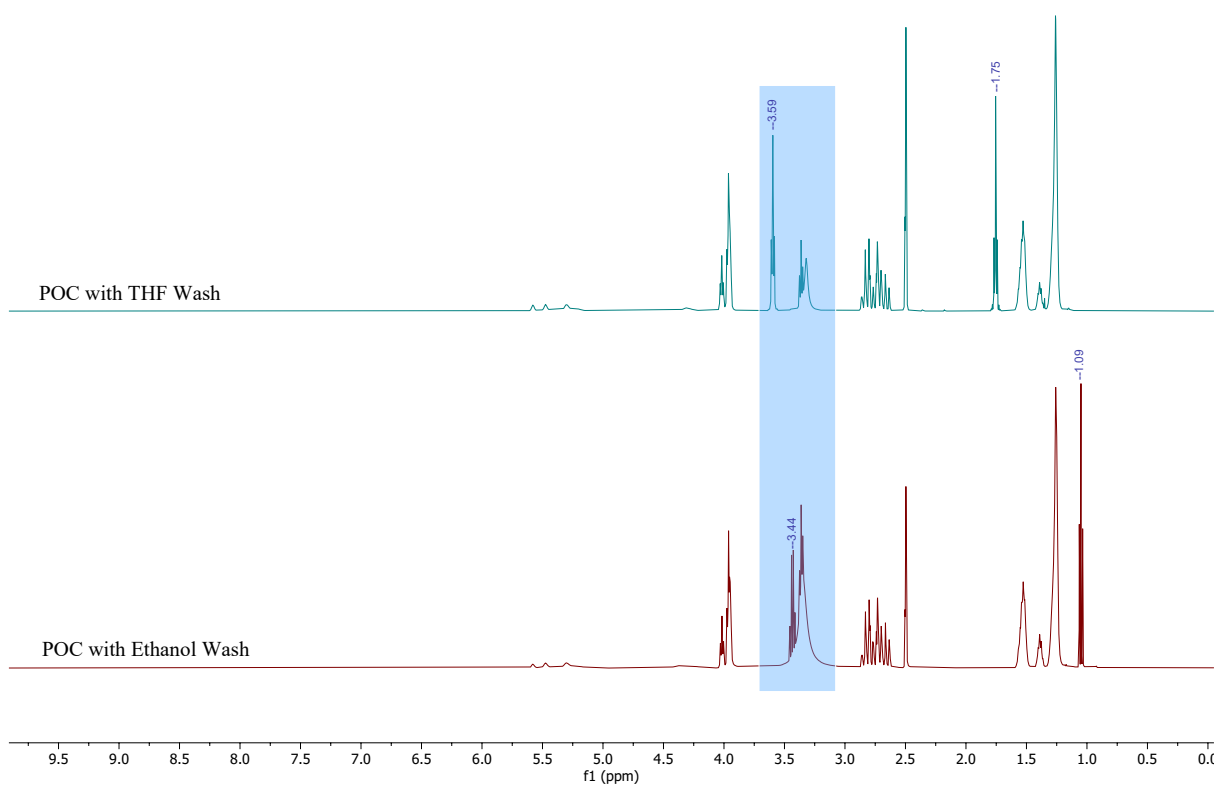


Figure S A.2: <sup>1</sup>H NMR spectra of POC washed in THF or ethanol. During the original synthesis of POC, the polymer is dissolved in ethanol before distilling the polymer in DI water. While the use of ethanol in this step does not impact the use of POC for further applications, it can affect further synthesis steps for mPOC. As such, ethanol was replaced by THF as THF is the primary solvent used during mPOC synthesis, resulting in distinct peaks at 3.59 and 1.75 ppm for the POC-THF workup. Ethanol peaks can be seen at 3.44 and 1.05 ppm.

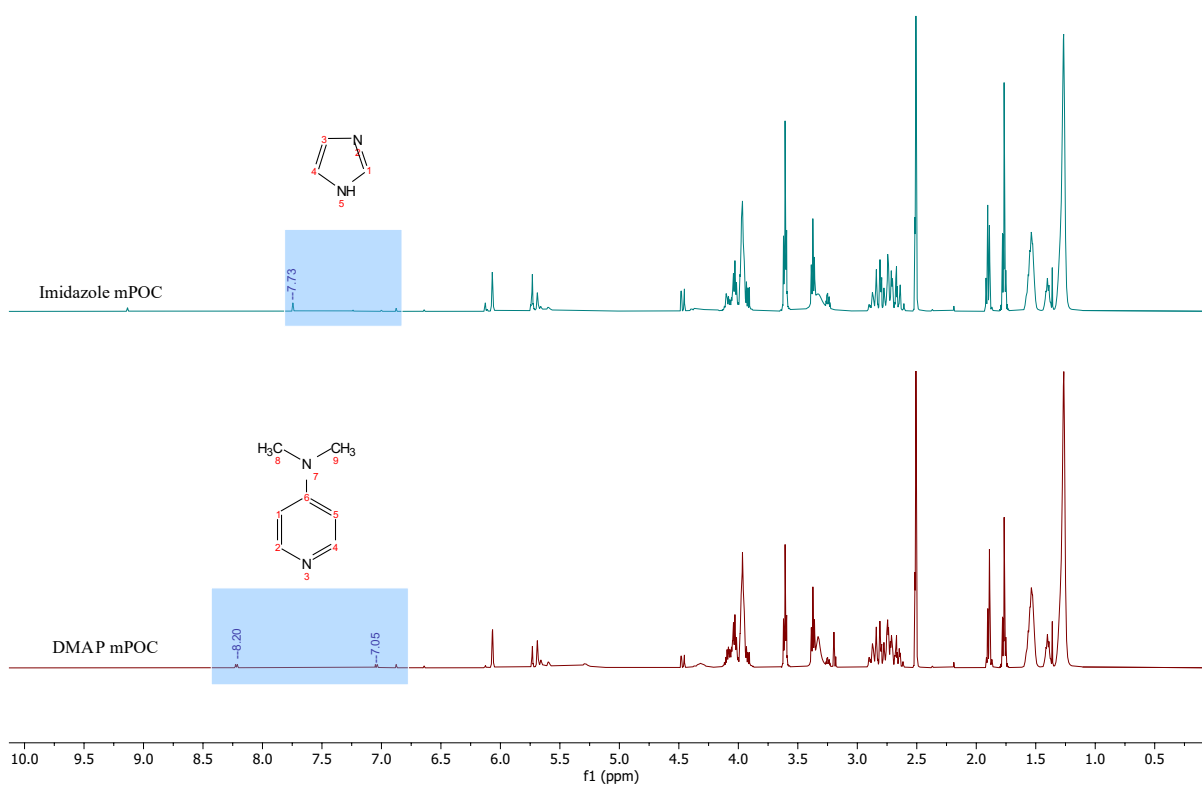


Figure S A.3: <sup>1</sup>H NMR spectra of mPOC with either imidazole or DMAP used as the ring-opening catalyst during mPOC synthesis. <sup>1</sup>H NMR spectra of both imidazole mPOC and DMAP mPOC are similar, except for the presence of aromatic groups associated with imidazole at 7.73 ppm and DMAP at 8.20 and 7.05 ppm. Using DMAP was hypothesized to increase the efficiency of attachment of methacrylate groups to the POC structure, potentially decreasing the amount of synthesis time.

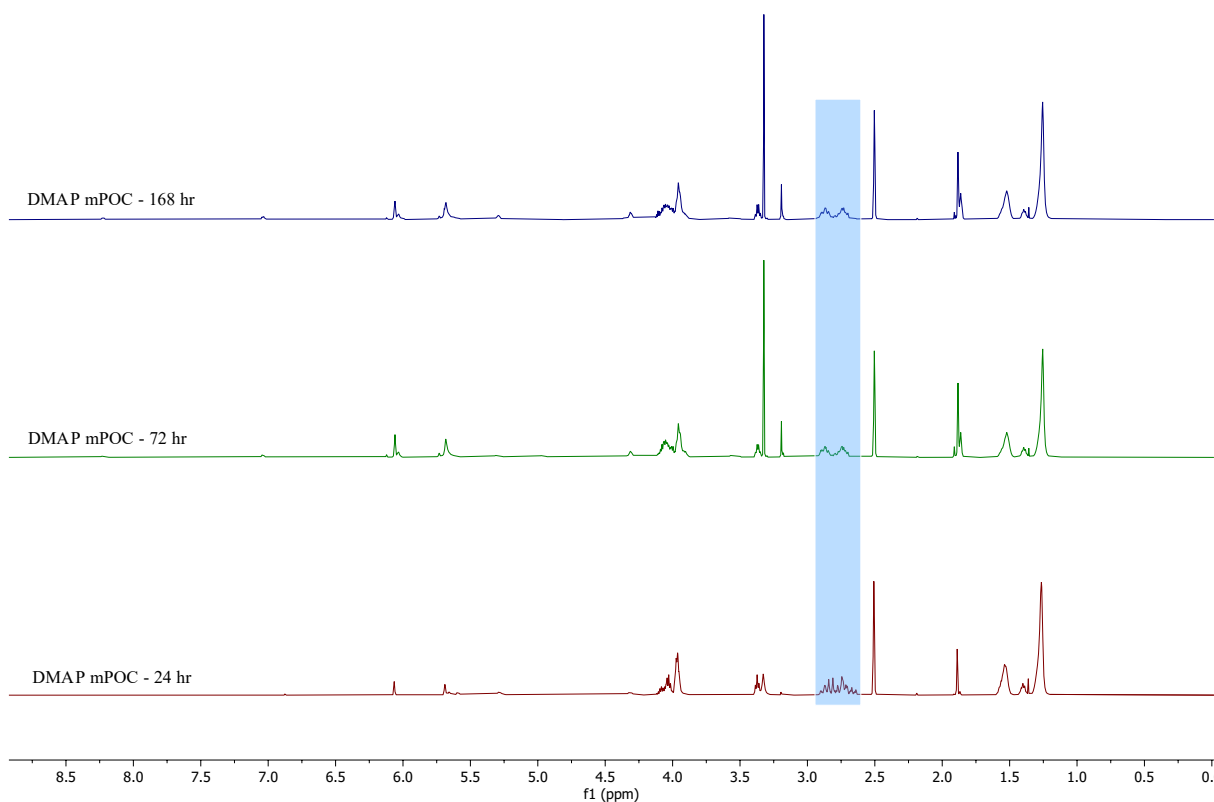


Figure S A.4:  $^1\text{H}$  NMR spectra of mPOC with DMAP used as the ring-opening catalyst during synthesis carried out for 24, 72, or 168 hours. It was hypothesized that letting the synthesis run for extended periods of time would increase the amount of methacrylate groups added to the POC structure. The change in synthesis times was also hypothesized to have effects on the mechanics and cytotoxicity of cured mPOC composites. Of note, the  $^1\text{H}$  NMR spectra shows distinct separation of the peaks associated with citric acid (blue highlight) which may indicate that the hydrogen atoms are in more stable environments after 72 hours of synthesis. These data also show that further synthesis past 72 hours is unnecessary, as the  $^1\text{H}$  NMR spectra between 72 and 168 hours are nearly identical.



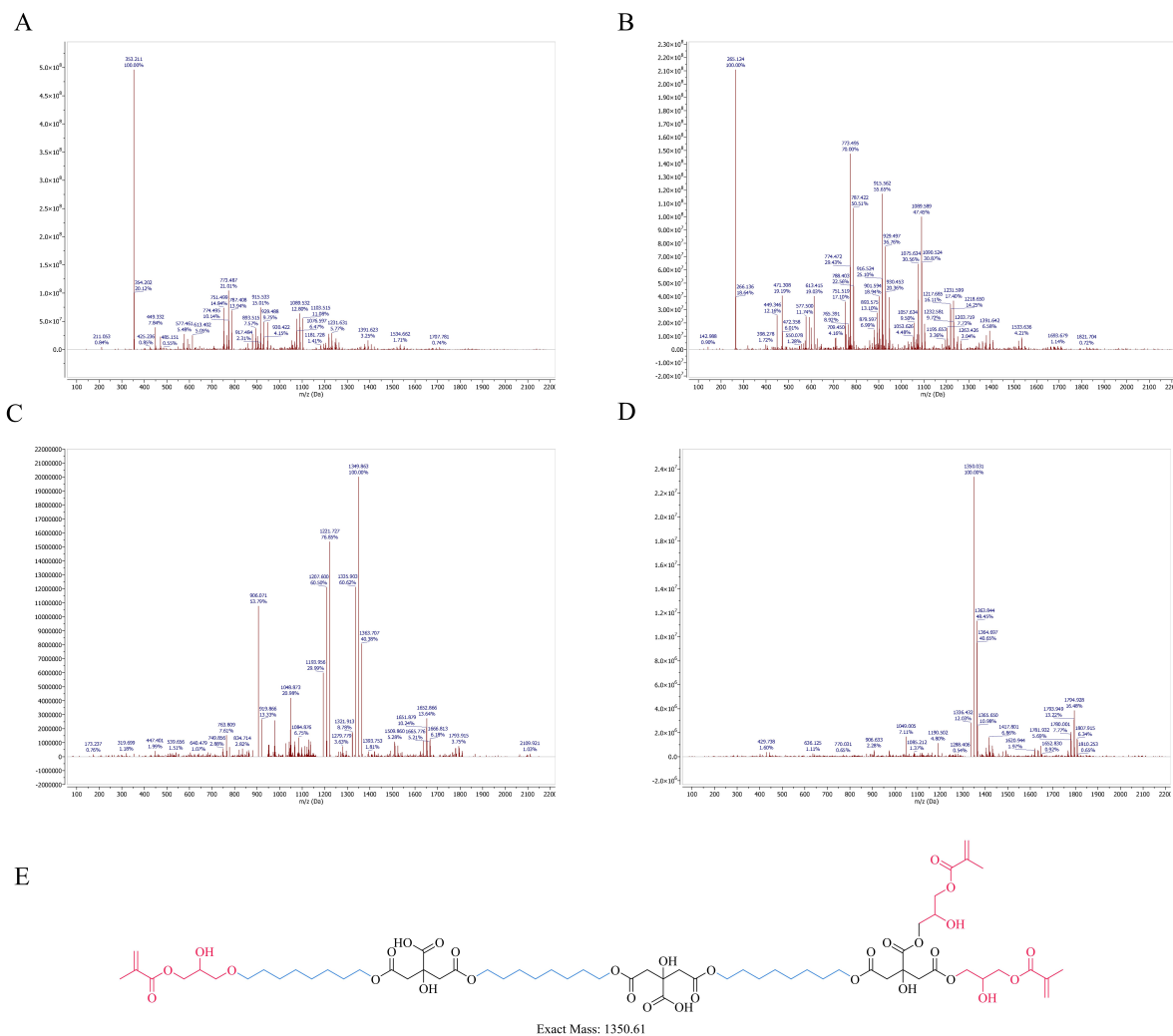


Figure S A.5: ESI data for mPOC synthesized with (A) imidazole for 6 hours, (B) DMAP for 6 hours, (C) DMAP for 24 hours, and (D) DMAP for 72 hours. Trace amounts of imidazole and DMAP can be seen in the 6-hour syntheses (A-B), noted by the molecular weights of 353.2 Daltons and 265.1 Daltons. Synthesis over 24 hours eliminates these trace compounds and greatly increases the size, occurrence, and variety of mPOC macromolecules (C). Synthesis over 72 hours (D) shows that one distinct structure of mPOC is likely to occur over other structures, namely a tri-1,8-octanediol – tri-citric acid – tri-glycidyl methacrylate (E). Moving forward from this data, mPOC synthesis time was increased from 6 hours to 24 hours for all subsequent polymer syntheses.

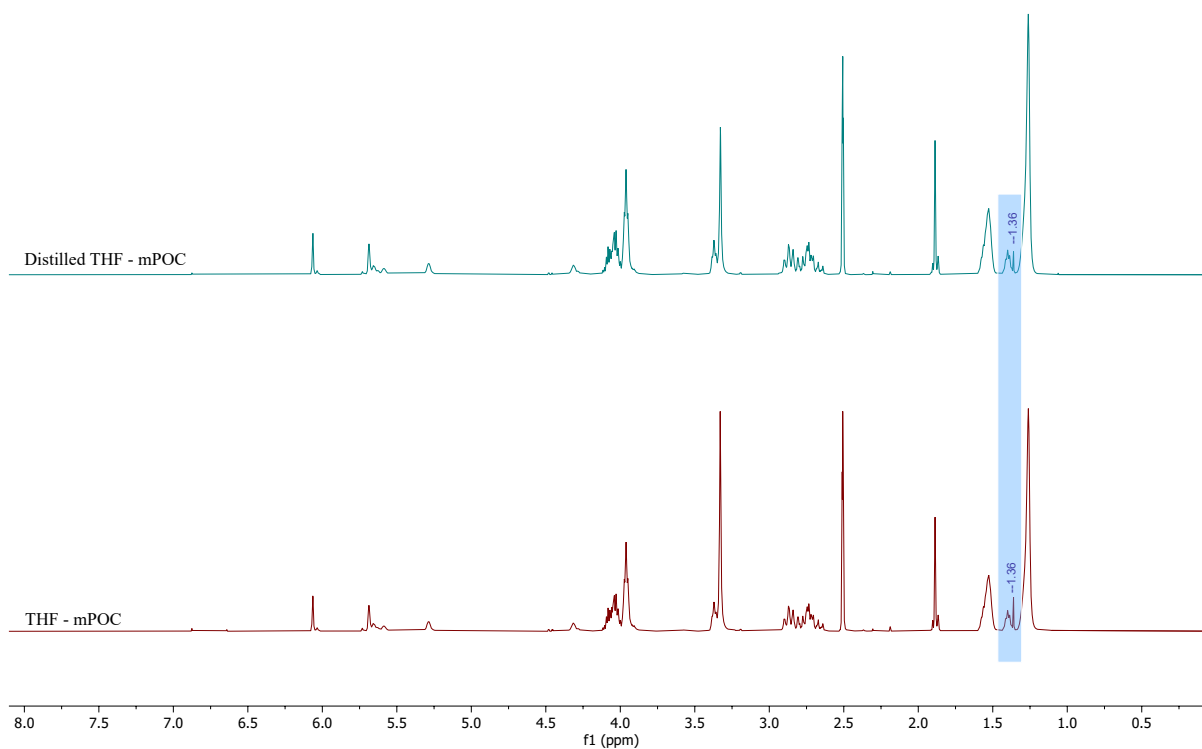


Figure S A.6:  $^1\text{H}$  NMR spectra of mPOC using non-distilled THF and distilled THF as a polymer solvent. It was noted that BHT, a trace component of THF, was found in the  $^1\text{H}$  NMR spectra of mPOC. In an effort to purify mPOC as much as possible, THF was distilled and used as an alternative solvent during mPOC synthesis. Using distilled THF showed a reduction of BHT within the  $^1\text{H}$  NMR spectra (blue highlight) noted at 1.36 ppm.

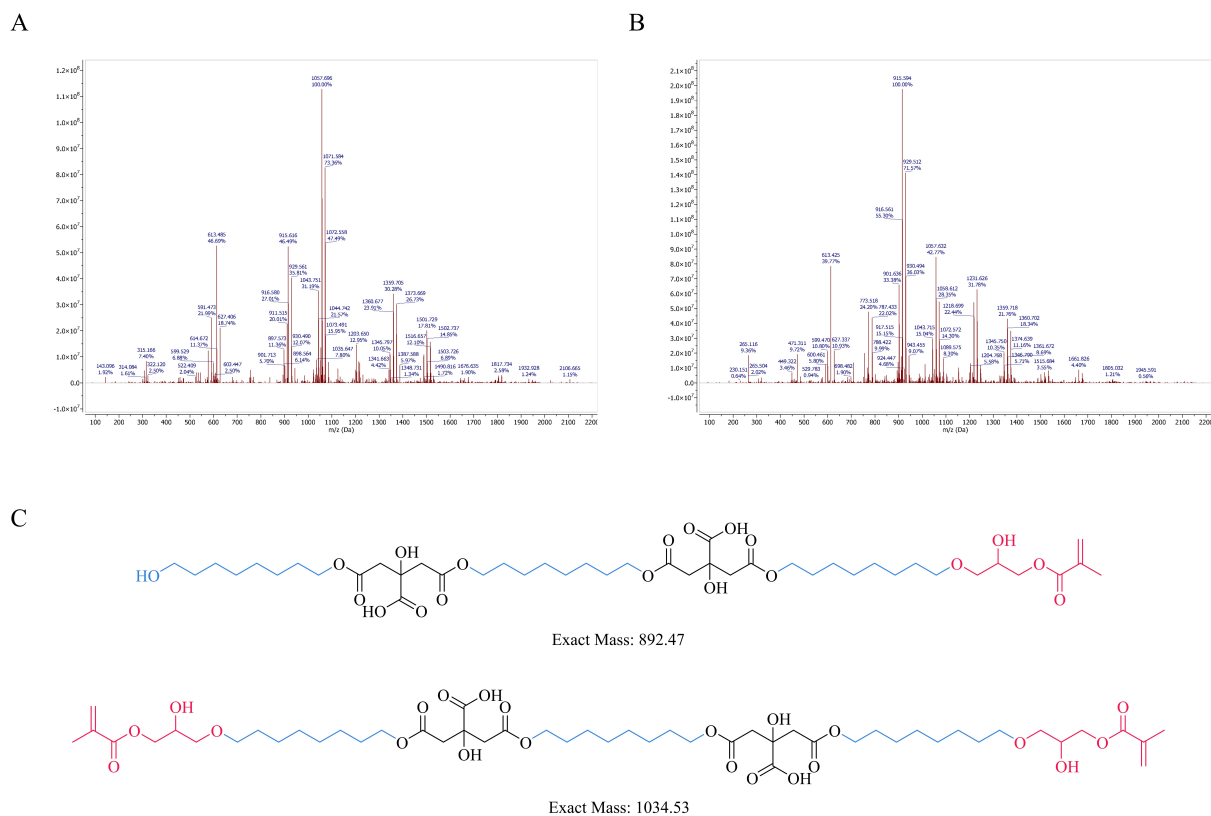


Figure S A.7: ESI data for mPOC run through chromatography with non-distilled THF (A) and distilled THF (B). The occurrence of macromolecules differs slightly between these samples, with non-distilled THF (A) resulting in primarily a 1034.53 Dalton macromolecule (C) and distilled THF (B) resulting in primarily an 892.47 Dalton macromolecule (C). Sodium adducts are noted within the ESI spectrum by an increase in macromolecule size of 23 Daltons.

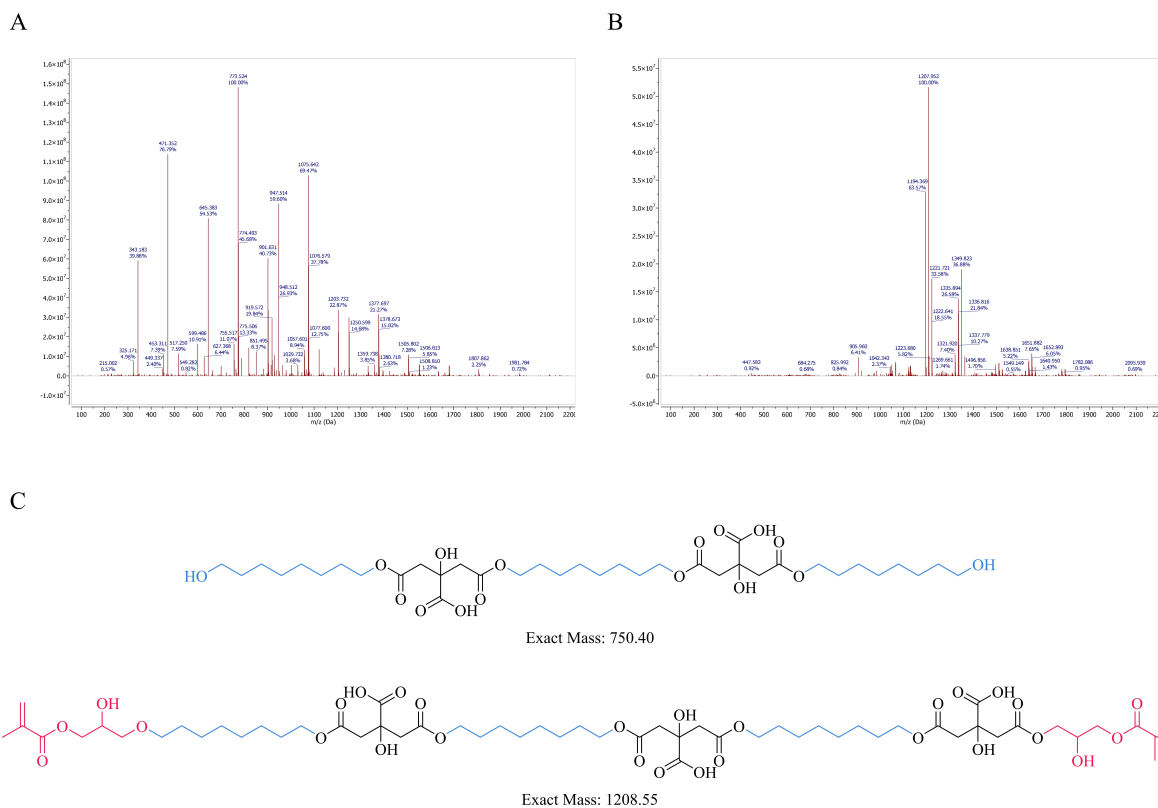


Figure S A.8: ESI data for a new molar synthesis of POC (A) and mPOC (B). Typical molar ratio between 1,8-octanediol and citric acid are 1:1. This figure instead shows ESI data for a 1.2:1 ratio, which aimed to attach more 1,8-octanediol groups to the overall macromolecule structure. (A) POC ESI data shows primarily a tri-1,8-octanediol – di-citric acid structure weighing 750.40 Daltons (C). Sodium adducts are noted within this spectrum by an increase in macromolecule size of 23 Daltons. (B) Primary structure of mPOC is a tri-1,8-octanediol – tri-citric acid – di-glycidyl methacrylate weighing 1207.95 Daltons (C). Increasing the amount of 1,8-octanediol compared to citric acid did increase the likelihood of POC macromolecules containing more units of 1,8-octanediol, but this was not seen in mPOC structures. Adjusting the ratio may have more precedent in POC applications over mPOC applications.

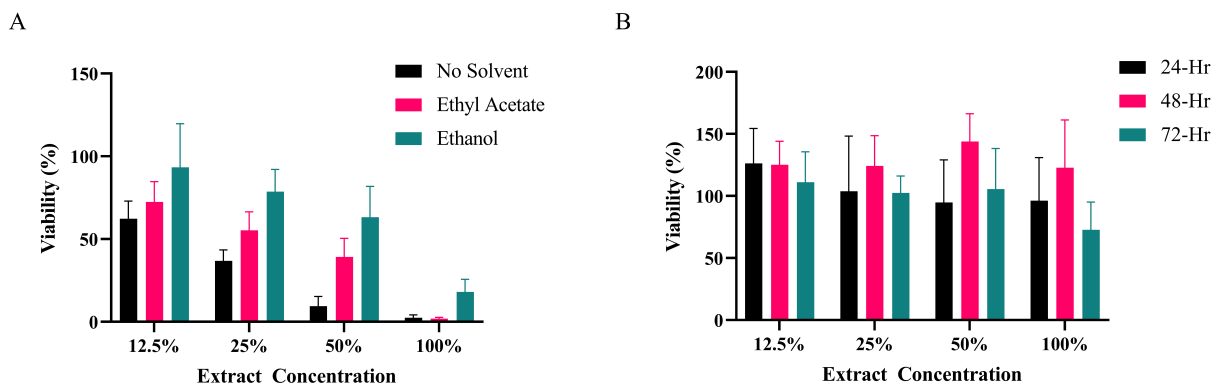


Figure S A.9: (A) *In vitro* cell cytotoxicity study comparing mPOC composites cured with no solvent, ethyl acetate as the solvent, or ethanol as the solvent. L929 murine fibroblasts (passage 7) were seeded onto 96-well plates at 10,000 cells/well and allowed to attach and grow for 24 hours. Cells were exposed to various extract concentrations and allowed to incubate over 24 hours, then an MTT assay was performed to determine viability. Viability decreases for all groups as the extract concentration increases, though ethanol samples performed the best. Ethanol was chosen as the solvent utilized in mPOC polymerization moving forward. (B) *In vitro* cell cytotoxicity study comparing mPOC composites cured at various time points. L929 murine fibroblasts (passage 7) were seeded onto 96-well plates at 10,000 cells/well and allowed to attach and grow for 24 hours. Cells were exposed to various extract concentrations and allowed to incubate over 24 hours, then an MTT assay was performed to determine viability. Viability remains above minimum viability levels (above 80%) for all extract concentrations and cure times.

mPOC scaffolds. It was found that increasing the amount of V70 was unnecessary as the viability was worse than 24 hour cured samples.

## A.2 Efficacy of Statins

An initial project design involved studying statins due to their ability to affect both angiogenesis and osteogenesis. It was hypothesized that incorporating either hydrophobic or hydrophilic statins into mPOC would help initiate both angiogenesis and osteogenesis at a quicker rate than naturally seen from the material itself. Statins are small molecules that inhibit 3-hydroxy-3-methylglutaryl (HMG) coenzyme A reductase and has been shown *in vitro* and *in vivo* to promote both angio-

Table A.2: Comparative statistical analysis of *in vitro* cell cytotoxicity for different solvents used in mPOC polymerization using student's t-test to compare pairs of means where  $*p < 0.05$  and  $**p < 0.01$ .

<b>12.5%</b>	<b>No Solvent</b>	<b>Ethyl Acetate</b>	<b>Ethanol</b>
<b>No Solvent</b>	-		**
<b>Ethyl Acetate</b>		-	*
<b>Ethanol</b>	**	*	-

<b>25%</b>	<b>No Solvent</b>	<b>Ethyl Acetate</b>	<b>Ethanol</b>
<b>No Solvent</b>	-	**	**
<b>Ethyl Acetate</b>	**	-	**
<b>Ethanol</b>	**	**	-

<b>50%</b>	<b>No Solvent</b>	<b>Ethyl Acetate</b>	<b>Ethanol</b>
<b>No Solvent</b>	-	**	**
<b>Ethyl Acetate</b>	**	-	**
<b>Ethanol</b>	**	**	-

<b>100%</b>	<b>No Solvent</b>	<b>Ethyl Acetate</b>	<b>Ethanol</b>
<b>No Solvent</b>	-		**
<b>Ethyl Acetate</b>		-	**
<b>Ethanol</b>	**	**	-

(a) Statistical comparison of viability between different solvents at the same concentration.

<b>No Solvent</b>	<b>12.5%</b>	<b>25%</b>	<b>50%</b>	<b>100%</b>
<b>12.5%</b>	-	**	**	**
<b>25%</b>	**	-	**	**
<b>50%</b>	**	**	-	**
<b>100%</b>	**	**	**	-

<b>Ethyl Acetate</b>	<b>12.5%</b>	<b>25%</b>	<b>50%</b>	<b>100%</b>
<b>12.5%</b>	-	**	**	**
<b>25%</b>	**	-	**	**
<b>50%</b>	**	**	-	**
<b>100%</b>	**	**	**	-

<b>Ethanol</b>	<b>12.5%</b>	<b>25%</b>	<b>50%</b>	<b>100%</b>
<b>12.5%</b>	-		*	**
<b>25%</b>		-		**
<b>50%</b>	*		-	**
<b>100%</b>	**	**	**	-

(b) Statistical comparison of viability between the same solvent at different concentrations.

Table A.3: Comparative statistical analysis of *in vitro* cell cytotoxicity for cure times for mPOC polymerization using student's t-test to compare pairs of means where  $*p < 0.05$  and  $**p < 0.01$ . 12.5% and 48-Hr tables showed no significance between groups and are thus not reported.

<b>25%</b>	<b>24-Hr</b>	<b>48-Hr</b>	<b>72-Hr</b>
<b>24-Hr</b>	-		
<b>48-Hr</b>		-	*
<b>72-Hr</b>		*	-

<b>50%</b>	<b>24-Hr</b>	<b>48-Hr</b>	<b>72-Hr</b>
<b>24-Hr</b>	-	**	
<b>48-Hr</b>	**	-	*
<b>72-Hr</b>		*	-

<b>100%</b>	<b>24-Hr</b>	<b>48-Hr</b>	<b>72-Hr</b>
<b>24-Hr</b>	-		
<b>48-Hr</b>		-	**
<b>72-Hr</b>		**	-

(a) Statistical comparison of viability between different cure times at the same concentration.

<b>24-Hr</b>	<b>12.5%</b>	<b>25%</b>	<b>50%</b>	<b>100%</b>
<b>12.5%</b>	-		*	
<b>25%</b>		-		
<b>50%</b>	*		-	
<b>100%</b>				-

<b>72-Hr</b>	<b>12.5%</b>	<b>25%</b>	<b>50%</b>	<b>100%</b>
<b>12.5%</b>	-			**
<b>25%</b>		-		**
<b>50%</b>			-	*
<b>100%</b>	**	**	*	-

(b) Statistical comparison of viability between the same cure time at different concentrations.

genic and osteogenic characteristics by upregulating endothelial nitric oxide synthase (eNOS), decreasing osteoclast differentiation and osteoblast apoptosis, and increasing osteoblast differentiation<sup>101,102</sup>. Hydrophobic simvastatin and lovastatin and hydrophilic pravastatin were chosen as potential statin additives based on their short elimination half-lives (statins purchased from Millipore Sigma, Burlington, MA). Cell cytotoxicity for various concentrations of statins were prepared and tested with L929 cells, human umbilical vein endothelial cells (HUVECs), and hMSCs (Figure SA.10 and SA.11). Cytotoxicity at 10  $\mu\text{M}$  in L929 cells was seen for both simvastatin and lovastatin, potentially due to their hydrophobicity. HUVECs were more sensitive to higher statin concentrations, so a range of 0-0.1  $\mu\text{M}$  was tested. It was determined that concentrations of up to 0.025  $\mu\text{M}$  did not cause cytotoxic effects to HUVECs. ALP activity and calcium production of hMSCs exposed to statin concentrations of 0.01-0.1  $\mu\text{M}$  was also addressed to determine if any of the tested statins promoted osteogenic lineages (Figure SA.12). After 10 days, there was no significant difference between negative and experimental statin groups, indicating that there was little to no pro-osteogenic effect of statins on hMSCs. Additionally, no calcium deposits were seen in experimental statin groups at day 21. Given the minimal evidence that the statins studied presented early pro-osteogenic expression, they were not pursued in following experiments and are thus not featured within the bulk portions of this thesis work.

### **A.3 Component Cell Cytotoxicity**

Each component relevant to mPOC polymerization, as well as components present in PMMA polymerization, or a relevant azo initiator were tested for cytotoxic effects at various concentrations following ISO 10993. Benzoyl peroxide (PMMA initiator), AIBN (azo initiator), V70, glycidyl methacrylate, and EDAB were tested at 0.1, 0.5, 1, 5, and 10  $\mu\text{M}$  concentrations in media over 24



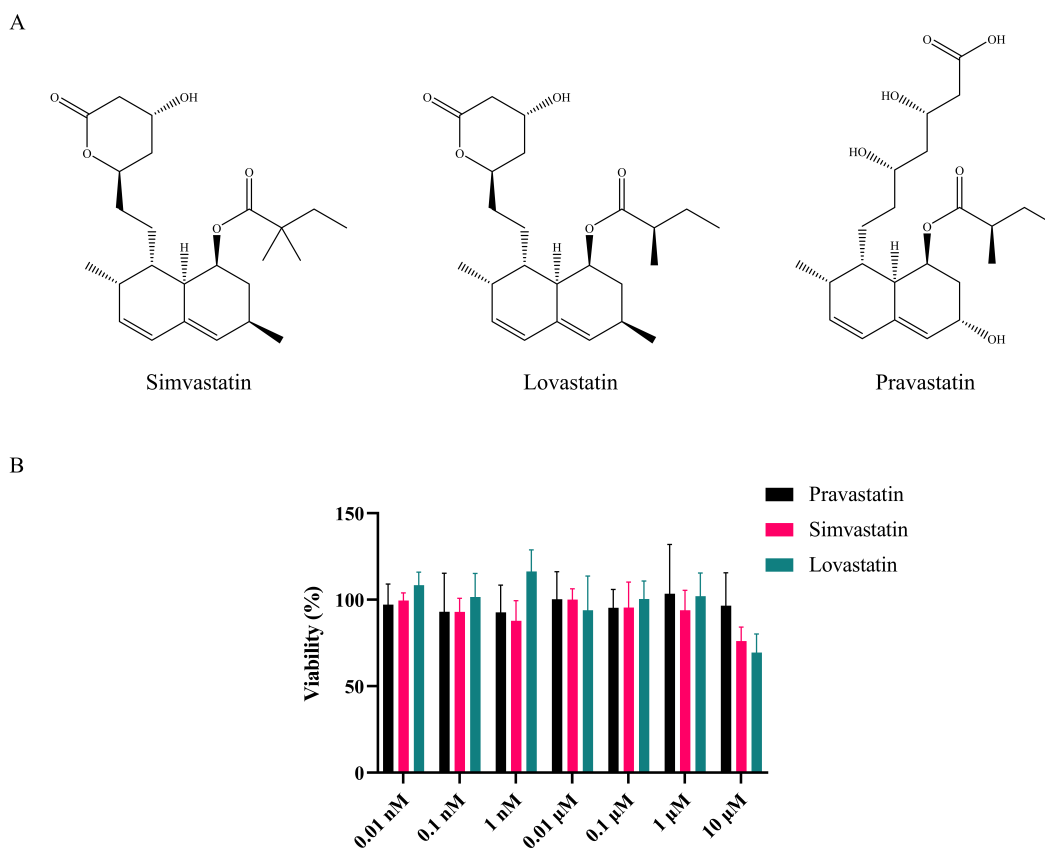


Figure S A.10: (A) Molecular structures for simvastatin, lovastatin, and pravastatin. (B) *In vitro* cell cytotoxicity study comparing statins at various concentrations. L929 murine fibroblasts (passage 7) were seeded onto 96-well plates at 10,000 cells/well and allowed to attach and grow for 24 hours. Cells were exposed to various statin concentrations and allowed to incubate over 24 hours, then an MTT assay was performed to determine viability. Cytotoxicity is noted in both simvastatin and lovastatin at 10  $\mu$ M. This concentration was not further pursued.

Table A.4: Comparative statistical analysis of *in vitro* cell cytotoxicity for statins (Figure SA.10B) at different concentrations using student's t-test to compare pairs of means where  $*p < 0.05$  and  $**p < 0.01$ . Pravastatin did not have any statistical significance between groups and is thus not reported here.

<b>Simvastatin</b>	<b>0.01 nM</b>	<b>0.1 nM</b>	<b>1 nM</b>	<b>0.01 <math>\mu</math>M</b>	<b>0.1 <math>\mu</math>M</b>	<b>1 <math>\mu</math>M</b>	<b>10 <math>\mu</math>M</b>
<b>0.01 nM</b>	-						**
<b>0.1 nM</b>		-					*
<b>1 nM</b>			-				
<b>0.01 <math>\mu</math>M</b>				-			**
<b>0.1 <math>\mu</math>M</b>					-		
<b>1 <math>\mu</math>M</b>						-	*
<b>10 <math>\mu</math>M</b>	**	*		**		*	-
<b>Lovastatin</b>	<b>0.01 nM</b>	<b>0.1 nM</b>	<b>1 nM</b>	<b>0.01 <math>\mu</math>M</b>	<b>0.1 <math>\mu</math>M</b>	<b>1 <math>\mu</math>M</b>	<b>10 <math>\mu</math>M</b>
<b>0.01 nM</b>	-						**
<b>0.1 nM</b>		-					*
<b>1 nM</b>			-				**
<b>0.01 <math>\mu</math>M</b>				-			
<b>0.1 <math>\mu</math>M</b>					-		**
<b>1 <math>\mu</math>M</b>						-	**
<b>10 <math>\mu</math>M</b>	**	*	**		**	**	-

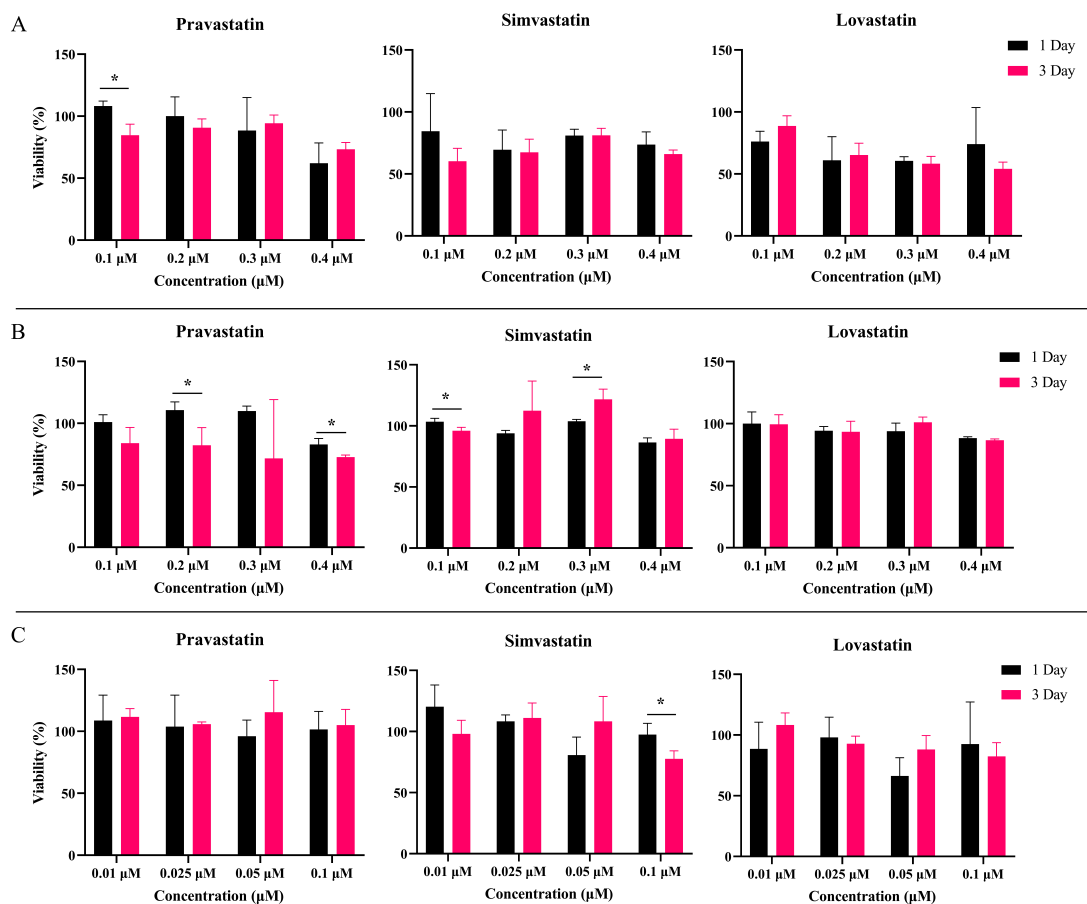


Figure S A.11: *In vitro* cell cytotoxicity study comparing statins at various concentrations and with various cell types. (A) HUVECs (passage 4) were seeded onto 96-well plates at 3,000 cells/well and allowed to attach and grow for 24 hours. Cells were exposed to various statin concentrations and allowed to incubate over 24 hours and 72 hours, then an MTT assay was performed to determine viability where  $*p < 0.05$ . Pravastatin presented a significant decrease in cell viability at day 3, so concentrations between 0 and 0.1  $\mu\text{M}$  were chosen for an additional cell viability study in HUVECs. (B) hMSCs (passage 1) were seeded onto 96-well plates at 5,000 cells/well and allowed to attach and grow for 24 hours. Cells were exposed to various statin concentrations and allowed to incubate over 24 hours and 72 hours, then an MTT assay was performed to determine viability where  $*p < 0.05$ . (C) Comparison of statins at concentrations between 0 and 0.1  $\mu\text{M}$ . HUVECs (passage 4) were seeded onto 96-well plates at 3,000 cells/well and allowed to attach and grow for 24 hours. Cells were exposed to various statin concentrations and allowed to incubate over 24 hours and 72 hours, then an MTT assay was performed to determine viability where  $*p < 0.05$ . Given all statins and concentrations fell above 80% viability, concentrations of up to 0.1  $\mu\text{M}$  were utilized for osteogenic cell studies.

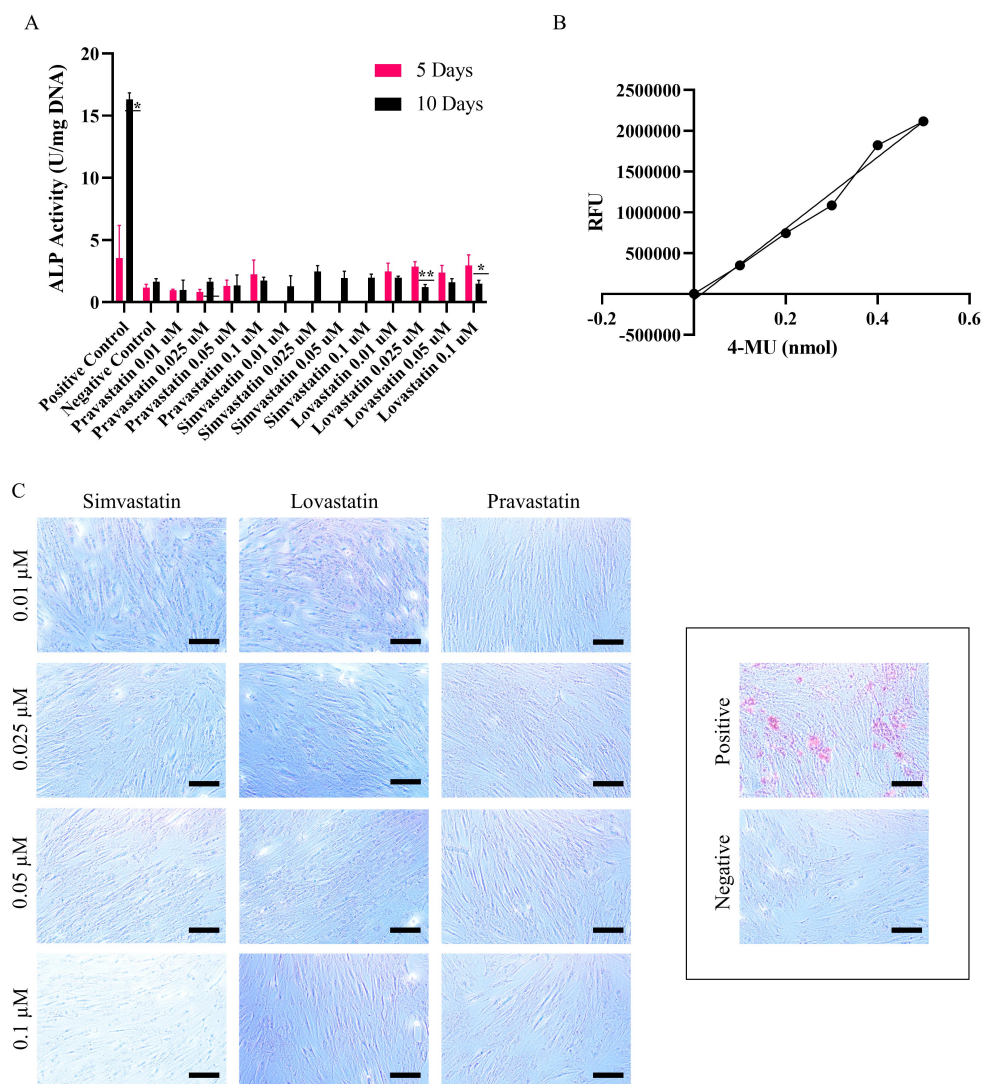


Figure S A.12: (A) Alkaline Phosphatase (ALP) expression at 5 and 10 days for control groups and statin experimental groups. Statistical significance between 5 and 10 days for each group are represented where  $*p < 0.05$  and  $**p < 0.01$ . Statins groups show statistically equivalent ALP expression at 10 days compared to negative controls, indicating that the statins do not promote early osteogenic expression. (B) ALP standard curve to determine ALP activity where  $y=4,375,468.57x-72,316.14$  and  $R^2=0.98$  for the fit linear regression. (C) Alizarin red staining of hMSCs after 21 days exposure to either simvastatin, lovastatin, or pravastatin of various concentrations. No calcium deposits are seen in any experimental group, whereas positive cells that were cultured in osteogenic media contain calcium deposits (red). Cell density remains consistent between groups. Scale bar inset is 100  $\mu$ m.

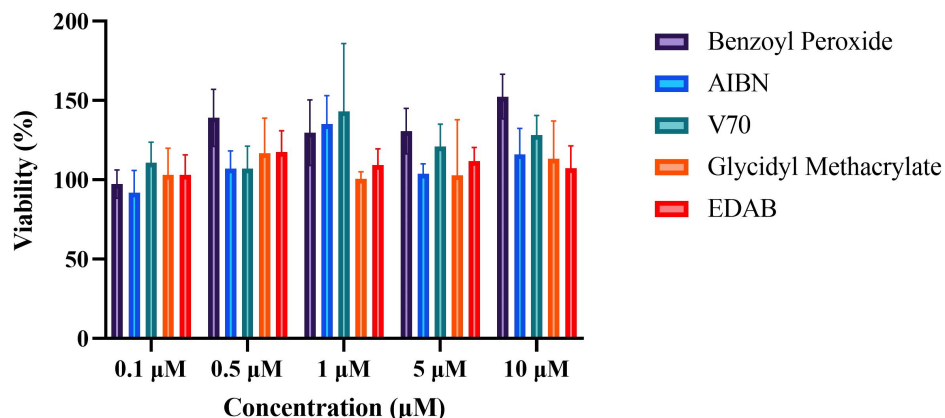


Figure S A.13: *In vitro* cell cytotoxicity study for various concentrations of chemical components and free radical polymerization initiators. L929 murine fibroblasts (passage 7) were seeded onto 96-well plates at 6000 cells/well and allowed to attach and grow for 24 hours. Each chemical component was mixed into media at concentrations of 0.1, 0.5, 1, 5, and 10 µM, filtered, and applied to cells for a 24-hour period following ISO 10993. Media was then aspirated, and 1mg/mL MTT solution was added into wells and allowed to react for 4 hours. MTT solution was removed, particulates were dissolved in DMSO to produce a colour change, and plates were read at 570nm. Viability is calculated as the average absorbance of experimental groups divided by the average absorbance of control groups, multiplied by 100 to obtain a percentage.

hours of exposure. Each component performed well within viable ranges at each tested concentration, showing that the included components in mPOC polymerization should not cause additional cytotoxic effects towards cells.

#### A.4 OPN *In Vivo* Results

Preliminary OPN immunofluorescent staining was performed to determine if any bone marker cells were present at and around the material tissue interface following the *in vivo* subcutaneous injection study. 4-week time points were sectioned at 5 µm and stained for OPN (Akm2A1, mouse

Table A.5: Comparative statistical analysis of *in vitro* cell cytotoxicity for various concentrations of chemical components and free radical polymerization initiators using student's t-test to compare pairs of means where  $*p < 0.05$  and  $**p < 0.01$ . No statistical significance was seen for (a) 0.1 and 0.5  $\mu\text{M}$  or (b) V70, GMA, and EDAB so are not reported here.

<b>1 <math>\mu\text{M}</math></b>	<b>BP</b>	<b>AIBN</b>	<b>V70</b>	<b>GMA</b>	<b>EDAB</b>
<b>BP</b>	-				
<b>AIBN</b>		-		*	
<b>V70</b>			-		
<b>GMA</b>		*		-	
<b>EDAB</b>					-

<b>5 <math>\mu\text{M}</math></b>	<b>BP</b>	<b>AIBN</b>	<b>V70</b>	<b>GMA</b>	<b>EDAB</b>
<b>BP</b>	-	*			
<b>AIBN</b>	*	-			
<b>V70</b>			-		
<b>GMA</b>				-	
<b>EDAB</b>					-

<b>10 <math>\mu\text{M}</math></b>	<b>BP</b>	<b>AIBN</b>	<b>V70</b>	<b>GMA</b>	<b>EDAB</b>
<b>BP</b>	-	*			*
<b>AIBN</b>	*	-			
<b>V70</b>			-		
<b>GMA</b>				-	
<b>EDAB</b>	*				-

(a) Statistical comparison of viability between different chemical components/initiators at the same concentration.

<b>BP</b>	<b>0.1 <math>\mu\text{M}</math></b>	<b>0.5 <math>\mu\text{M}</math></b>	<b>1 <math>\mu\text{M}</math></b>	<b>5 <math>\mu\text{M}</math></b>	<b>10 <math>\mu\text{M}</math></b>
<b>0.1 <math>\mu\text{M}</math></b>	-	*		*	**
<b>0.5 <math>\mu\text{M}</math></b>	*	-			
<b>1 <math>\mu\text{M}</math></b>			-		
<b>5 <math>\mu\text{M}</math></b>	*			-	
<b>10 <math>\mu\text{M}</math></b>	**				-

<b>AIBN</b>	<b>0.1 <math>\mu\text{M}</math></b>	<b>0.5 <math>\mu\text{M}</math></b>	<b>1 <math>\mu\text{M}</math></b>	<b>5 <math>\mu\text{M}</math></b>	<b>10 <math>\mu\text{M}</math></b>
<b>0.1 <math>\mu\text{M}</math></b>	-		*		
<b>0.5 <math>\mu\text{M}</math></b>		-			
<b>1 <math>\mu\text{M}</math></b>	*		-	*	
<b>5 <math>\mu\text{M}</math></b>			*	-	
<b>10 <math>\mu\text{M}</math></b>					-

(b) Statistical comparison of viability between the same chemical component/initiator at different concentrations.

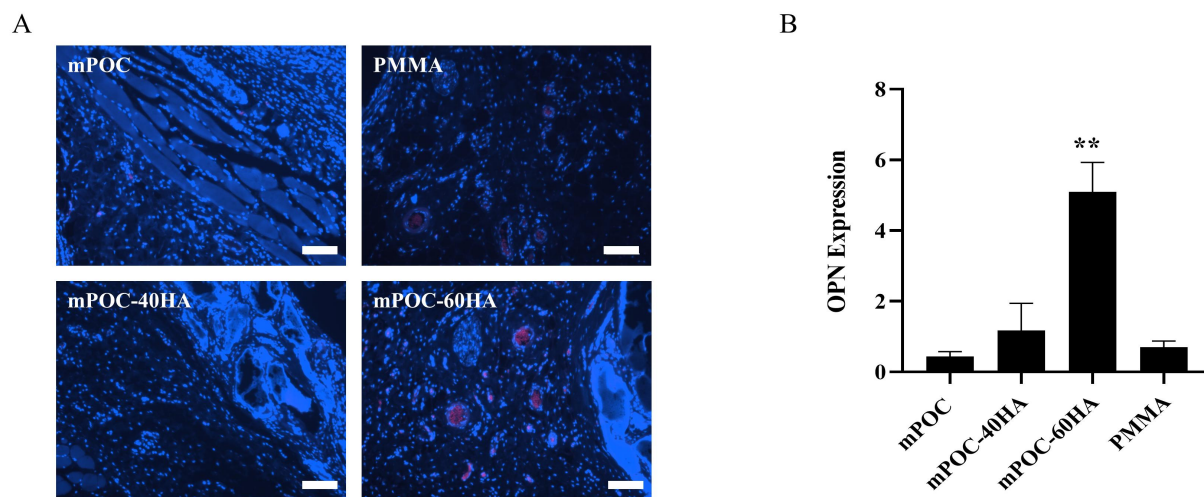


Figure S A.14: (A) Immunohistochemistry staining for osteopontin (OPN) and (B) quantitative analysis. (A) OPN (red) was qualitatively noted at a higher occurrence in mPOC-60HA samples, verified through quantitative analysis (B) where OPN expression in mPOC-60HA is statistically significant compared to other experimental groups. Additional, extended *in vivo* models should be carried out in a bone defect model to verify the expression of bone marker cells in response to mPOC-xHA composites over controls. Scale bars are set at 100  $\mu\text{m}$  and \*\* $p < 0.01$ .

anti-OPN antibody, Santa Cruz Biotechnology, 1:50 dilution). ImageJ was used to quantitatively assess the expression of markers against control samples. OPN expression in mPOC-60HA composites is significantly increased compared to all other sample groups, indicating that the presence of HA may increase the response and influx of early bone marker cells. While these results may be promising, staining for OPN should be done in an *in vivo* bone model, as the OPN could be staining for other cell types such as immune responsive cells.

## VITA

### Samantha E Huddleston

Place of Birth: St. Louis, Missouri

Year: April 6, 1994

#### Education

**Northwestern University**

Class of 2022

Ph.D. Biomedical Engineering Program

**University of Missouri, Columbia**

Class Of 2016

Major: B.S. Bioengineering

Minor: Mathematics

GPA: 3.904

#### Research Experience

**Graduate Researcher|Biomedical Engineering**

Sept 2016-May 2022

*Northwestern University, Evanston, IL — Ameer Group*

- Synthesizing new citrate-based thermoresponsive polymers for bone tissue engineering applications

**Undergraduate Researcher|Bioengineering**

May 2013-May 2016

*University of Missouri, Columbia, MO — Grant and McClellan Group*

- Synthesizing new biodegradable hydrogels for soft tissue repair
- Creating computer program for analysis of spinal cord activity

#### Professional Experience

*Acuitive Technologies, Allendale, NJ*

May 2020-Oct 2020

- Performing all in-house cell culture experiments
- Synthesizing new citrate-based materials for orthopedic applications

#### Publications

1. Huddleston SE, Duan C, Ameer GA. Azo Polymerization of Citrate-Based Biomaterial-Ceramic Composites at Physiological Temperatures. *Nano Select* **2022** 0(0). DOI: 10.1002/nano.202200080.
2. Xiao J, Zhu Y, Huddleston S, Li P, Xiao B, Farha O, Ameer G. Copper Metal-Organic Framework Nanoparticles Stabilized with Folic Acid Improve Wound Healing in Diabetes. *ACS Nano* **2018** 12(2), 1023-1032. DOI: 10.1021/acsnano.7b01850.